

6189

NATIONAL LIBRARY
OTTAWABIBLIOTHÈQUE NATIONALE
OTTAWA

NAME OF AUTHOR.....GORDON...PAUL.....BERARD...
TITLE OF THESIS.....The...Transition...Boundary...
.....Layer...Near the...Leading...
.....Edge.....
UNIVERSITY.....of...Alberta.....
DEGREE FOR WHICH THESIS WAS PRESENTED.....Ph.D.....
YEAR THIS DEGREE GRANTED....Spring...1970.....

Permission is hereby granted to THE NATIONAL LIBRARY
OF CANADA to microfilm this thesis and to lend or sell copies
of the film.

The author reserves other publication rights, and
neither the thesis nor extensive extracts from it may be
printed or otherwise reproduced without the author's
written permission.

(Signed).....P. Berard.....

PERMANENT ADDRESS:

5930 West Park Cr.
Red Deer, Alberta

DATED...March 13...1970

THE UNIVERSITY OF ALBERTA

THE TRANSITION BOUNDARY LAYER NEAR THE LEADING EDGE

by



Gordon Paul Berard, B.Sc. (Alberta)

A THESIS

SUBMITTED TO THE FACULTY OF GRADUATE STUDIES
IN PARTIAL FULFILMENT OF THE REQUIREMENTS FOR THE DEGREE
OF DOCTOR OF PHILOSOPHY

DEPARTMENT OF MECHANICAL ENGINEERING

EDMONTON, ALBERTA

Spring, 1970

UNIVERSITY OF ALBERTA

FACULTY OF GRADUATE STUDIES

The undersigned certify that they have read, and recommend to the Faculty of Graduate Studies for acceptance, a thesis entitled THE TRANSITION BOUNDARY LAYER NEAR THE LEADING EDGE submitted by Gordon Paul Berard in partial fulfilment of the requirements for the degree of Doctor of Philosophy.

David Marsden.....
Supervisor

H. C. Cheng.....

U. S. Hock.....

R. W. L. Lavoie.....

J. Barry Fush.....
External Examiner

Date *6 March 1970*.....

ABSTRACT

An experimental investigation was undertaken in the low density wind tunnel to test the validity of the boundary layer equations when used with "slip" and "temperature jump" boundary conditions in the transition regime.

The boundary layer equations were solved using a numerical technique developed by D. Clutter and A.M.O. Smith, using as boundary conditions the classical slip and temperature jump boundary conditions, and also by using experimentally determined slip and temperature jump results. The slip theory predicts lower values of slip than were experimentally obtained, and the boundary layer profiles begin to correlate with experiment after approximately one inch from the leading edge, where the local Reynolds number is of the order of 11.

Inclusion of temperature jump in the theory indicates that its effect on the slip results is small at least for Knudsen number less than 0.1.

Changing the initial value of slip velocity at the leading edge does not change the slip profile appreciably after three or four mean free paths from this point.

ACKNOWLEDGEMENTS

The author wishes to extend his appreciation to Dr. D.J. Marsden for providing the opportunity to undertake this project and for his guidance and supervision of this thesis. He also gratefully acknowledges the financial support of this research by the National Research Council and by the University of Alberta.

Thanks are extended to the staff members of the Mechanical Engineering Shop for the construction of the apparatus and to Dr. Gerard De Vries for his assistance on many occasions.

Additional thanks are also extended to Susan Schultz for her patience in typing this thesis.

TABLE OF CONTENTS

	Page
CHAPTER I - INTRODUCTION	1
CHAPTER II - THEORETICAL ANALYSIS	
2.1 Order of Magnitude Analysis	9
2.2 Numerical Analysis	19
2.2.1 Solution of the Momentum Equation	24
2.2.2 Solution of the Energy Equation	26
2.3 Boundary Conditions	28
2.3.1 Experimental Results	29
2.3.2 Classical Boundary Conditions	29
2.3.3 Linearized Boltzmann Solution	30
2.3.4 Incorporation of the Boundary Conditions in the Problem	31
2.4 Theory of the Equilibrium Temperature Probe	32
CHAPTER III - APPARATUS	
3.1 The Low Density Wind Tunnel	35
3.1.1 The Wind Tunnel Nozzle	36
3.2 Instrumentation	37
3.2.1 The Impact Probe	37
3.2.2 The Static Probe	38
3.2.3 The Equilibrium Temperature Probe	38
3.2.4 The Flat Plate Model	39
CHAPTER IV - PROCEDURE	
4.1 General Experimental Procedure	41
4.2 Reduction of Experimental Data	42
4.2.1 Impact Probe Calibration	43

CHAPTER V - RESULTS AND DISCUSSION OF EXPERIMENTAL AND THEORETICAL INVESTIGATION

5.1	Slip and Temperature Jump Boundary Conditions	46
5.1.1	Results	46
5.1.1.1	Measurement of Slip Velocity on a Cold Plate	46
5.1.1.2	Measurement of Slip and Temperature Jump on an Uncooled Plate at $P = 30.4$ Microns	47
5.1.1.3	Measurement of Slip and Temperature Jump on an Uncooled Plate at $P = 65.0$ Microns	48
5.1.2	Discussion	48
5.1.2.1	Experimental Results	48
5.1.2.2	Theoretical Results	50
5.2	Velocity and Temperature Profiles	52
5.2.1	Results	52
5.2.1.1	Velocity and Temperature Profiles on a Cold Plate	52
5.2.1.2	Velocity and Temperature Profiles on an Uncooled Plate	52
5.2.2	Discussion	53
5.3	Error Analysis	53
5.3.1	Experimental Accuracy	53
5.3.1.1	Resolution of the Static and Impact Probes	53
5.3.1.2	Accuracy of Temperature Measurements	54
5.3.1.3	Error in Reading the Dial Indicator	54
5.3.1.4	Other Possible Sources of Error	55
5.3.2	Accuracy of the Numerical Analysis	55
CHAPTER VI - SUMMARY AND CONCLUSIONS		57
BIBLIOGRAPHY		59

	Page
APPENDIX A - THEORY OF THE EQUILIBRIUM TEMPERATURE PROBE	62
A.1 Radiation Effects	67
APPENDIX B - PRESSURE RESPONSE TO THERMOCOUPLE WALL TEMPERATURE VARIATION	69
APPENDIX C - ERROR IN NUMERICAL ANALYSIS	72
C.1 Finite Difference Representations	73
C.2 Integration Expressions	74
C.2.1 Extrapolation Formulas	74
C.2.2 Interpolation Formulas	75

LIST OF TABLES

	Page
1. Experimental Data at the Wall (Cooled Plate)	120
2. Experimental Data at the Wall (Uncooled Plate): $P = 30.4$ Microns	121
3. Experimental Data at the Wall (Uncooled Plate): $P = 65.0$ Microns	122
4. Experimental Data at $P = 65.0$ Microns (Cooled Plate): $x = 0.2$ Inches	123
5. Experimental Data at $P = 65.0$ Microns (Cooled Plate): $x = 0.4$ Inches	124
6. Experimental Data at $P = 65.0$ Microns (Cooled Plate): $x = 0.6$ Inches	125
7. Experimental Data at $P = 65.0$ Microns (Cooled Plate): $x = 0.8$ Inches	126
8. Experimental Data at $P = 65.0$ Microns (Cooled Plate): $x = 1.0$ Inches	127
9. Experimental Data at $P = 29.0$ Microns (Uncooled Plate): $x = 0.2$ Inches	128
10. Experimental Data at $P = 29.0$ Microns (Uncooled Plate): $x = 0.4$ Inches	129
11. Experimental Data at $P = 29.0$ Microns (Uncooled Plate): $x = 0.8$ Inches	130
12. Experimental Data at $P = 29.0$ Microns (Uncooled Plate): $x = 1.0$ Inches	131
13. Experimental Data at $P = 64.0$ Microns (Uncooled Plate): $x = 0.2$ Inches	132
14. Experimental Data at $P = 64.0$ Microns (Uncooled Plate): $x = 0.4$ Inches	133
15. Experimental Data at $P = 64.0$ Microns (Uncooled Plate): $x = 0.6$ Inches	134

	Page
16. Experimental Data at $P = 64.0$ Microns (Uncooled Plate): $x = 0.8$ Inches	135
17. Experimental Data at $P = 64.0$ Microns (Uncooled Plate): $x = 1.0$ Inches	136

LIST OF FIGURES

	Page
1. Schematic Diagram of Low Density Wind Tunnel	77
2. Photograph of Low Density Wind Tunnel	78
3. Photograph of Test Section with Equilibrium Temperature Probe	79
4. Photograph of Test Section showing Traversing Mechanism	80
5. Photograph of Impact Probe	81
6. Schematic Diagram of the Nozzle	82
7. Thermocouple Calibration Curve	83
8. Schematic Diagram of Plate Model	83
9. Velocity Profile at Nozzle Exit: P = 78 Microns	84
10. Velocity Profile at Nozzle Exit: P = 95 Microns	85
11. Impact Probe Calibration	86
12. Slip along a Cold Flat Plate	87
13. Slip along a Flat Plate: P = 30.4 Microns	88
14. Temperature Jump along Flat Plate: P = 30.4 Microns	89
15. Slip along a Flat Plate: P = 65.0 Microns	90
16. Temperature Jump along a Flat Plate: P = 65.0 Microns	91
17. Velocity Profile on a Cold Flat Plate: x = 0.2 Inches	92
18. Velocity Profile on a Cold Flat Plate: x = 0.4 Inches	93
19. Velocity Profile on a Cold Flat Plate: x = 0.6 Inches	94

	Page
20. Velocity Profile on a Cold Flat Plate: x = 0.8 Inches	95
21. Velocity Profile on a Cold Flat Plate: x = 1.0 Inches	96
22. Temperature Profile on a Cold Flat Plate: x = 0.2 Inches	97
23. Temperature Profile on a Cold Flat Plate: x = 0.4 Inches	98
24. Temperature Profile on a Cold Flat Plate: x = 0.6 Inches	99
25. Temperature Profile on a Cold Flat Plate: x = 0.8 Inches	100
26. Temperature Profile on a Cold Flat Plate: x = 1.0 Inches	101
27. Velocity Profile on a Flat Plate: P = 29.0 Microns, x = 0.2 Inches	102
28. Velocity Profile on a Flat Plate: P = 29.0 Microns, x = 0.4 Inches	103
29. Velocity Profile on a Flat Plate: P = 29.0 Microns, x = 0.8 Inches	104
30. Velocity Profile on a Flat Plate: P = 29.0 Microns, x = 1.0 Inches	105
31. Temperature Profile on a Flat Plate: P = 29.0 Microns, x = 0.2 Inches	106
32. Temperature Profile on a Flat Plate: P = 29.0 Microns, x = 0.4 Inches	107
33. Temperature Profile on a Flat Plate: P = 29.0 Microns, x = 0.8 Inches	108
34. Temperature Profile on a Flat Plate: P = 29.0 Microns, x = 1.0 Inches	109
35. Velocity Profile on a Flat Plate: P = 64.0 Microns, x = 0.2 Inches	110
36. Velocity Profile on a Flat Plate: P = 64.0 Microns, x = 0.4 Inches	111

	Page
37. Velocity Profile on a Flat Plate: P = 64.0 Microns, x = 0.6 Inches	112
38. Velocity Profile on a Flat Plate: P = 64.0 Microns, x = 0.8 Inches	113
39. Velocity Profile on a Flat Plate: P = 64.0 Microns, x = 1.0 Inches	114
40. Temperature Profile on a Flat Plate: P = 64.0 Microns, x = 0.2 Inches	115
41. Temperature Profile on a Flat Plate: P = 64.0 Microns, x = 0.4 Inches	116
42. Temperature Profile on a Flat Plate: P = 64.0 Microns, x = 0.6 Inches	117
43. Temperature Profile on a Flat Plate: P = 64.0 Microns, x = 0.8 Inches	118
44. Temperature Profile on a Flat Plate: P = 64.0 Microns, x = 1.0 Inches	119

NOMENCLATURE

μ	coefficient of viscosity
ρ	density
p, P	hydrostatic pressure
Kn	Knudsen Number
λ	mean free path
σ	tangential momentum accommodation coefficient
y, Y	distance normal to surface
T	temperature
α	thermal accommodation coefficient
x, X	distance parallel to surface
u, U	velocity in X direction
v, V	velocity in Y direction
C_p	specific heat at constant pressure
κ	thermal conductivity
k	Boltzmann's Constant
G	gravitational acceleration
L	plate length
Re_L	Reynolds Number based on plate length
Pr	Prandtl Number
η	$\left(\frac{U_\infty}{\rho_\infty \mu_\infty X} \right) \int_0^y \rho \, dy$
C	$\frac{\rho \mu}{\rho_\infty \mu_\infty}$

R	gas constant
v_m	$\sqrt{2RT}$
S	$\frac{U}{\sqrt{2RT}}$
T_c	wire temperature
T_1	temperature of gas at the wall
P_t	total pressure
γ	$\frac{C_p}{C_v}$
ϵ	emmissivity
m	mass of gas molecule
'	denotes differentiation with respect to η

SUBSCRIPTS

c	characteristic
w	surface
∞	infinity

Other symbols are defined where they appear

CHAPTER I

INTRODUCTION

An analytical solution of the equations governing a physical system is facilitated by a mathematical model which describes the behavior of such a system. The relationships describing such a mathematical model are known as constitutive equations. The constitutive equations, which are necessary for a solution to the problem, incorporate the material response in the formulation of the problem. Eringen [1]* notes that "The character of the material is brought into the formulation through appropriate constitutive equations for each material with the constitutive variables being restricted in their regions of definitions".

Certain material properties, such as elasticity, viscosity, and plasticity, appear as parameters in the constitutive equations; these properties are termed by Reiner [2] as fundamental; and other properties, such as visco-elasticity and visco-plasticity, as complex properties. The fundamental material properties may be associated with the manner in which mechanical energy is dissipated by the material. In the case of gases at low pressure the linear Newtonian model for the relationship between shear stress and shear strain

* [] denotes reference.

rate is appropriate.

The constitutive equation for simple shear of a Newtonian fluid is,

$$\tau_{xy} = 2\mu \, dxy$$

where τ_{xy} is the shear stress and dxy is the shearing strain rate. The viscosity coefficient, μ , depends only on temperature and pressure, and not on the rate of deformation. The Newtonian fluid dissipates energy by the transfer of momentum on a molecular scale.

A theoretical investigation of flow problems involves the solution of the equations of motion, along with the energy equation.

The equations of motion are:

$$\frac{\partial \sigma_{xx}}{\partial x} + \frac{\partial \tau_{xy}}{\partial y} + \frac{\partial \tau_{xz}}{\partial z} + \rho f_x = \rho a_x ,$$

$$\frac{\partial \tau_{xy}}{\partial x} + \frac{\partial \sigma_{yy}}{\partial y} + \frac{\partial \tau_{yz}}{\partial z} + \rho f_y = \rho a_y ,$$

$$\frac{\partial \tau_{xz}}{\partial x} + \frac{\partial \tau_{yz}}{\partial y} + \frac{\partial \sigma_{zz}}{\partial z} + \rho f_z = \rho a_z$$

where f_x , f_y , f_z , and a_x , a_y , and a_z are the x , y , and z components of the body force and acceleration vector

respectively. Furthermore, if the material under consideration is a Newtonian fluid, then the governing equations may be further reduced to the Navier-Stokes equations, which in vector notation are given by [3]

$$\begin{aligned} \rho \frac{D\bar{V}}{Dt} = & \rho \bar{f} - \nabla P - \frac{2}{3} \nabla(\mu \nabla \cdot \bar{V}) + 2(\nabla \mu) \cdot \nabla \bar{V} \\ & + (\nabla \mu) \times (\nabla \times \bar{V}) + \mu [\nabla^2 \bar{V} + \nabla(\nabla \cdot \bar{V})] \end{aligned}$$

where \bar{V} is the velocity vector, \bar{f} is the body force per unit mass, and P is the static pressure. The Navier-Stokes equations are not readily solvable in their general form. However, in some important special cases these equations reduce to a solvable form.

The Knudsen number, Kn , is a non-dimensional parameter which is important in rarefied gas flows, although not derivable from the Navier-Stokes equations.

The Knudsen number which is defined by [4] as,

$$Kn = \frac{\lambda}{D},$$

where λ is the mean free path and D a characteristic length which will be taken to be the plate length in this study, distinguishes between flow regimes within the laminar region.

Depending on the relative magnitude of the Knudsen number,

the laminar flow regime may be divided [5] into the following regimes:

- (a) the continuum regime, which is defined when Knudsen number is less than 0.01,
- (b) the free molecular regime, which occurs when $Kn > 1$, and
- (c) the transition regime, which is the regime in which a transition occurs between the continuum and free molecular regime.

The regime of interest in the study presented in this thesis is the transition regime; experimental investigations were carried out at $Kn \approx 0.11$ and $Kn \approx 0.06$.

Since this thesis primarily uses the Navier-Stokes equations in the transition regime, it is important that the validity of the use of these equations in this regime is investigated. The most important point to be considered is the boundary conditions. The "no-slip" boundary condition is usually assumed for Newtonian viscous flow and its range of validity is defined by Knudsen number less than 0.01.

The no-slip boundary condition, as assumed in classical aerodynamics, is clearly inconsistent with the observed behavior [6] of the flow in the transition flow regime; that is for Knudsen number in the range

$$0.01 < Kn < 1 .$$

The phenomenon of slip was first observed by Kundt and Warburg [7]. These investigators found that the damping of a vibrating disk by a surrounding gas decreased at low pressures. They attributed this to slip of the gas at the boundaries. It was not until four years later that a theoretical expression describing this phenomenon was obtained by Maxwell [8]. Maxwell concluded that the amount of slip at the wall is a function of the velocity gradient at that point, and is given by

$$U = \frac{\mu}{p} a_1 \sqrt{RT} \left. \frac{\partial u}{\partial y} \right|_{y=0},$$

$$a_1 = \frac{2-\sigma}{\sigma} \sqrt{\frac{\pi}{2}}$$

Similar conclusions were obtained, but in a simpler manner, by Millikan [9] and reproduced by Kennard [10]. Notwithstanding some slight modifications in the slip coefficient, this theory is still widely used today. It has been shown experimentally [11] that the accommodation coefficient must depend on the physical condition of the surface and on the gas under consideration. A theoretical expression relating these quantities has not been found as yet, consequently the slip coefficients used in any theoretical investigation are based on experimental results. The slip coefficients adopted in this investigation are

$$a_1 = 2.333 ,$$

$$a_1 = 1.857 ,$$

and

$$a_1 = 1.222 ,$$

which correspond to the following tangential momentum accommodation coefficients

$$\sigma = 0.6 ,$$

$$\sigma = 0.7 ,$$

and

$$\sigma = 0.9 \text{ respectively.}$$

These values cover the range of values obtained experimentally by Merlic [12].

So far attention has been focused on the velocity boundary condition. The other boundary condition to be considered is on the gas temperature at the surface. In the continuum regime the gas temperature at the wall is equal to the wall temperature. However, in the transition regime the gas temperature at the surface can differ from the wall temperature, giving a "temperature jump" boundary condition [13]. The presence of such a temperature jump was first assumed by Poisson, and later confirmed experimentally by Smoluchowski [14]. A theory describing the temperature jump, similar to the slip theory derived by Maxwell, was derived by Poisson.

Poisson's temperature jump boundary condition is,

$$T_k - T_w = g' \frac{\partial T}{\partial y} ,$$

where T_k is the temperature of the gas that would exist if the temperature gradient along the outward-drawn normal to the wall, $\frac{\partial T}{\partial y}$, continued without change up to the wall itself [15], and g' represents the "temperature jump distance".

Again it is clear that the temperature jump is a function of an accommodation coefficient, which is referred to as the thermal accommodation coefficient.

It is worth noting that the thermal accommodation coefficient and the tangential accommodation coefficient are not necessarily equal. The temperature jump coefficient used in this thesis is,

$$a_2 = 1.875 ,$$

which is based on the thermal accommodation coefficient

$$\alpha = 1.0 ,$$

and is the coefficient usually assumed for diffuse reflection.

The possibility of using the Navier-Stokes equations subject to the slip boundary condition as a model to study viscous flow problems in the transition regime was investi-

gated by Patterson [16] and by Street [17]. Street concluded that the slip condition is compatible with the Navier-Stokes equations, and furthermore that it may be possible to study viscous flow problems in the transition regime using the boundary layer equations, which take the first order slip effects into account.

The objective of this work is to experimentally investigate the range of validity of the boundary layer equations and transition boundary conditions.

CHAPTER II

THEORETICAL ANALYSIS

2.1 Order of Magnitude Analysis

The solution of many flow problems can be facilitated by an order of magnitude analysis of the continuity, energy, and momentum equations. The purpose is to retain those terms which are essential to describe the flow.

The governing equations for a two dimensional steady flow in rectangular Cartesian coordinates (see reference [18] or [19] for derivation) become:

Continuity:

$$\frac{\partial(\rho U)}{\partial X} + \frac{\partial(\rho V)}{\partial Y} = 0$$

Longitudinal Momentum

$$\begin{aligned} \rho \left(U \frac{\partial U}{\partial X} + V \frac{\partial U}{\partial Y} \right) = & - \frac{\partial P}{\partial X} + \frac{\partial(-2/3 \mu)}{\partial X} \cdot \left(\frac{\partial U}{\partial X} + \frac{\partial V}{\partial Y} \right) \\ & + \left(-\frac{2}{3} \mu \right) \frac{\partial}{\partial X} \left(\frac{\partial U}{\partial X} + \frac{\partial V}{\partial Y} \right) + 2 \frac{\partial \mu}{\partial X} \frac{\partial U}{\partial X} \\ & + \frac{\partial \mu}{\partial Y} \left(\frac{\partial U}{\partial Y} + \frac{\partial V}{\partial X} \right) + \mu \left(\frac{\partial^2 U}{\partial X^2} + \frac{\partial^2 U}{\partial Y^2} \right) + \mu \frac{\partial}{\partial X} \left(\frac{\partial U}{\partial X} + \frac{\partial V}{\partial Y} \right) \end{aligned}$$

Lateral Momentum

$$\begin{aligned}
\rho \left(U \frac{\partial V}{\partial X} + V \frac{\partial U}{\partial Y} \right) = & - \frac{\partial P}{\partial Y} + \frac{\partial (-2/3 \mu)}{\partial Y} \left(\frac{\partial U}{\partial X} + \frac{\partial V}{\partial Y} \right) \\
& + \left(-\frac{2}{3} \mu \right) \frac{\partial}{\partial Y} \left(\frac{\partial U}{\partial X} + \frac{\partial V}{\partial Y} \right) + \frac{\partial \mu}{\partial X} \left(\frac{\partial V}{\partial X} + \frac{\partial U}{\partial Y} \right) \\
& + 2 \frac{\partial \mu}{\partial Y} \frac{\partial V}{\partial Y} + \mu \left(\frac{\partial^2 V}{\partial X^2} + \frac{\partial^2 V}{\partial Y^2} \right) + \mu \frac{\partial}{\partial Y} \left(\frac{\partial U}{\partial X} + \frac{\partial V}{\partial Y} \right) - \rho G
\end{aligned}$$

Energy:

2.2-1

$$\begin{aligned}
\rho C_p \left(U \frac{\partial T}{\partial X} + V \frac{\partial T}{\partial Y} \right) + U \frac{\partial P}{\partial X} + V \frac{\partial P}{\partial Y} = & k \left(\frac{\partial^2 T}{\partial X^2} + \frac{\partial^2 T}{\partial Y^2} \right) + \frac{\partial k}{\partial X} \frac{\partial T}{\partial X} + \frac{\partial k}{\partial Y} \frac{\partial T}{\partial Y} \\
& + \left(-\frac{2}{3} \mu \right) \left(\frac{\partial U}{\partial X} + \frac{\partial V}{\partial Y} \right)^2 + 2\mu \left[\left(\frac{\partial U}{\partial X} \right)^2 \right. \\
& \left. + \left(\frac{\partial V}{\partial Y} \right)^2 \right] + \mu \left(\frac{\partial U}{\partial Y} + \frac{\partial V}{\partial X} \right)^2
\end{aligned}$$

The boundary conditions at the wall will be taken to be the Maxwell slip condition, and for convenience, the temperature of the gas at the wall will be assumed constant.

Therefore, at $Y = 0$,

$$U(X,0) = \lambda a_1 \frac{\partial U}{\partial Y} \quad \text{where } a_1 \text{ is a constant.}$$

$$T(X,0) = T_w \quad 2.1-2$$

$$V(X,0) = 0 \quad (\text{no blowing or suction})$$

$$P(X,0) = P_w$$

$$\text{At } Y = \infty :$$

$$U = U_\infty$$

$$T = T_\infty$$

$$V = 0$$

$$P = P_\infty$$

The terms in the equations are nondimensionalized by dividing all the variables by characteristic quantities, denoted by subscript C.

$$\left[\frac{\rho_c U_c}{X_c} \right] \left(\omega \frac{\partial u}{\partial x} + u \frac{\partial \rho}{\partial x} \right) + \left[\frac{\rho_c V_c}{Y_c} \right] \left(\omega \frac{\partial v}{\partial y} + u \frac{\partial \rho}{\partial y} \right) = 0$$

$$\left[\frac{\rho_c U_c^2}{X_c} \right] \omega u \frac{\partial u}{\partial x} + \left[\frac{\rho_c V_c U_c}{Y_c} \right] \omega v \frac{\partial u}{\partial y} = - \left[\frac{P_c}{X_c} \right] \frac{\partial P}{\partial x}$$

$$+ \left[\frac{\mu_c U_c}{X_c^2} \right] \left(\frac{4}{3} \frac{\partial M}{\partial x} \frac{\partial u}{\partial x} + \frac{4}{3} M \frac{\partial^2 u}{\partial x^2} \right)$$

$$+ \left[\frac{\mu_c V_c}{X_c Y_c} \right] \left(-\frac{2}{3} \frac{\partial M'}{\partial x} \frac{\partial v}{\partial y} + \frac{M'}{3} \frac{\partial^2 v}{\partial x \partial y} + \frac{\partial M'}{\partial y} \frac{\partial v}{\partial x} \right)$$

$$+ \left[\frac{\mu_c U_c}{Y_c^2} \right] \left(\frac{\partial M'}{\partial y} \frac{\partial u}{\partial y} + M' \frac{\partial^2 u}{\partial y^2} \right)$$

$$\left[\frac{\rho_c U_c V_c}{X_c} \right] \omega u \frac{\partial v}{\partial x} + \left[\frac{\rho_c V_c^2}{Y_c} \right] \omega v \frac{\partial v}{\partial y} = - \left[\frac{P_c}{Y_c} \right] \frac{\partial P}{\partial y}$$

$$+ \left[\frac{\mu_c U_c}{Y_c X_c} \right] \left(-\frac{2}{3} \frac{\partial M'}{\partial y} \frac{\partial u}{\partial x} + \frac{M'}{3} \frac{\partial^2 u}{\partial y \partial x} + \frac{\partial M'}{\partial x} \frac{\partial u}{\partial y} \right)$$

$$+ \left[\frac{\mu_c V_c}{Y_c^2} \right] \left(\frac{4}{3} \frac{\partial M'}{\partial y} \frac{\partial v}{\partial y} + \frac{4}{3} M' \frac{\partial^2 v}{\partial y^2} \right)$$

2.1-3

$$+ \left[\frac{\mu_c V_c}{X_c^2} \right] \left(\frac{\partial M'}{\partial x} \frac{\partial v}{\partial x} + M' \frac{\partial^2 v}{\partial x^2} \right) - [\rho_c G] \omega$$

$$\left[\frac{\rho_c C_p U_c \theta_c}{X_c} \right] \omega u \frac{\partial \phi}{\partial x} + \left[\frac{\rho_c C_p V_c \theta_c}{Y_c} \right] \omega v \frac{\partial \phi}{\partial y} - \left[\frac{U_c P_c}{X_c} \right] u \frac{\partial P}{\partial x} - \left[\frac{V_c P_c}{Y_c} \right] v \frac{\partial P}{\partial y}$$

$$= \left[\frac{\kappa_c \theta_c}{X_c^2} \right] \left(\kappa \frac{\partial^2 \phi}{\partial x^2} + \frac{\partial \kappa}{\partial x} \frac{\partial \phi}{\partial x} \right) + \left[\frac{\kappa_c \theta_c}{Y_c^2} \right] \left(\kappa \frac{\partial^2 \phi}{\partial y^2} + \frac{\partial \kappa}{\partial y} \frac{\partial \phi}{\partial y} \right)$$

$$+ \left[\frac{\mu_c U_c^2}{X_c^2} \right] \frac{4M'}{3} \left(\frac{\partial u}{\partial x} \right)^2 + \left[\frac{\mu_c V_c^2}{Y_c^2} \right] \frac{4M'}{3} \left(\frac{\partial v}{\partial y} \right)^2$$

$$+ \left[\frac{\mu_c v_c u_c}{x_c y_c} \right] \left(- \frac{4M'}{3} \frac{\partial u}{\partial x} \frac{\partial v}{\partial y} + 2M' \frac{\partial u}{\partial y} \frac{\partial v}{\partial x} \right)$$

$$+ \left[\frac{\mu_c u_c^2}{y_c^2} \right] M' \left(\frac{\partial u}{\partial y} \right)^2 + \left[\frac{\mu_c v_c^2}{x_c^2} \right] M' \left(\frac{\partial v}{\partial x} \right)^2$$

$$[U_c] u(x,0) = \left[\frac{\lambda U_c}{Y_c} \right] c_1 \frac{\partial u}{\partial y}$$

where

$$K = \kappa / \kappa_c$$

$$M' = \mu / \mu_c$$

$$\omega = \rho / \rho_c$$

$$\theta = T - T_\infty$$

$$\phi = \theta / \theta_c$$

Assume

$$U_c = U_\infty$$

$$X_c = L \quad (\text{the plate length})$$

$$\rho_c = \rho_\infty$$

$$\theta_c = T_w - T_\infty = \theta_w$$

$$\kappa_c = \kappa_\infty$$

$$\mu_c = \mu_\infty$$

If it is assumed that in the laminar boundary layer the order of magnitude of the viscous forces is equal to the order of magnitude of the inertia forces, this implies,

$$\frac{\rho_\infty U_\infty^2}{L} = O\left(\frac{\mu_\infty U_\infty}{y_c^2}\right)$$

or $y_c = \sqrt{\frac{\mu_\infty L}{\rho_\infty U_\infty}} = \frac{L}{(Re_L)^{1/2}}$, where Re_L is the Reynolds number based on plate length.

However, from the slip boundary condition,

$$y_c = \lambda$$

Therefore let,

$$y_c = KnL + \frac{L}{(Re_L)^{1/2}}, \quad 0 \leq Kn \leq 1$$

All terms in the continuity equation are taken to be of equal order. Then

$$\frac{\rho_{\infty} U_{\infty}}{L} = 0 \left(\frac{\rho_{\infty} V_c}{Y_c} \right)$$

or

$$V_c = \frac{U_{\infty} Y_c}{L} = U_{\infty} \left(Kn + \frac{1}{(Re_L)^{1/2}} \right)$$

Substituting the values for the characteristic quantities into the equations and re-arranging

$$\omega \frac{\partial u}{\partial x} + u \frac{\partial \rho}{\partial x} + \omega \frac{\partial v}{\partial y} + u \frac{\partial \rho}{\partial y} = 0$$

$$\omega u \frac{\partial u}{\partial x} + \omega v \frac{\partial u}{\partial y} = - [Eu] \frac{\partial p}{\partial x} + \left[\frac{1}{Re_L} \right] \left(\frac{4}{3} \frac{\partial M'}{\partial x} \frac{\partial u}{\partial x} + \frac{4}{3} M' \frac{\partial^2 u}{\partial x^2} \right)$$

$$+ \left[\frac{1}{Re_L} \right] \left(- \frac{2}{3} \frac{\partial M'}{\partial x} \frac{\partial v}{\partial y} + \frac{M'}{3} \frac{\partial^2 v}{\partial x \partial y} + \frac{\partial M'}{\partial y} \frac{\partial v}{\partial x} \right)$$

$$+ \left[\frac{\frac{1}{Re_L}}{(Kn + (1-Kn)/(Re_L)^{1/2})^2} \right] \left(\frac{\partial M'}{\partial y} \frac{\partial u}{\partial y} + M' \frac{\partial^2 u}{\partial y^2} \right)$$

$$\omega u \frac{\partial v}{\partial x} + \omega v \frac{\partial v}{\partial y} = - \left[\frac{Eu}{(Kn + (1-Kn)/(Re_L)^{1/2})^2} \right] \frac{\partial p}{\partial y}$$

$$\begin{aligned}
& + \left[\frac{\frac{1}{Re_L}}{(Kn + (1-Kn)/(Re_L)^{1/2})^2} \right] \left(-\frac{2}{3} \frac{\partial M'}{\partial y} \frac{\partial u}{\partial x} + \frac{M'}{3} \frac{\partial^2 u}{\partial y \partial x} + \frac{\partial M'}{\partial x} \frac{\partial u}{\partial y} \right) \\
& + \left[\frac{\frac{1}{Re_L}}{(Kn + (1-Kn)/(Re_L)^{1/2})^2} \right] \left(\frac{4}{3} \frac{\partial M'}{\partial y} \frac{\partial v}{\partial y} + \frac{4M'}{3} \frac{\partial^2 v}{\partial y^2} \right) \\
& + \frac{1}{Re_L} \left(\frac{\partial M'}{\partial x} \frac{\partial v}{\partial x} + M' \frac{\partial^2 v}{\partial x^2} \right) - \left[\frac{1}{F} \right] \omega
\end{aligned} \tag{2.1-4}$$

$$\omega u \frac{\partial \phi}{\partial x} + \omega v \frac{\partial \phi}{\partial y} - [E E_u] \left(u \frac{\partial P}{\partial x} - v \frac{\partial P}{\partial y} \right) = \left[\frac{1}{Pr Re_L} \right] \left(K \frac{\partial^2 \phi}{\partial x^2} + \frac{\partial K}{\partial x} \frac{\partial \phi}{\partial x} \right)$$

$$+ \left[\frac{\frac{1}{(Pr \times Re_L)}}{(Kn + (1-Kn)/(Re_L)^{1/2})^2} \right] \left(K \frac{\partial^2 \phi}{\partial y^2} + \frac{\partial K}{\partial y} \frac{\partial \phi}{\partial y} \right)$$

$$+ \left[\frac{E}{Re_L} \right] \frac{4M'}{3} \left(\frac{\partial u}{\partial x} \right)^2 + \left[\frac{E}{Re_L} \right] \frac{4M'}{3} \left(\frac{\partial v}{\partial y} \right)^2$$

$$+ \left[\frac{E}{Re_L} \right] \left(-\frac{4M'}{3} \frac{\partial u}{\partial x} \frac{\partial v}{\partial y} + 2M' \frac{\partial u}{\partial y} \frac{\partial v}{\partial x} \right)$$

$$+ \left[\frac{\frac{E}{Re_L}}{(Kn + (1-Kn)/(Re_L)^{1/2})^2} \right] M' \left(\frac{\partial u}{\partial y} \right)^2$$

$$+ \left[\frac{E}{Re_L} \right] [Kn + (1-Kn)/(Re_L)^{1/2}]^2 \left(\frac{\partial v}{\partial x} \right)^2$$

where

$$\text{Eckert number, } E = \frac{U_\infty^2}{C_p \theta_w}$$

$$\text{Euler number, } E_u = \frac{P_\infty}{\rho_\infty U_\infty^2}$$

$$\text{Froude number, } F = \frac{U_\infty^2}{LG}$$

$$\text{Prandtl number, } Pr = \frac{C_p \mu_\infty}{\kappa_\infty}$$

Consider the flow where $E \leq 0(1)$, $F > 0(1)$, $Pr = 0(1)$, and $0.5 \leq M \leq 1$; the bounds on Mach number implying that $E_u = 0(1)$.

From the "y"-momentum equation

$$\frac{\partial P}{\partial y} = O\left(\frac{[Kn + (1-Kn)/(Re_L)^{1/2}]^2}{E_u}\right) < 0(1).$$

Since P is assumed to be constant in the free stream and $\frac{\partial P}{\partial y} \approx 0$, then $\frac{\partial P}{\partial x} \approx 0$.

For the conditions stated above the dimensional equations governing the flow become:

$$\frac{\partial}{\partial X}(\rho U) + \frac{\partial}{\partial Y}(\rho V) = 0 \quad 2.1-5$$

$$\rho \left[U \frac{\partial U}{\partial X} + V \frac{\partial U}{\partial Y} \right] = \frac{\partial}{\partial Y} \left[\mu \frac{\partial U}{\partial Y} \right] \quad 2.1-6$$

$$\rho \left[U \frac{\partial h}{\partial X} + V \frac{\partial h}{\partial Y} \right] = \mu \left(\frac{\partial U}{\partial Y} \right) + \frac{\partial}{\partial Y} \left(\kappa \frac{\partial T}{\partial Y} \right) \quad 2.1-7$$

where $C_p = \frac{dh}{dT}$

The boundary conditions at the wall are:

$$U(X,0) = U_w \quad (\text{slip})$$

$$T(X,0) = T_1 \quad (\text{temperature jump})$$

$$V(X,0) = 0$$

outside the boundary layer,

2.1-8

$$U = U_\infty$$

$$T = T_\infty$$

$$V = 0$$

and at $X = 0$

$$U = U_\infty$$

$$T = T_\infty$$

The solution to the problem has been attempted by Maslen [20] who perturbed around a similar solution in order to take into account slip and temperature jump boundary conditions. This approach can be improved upon by numerically solving the above system.

2.2 Numerical Analysis

Since a closed form solution to the system in Section 2.1 did not seem possible a numerical solution of the equations was attempted.

Introducing total enthalpy,

$$H = h + \frac{U^2}{2} ,$$

the energy equation becomes,

$$(U \frac{\partial H}{\partial X} + V \frac{\partial H}{\partial Y}) = \frac{\partial}{\partial Y} \left(\frac{\mu}{Pr} \frac{\partial H}{\partial Y} + \mu \left(1 - \frac{1}{Pr}\right) U \frac{\partial U}{\partial Y} \right) \quad 2.2-1$$

Following the numerical method presented by D. Clutter and A.M.O. Smith [21], the equations are transformed using a modified Howarth-Dorodnitsyn transformation to a more convenient coordinate system. The transformation has the advantage that for this problem the singularity at $x = 0$ is removed and the

boundary layer thickness in the transformed plane does not grow as rapidly along the plate as in the x, y coordinate system.

The Howarth-Dorodnitsyn transformation is

$$\eta_H = \int_0^y \rho \, dy$$

$$\xi = x$$

Clutter and Smith have introduced a modified transformation which reduces to a form studied in previous work on incompressible flow.

Thus,

$$\eta = \left(\frac{U_\infty}{\rho_\infty \mu_\infty x} \right)^{1/2} \int_0^y \rho \, dy$$

$$x = x$$

A stream function is defined such that

$$\rho u = \frac{\partial \psi}{\partial y} \quad \rho v = - \frac{\partial \psi}{\partial x}$$

If we define another stream function f such that,

$$\frac{\partial f}{\partial \eta} = f' = \frac{U}{U_{\infty}}$$

the relationship between ψ and f becomes

$$\psi = \sqrt{\rho_{\infty} \mu_{\infty} x U_{\infty}} f .$$

Introducing the non-dimensional variables, $g = \frac{H}{H_{\infty}}$ and $C = \frac{\rho \mu}{\rho_{\infty} \mu_{\infty}}$, the transformed equations become;

$$\frac{\partial}{\partial \eta} [C f''] + \frac{f f''}{2} - x [f' - f'' \frac{\partial f}{\partial x}] = 0 \quad 2.2-2$$

$$\frac{\partial}{\partial \eta} \left[\frac{C}{Pr} g' + \frac{U_{\infty}^2}{H_{\infty}} C \left(1 - \frac{1}{Pr}\right) f' f'' \right] = - \frac{f g'}{2} \quad 2.2-3$$

$$+ x [f' \frac{\partial g}{\partial x} - g' \frac{\partial f}{\partial x}]$$

All primes denote differentiation with respect to η .

Round off errors in the computer program can be reduced [21] by introducing the following variables:

$$\begin{aligned}
 \phi &= f-\eta & \theta &= g-1 \\
 \phi' &= f'-1 & \theta' &= g' \\
 \phi'' &= f'' & \theta'' &= g'' \\
 \phi''' &= f'''
 \end{aligned}
 \tag{2.2-4}$$

With these new variables, equations 2.2-2 and 2.2-3 become:

$$\frac{\partial}{\partial \eta} [C\phi''] = - \frac{(\phi+\eta)\phi''}{2}
 \tag{2.2-5}$$

$$+ x[(\phi'+1) \frac{\partial \phi'}{\partial x} - \phi'' \frac{\partial \phi}{\partial x}]$$

$$\frac{\partial}{\partial \eta} \left[\frac{C\theta'}{Pr} + \frac{U_{\infty}^2}{H_{\infty}} C(1-\frac{1}{Pr}) (\phi'+1)\phi'' \right] = - \frac{(\phi+\eta)}{2} \theta'
 \tag{2.2-6}$$

$$+ [(\phi'+1) \frac{\partial \theta}{\partial x} - \theta' \frac{\partial \phi}{\partial x}]$$

The boundary conditions are; at $\eta = 0$:

$$\phi_w = 0 \quad (\text{no blowing or suction})$$

$$\phi'_w = f'_w - 1 \quad (\text{for no slip } f'_w = 0)$$

$$\phi_w'' = \text{unknown to be solved for} \quad 2.2-7$$

$$\theta_w = g_w^{-1} \text{ (specified)}$$

$$\theta_w' = g_w'$$

as $\eta \rightarrow \infty$:

$$\phi' \rightarrow 0$$

2.2-8

$$\theta \rightarrow 0$$

Equations 2.2-5 and 2.2-6 are coupled and therefore must be solved simultaneously. The method employed here is to assume $C = 1$ for the first iteration which uncouples the momentum equation from the energy equation. The momentum equation can be solved and the results used to solve the energy equation. The ratio C can now be expressed as a function to enthalpy for all grid points using the values of enthalpy found from solving the energy equation. The momentum equation is solved again with C a variable and then the solution to the energy equation is obtained. This calculation is repeated until the results converge.

The equations are solved by replacing the partial derivatives with respect to x by finite difference quotients while retaining the derivatives in the η direction. This allows the partial derivatives to be approximated by ordinary differential equations. The equations are solved as an initial

value problem.

2.2.1 Solution of the Momentum Equation The first step in solving the momentum equation as an initial value problem is to determine

$$C\phi'' = \int_0^\eta \frac{\partial}{\partial \eta}(C\phi'') d\eta + C_w\phi_w'' \quad 2.2-9$$

The next step is to solve for,

$$\phi'' = \frac{(C\phi'')}{C} \quad 2.2-10$$

$$\phi' = \int_0^\eta \phi'' d\eta + \phi_w' \quad 2.2-11$$

$$\phi = \int_0^\eta \phi' d\eta + \phi_w \quad 2.2-12$$

An initial guess is made for the value of ϕ_w'' . Since the boundary conditions at the outer edge of the boundary layer are known it is possible to vary ϕ_w'' until the correct outer boundary conditions are met. The solution, however, can be obtained more rapidly by using an interpolation procedure. This involves obtaining three solutions that extend out to η_∞ within the bounds of $\phi'(\eta_\infty) \pm 1.0$; the three solu-

tions must not all be on the same side of the zero axis. For example, two solutions can have $\phi'(\eta_\infty)$ between zero and 1.0 and the third between zero and -1.0. Lagrangian three point interpolation is used to find the solution which meets the outer boundary conditions $\phi'(\eta_\infty) = 0$.

Denoting the three solutions as

$$\phi_1, \quad \phi_2, \quad \phi_3$$

$$\phi_1', \quad \phi_2', \quad \phi_3'$$

$$\phi_1'', \quad \phi_2'', \quad \phi_3''$$

the interpolated solution is given by

$$\phi(\eta) = A_1 \phi_1(\eta) + A_2 \phi_2(\eta) + A_3 \phi_3(\eta)$$

$$\phi'(\eta) = A_1 \phi_1'(\eta) + A_2 \phi_2'(\eta) + A_3 \phi_3'(\eta) \quad 2.2-13$$

$$\phi''(\eta) = A_1 \phi_1''(\eta) + A_2 \phi_2''(\eta) + A_3 \phi_3''(\eta)$$

where the coefficients are

$$A_1 = \frac{\phi_2'(\eta_\infty) \phi_3'(\eta_\infty)}{[\phi_1'(\eta_\infty) - \phi_2'(\eta_\infty)][\phi_1'(\eta_\infty) - \phi_3'(\eta_\infty)]}$$

$$\Delta_2 = \frac{\phi_1'(\eta_\infty) \phi_3'(\eta_\infty)}{[\phi_2'(\eta_\infty) - \phi_1'(\eta_\infty)] [\phi_2'(\eta_\infty) - \phi_3'(\eta_\infty)]} \quad 2.2-14$$

$$\Delta_3 = \frac{\phi_1'(\eta_\infty) \phi_2'(\eta_\infty)}{[\phi_3'(\eta_\infty) - \phi_1'(\eta_\infty)] [\phi_3'(\eta_\infty) - \phi_2'(\eta_\infty)]}$$

2.2.2 Solution of the Energy Equation In equation 2.2-6, θ and θ' are the only unknowns. Since the equation is treated as linear it is possible to take two solutions of equation 2.2-6 and combine them to meet the outer boundary condition.

For simplicity introduce Δ where

$$\Delta = \frac{C}{Pr} \theta' + \frac{U_\infty^2}{H_\infty} C(1 - \frac{1}{Pr}) (\phi' + 1) \phi'' \quad 2.2-15$$

Hence equation 2.2-6 becomes

$$\frac{\partial(\Delta)}{\partial \eta} = - \frac{(\phi + \eta)}{2} \theta' + x[(\phi' + 1) \frac{\partial \theta}{\partial x} - \theta' \frac{\partial \phi}{\partial x}] \quad 2.2-16$$

Integrating,

$$\Delta = \int_0^\eta \Delta' d\eta + \Delta_w \quad 2.2-17$$

From equation 2.2-15

$$\theta' = \frac{Pr}{C} \left[\Delta - \frac{U_{\infty}^2}{H_{\infty}} C \left(1 - \frac{1}{Pr} \right) (\phi' + 1) \phi'' \right] \quad 2.2-18$$

and,

$$\theta = \int_0^{\eta} \theta' d\eta + \theta_w \quad 2.2-19$$

To start the iteration assume some value of θ'_w . In the present solution a value of 0.2 was used and the solution is denoted as $\theta_1(\eta)$. If $\theta_1(\eta_{\infty})$ is greater than zero a smaller value of θ'_w is tried; if it is less a larger value is used. The second solution is denoted as $\theta_2(\eta)$.

The two solutions are linearly independent and can be added to give the general solution which is made to meet the boundary conditions.

The general solution is

$$\theta(\eta) = A\theta_1(\eta) + B\theta_2(\eta) \quad 2.2-20$$

The boundary conditions at the outer edge are

$$\theta(\eta_{\infty}) = A\theta_1(\eta_{\infty}) + B\theta_2(\eta_{\infty}) = 0$$

$$\theta'(\eta_{\infty}) = A\theta'_1(\eta_{\infty}) + B\theta'_2(\eta_{\infty}) = 0$$

At the wall the boundary conditions are

$$\theta_w = A\theta_{w1} + B\theta_{w2}$$

However,

$$\theta_w = \theta_{w1} = \theta_{w2}$$

Therefore,

$$A + B = 1$$

and

$$A = \frac{-\theta_2(\eta_\infty)}{\theta_1(\eta_\infty) - \theta_2(\eta_\infty)}$$

The correction solution is,

$$\theta(\eta) = A\theta_1(\eta) + (1-A)\theta_2(\eta)$$

2.2-21

$$\theta'(\eta) = A\theta_1'(\eta) + (1-A)\theta_2'(\eta)$$

2.3 Boundary Conditions

The velocity and temperature profiles are obtained from the solution of the boundary layer equations with appropriate boundary conditions. Two sets of boundary conditions have been used in this thesis; experimentally determined boundary

conditions, and the classical boundary conditions which are defined in Section 2.3.2 below.

Boundary conditions obtained from a solution of the linearized Boltzmann equation will be used to compare with the other slip results.

2.3.1 Experimental Results Velocity and temperature profiles can be calculated using experimental values of temperature and velocity at the wall as input data, together with free stream static pressure, temperature, and velocity.

2.3.2 Classical Boundary Conditions A semi macroscopic argument leads to the following relations for slip and temperature jump [22, 23],

$$U(x,0) = \frac{\mu}{P} (a_1 \sqrt{RT} \frac{\partial U}{\partial y} + \frac{3}{4} R \frac{\partial T}{\partial x})_0 \quad 2.3-1$$

and

$$T(x,0) - T_w = a_2 \frac{\mu}{P} \sqrt{RT} \frac{\partial T}{\partial y} \Big|_0 \quad 2.3-2$$

where

$$a_1 = \frac{2-\sigma}{\sigma} \sqrt{\frac{\pi}{2}},$$

and

$$a_2 = \frac{2-\alpha}{\alpha} \frac{15}{8} \sqrt{\frac{\pi}{2}}$$

The second term in 2.3-1 is small and will be neglected in this analysis.

Therefore,

$$U(x,0) = \frac{\mu}{p}(a_1 \sqrt{RT} \frac{\partial U}{\partial y}) \quad 2.3-3$$

Equation 2.3-2 is in the form first developed by Poisson and equation 2.3-3 is Maxwell's equation for slip. These boundary conditions will be referred to as classical boundary conditions in this thesis.

Slip velocities were calculated for values of the tangential accommodation, σ , equal to 0.6, 0.7, and 0.9 with the thermal accommodation coefficient, α , taken to be 1.0. The assumption that $\sigma = 0.9$ in equation 2.3-3 corresponds to Welander's value for the slip coefficient [24].

2.3.3 Linearized Boltzmann Solution When Rayleigh investigated the unsteady flow of an infinite flat plate in an incompressible fluid, he was able to draw some conclusions about the two-dimensional flow around the leading edge of an infinite plate by introducing the transformation $x = KUt$, where U is the plate velocity, K is a constant taken to be close to one [25], and x is the distance from the leading edge.

A solution of the linearized time variant Boltzmann

equation using the B.G.K. model for collisions has been obtained by C. Cercignani and F. Sernagiotto [26]. It is possible to transform this solution to a steady solution using the Rayleigh transformation and thereby obtain a slip boundary condition. It must be noted, however, that applying this transformation to compressible flow may give only qualitative results [27]. Nevertheless the results should be useful to compare with the classical boundary conditions which are also derived from a somewhat simplified model.

2.3.4 Incorporation of the Boundary Conditions in the Problem The technique used to solve the boundary layer equations varies slightly depending on the form of the boundary conditions. One set of velocity profiles has been obtained using experimental velocity and temperature boundary conditions. The temperature and velocity for stations along the plate are read into the program as starting data and the solution obtained as previously described. The only expression which must be iterated is the term $C = \frac{\rho\mu}{\rho_\infty\mu_\infty}$ which is taken to be equal to one for the first set of calculations. In subsequent calculations the previous calculation is used to obtain new values of C. It was found that after two iterations of C the velocity profiles remained unchanged for the first six decimal places.

To solve the boundary layer equations with the classical boundary conditions, profiles are first obtained for the case of zero slip, constant wall temperature, and $C = 1$. The

velocity and temperature profiles at the wall are used to calculate slip and temperature jump along the plate. New values for C are obtained as in the previous case. This process is repeated until the values of slip and temperature jump have converged to some final value. In practice, however, the number of iterations is limited by the amount of computer time available. It was found that five iterations could be obtained in 15 minutes on the IBM 360-65, and that this gave results which converged to the first three decimal places. This is consistent with the accuracy of the interpolation procedure (see error analysis in Chapter V).

2.4 Theory of the Equilibrium Temperature Probe

A thermocouple in the form of a thin wire mounted in a free molecular flow will assume an equilibrium temperature which can be related to the local gas temperature in terms of speed ratio, S . The speed ratio is obtained directly from impact and static probe measurements.

The relationship between equilibrium wire temperature, T_w , and local gas temperature, T , is obtained from the solution for heat transfer between a gas and a transverse cylinder in free molecular flow which has been derived in reference [28]. The results will be stated here and the details of the derivation shown in Appendix A.

The relationship between local temperature, wire temperature, and speed ratio is,

$$\frac{3T_c}{T} (z_1 + z_2) - [z_1(s^2 + 3) + z_2(s^2 + \frac{7}{2})]$$

2.4-1

$$+ \frac{2\pi^{3/2}}{PV_m\alpha} [\epsilon\sigma(T_c^4 - T_t^4) - Q] = 0$$

where

$$z_1 = \pi e^{-\frac{s^2}{2}} I_0\left(\frac{s^2}{2}\right)$$

and

$$z_2 = \pi s^2 e^{-\frac{s^2}{2}} [I_0\left(\frac{s^2}{2}\right) + I_1\left(\frac{s^2}{2}\right)]$$

Q = internal energy input to the cylinder per unit area

T_t = effective temperature of the surroundings

T_c = wire temperature

T = local temperature

S = speed ratio

I_0 and I_1 are modified Bessel Functions of the first and second kind. Equation 2.4-1 is simplified further since $Q = 0$.

A calculation in Appendix A shows that the radiation term is small compared to the other terms.

Neglecting radiation effects the equation becomes,

$$3\frac{T}{T_c}(z_1+z_2) - [z_1(s^2+3) + z_2(s^2+\frac{7}{2})] = 0$$

2.4-2

CHAPTER III

APPARATUS

3.1 The Low Density Wind Tunnel

The schematic layout and a photograph of the low density wind tunnel is shown in Figures 1 and 2. A picture of the test section containing the flat plate model is shown in Figures 3 and 4.

The tunnel shell is 24 inches in diameter by six feet long and is constructed from 1/8 inch stainless steel. The settling chamber is a 12 inch diameter by 17 inches long cylinder fitted with a removeable nozzle at the entrance section. Gas enters the settling chamber through a length of copper line with a 1/4 inch needle valve to control the gas flow.

The system is roughed with two Edwards ES3000 mechanical pumps each capable of handling up to 3000 cubic feet of gas per minute.

Two Edwards B18 vapour pumps which together pump 5000 liters per second maintain the tunnel at test conditions. The pumps are oil charged and have a water cooling system; a 12 inch butterfly valve directly above each diffusion pump controls the pumping speed.

In order to pump still larger amounts of gas a 22 inch diameter hollow cylinder has been placed downstream from the test section which, when filled with a suitably cold fluid,

removes large quantities of gas by cryogenic pumping. With a tank this size it is possible to attain pumping speeds of the order of several hundred thousand liters per second [29]. A convenient arrangement is to use CO_2 as the working gas and maintain a cold surface with liquid nitrogen. The liquid nitrogen level may be controlled by an automatic level control system filling from a large storage Dewar.

Instrumentation requiring movement in the axial direction of the tunnel, such as the impact probe, can be mounted from a moveable flat plate which is part of the electron gun housing mechanism. The plate is propelled from outside the tunnel by an electric motor operating through a mechanical feed through with a series of gear reductions (see Figure 1).

3.1.1 The Wind Tunnel Nozzle A schematic drawing of the wind tunnel nozzle is shown in Figure 6. It was formed out of two pieces of brass with the throat area milled from a solid block and joined to a length of brass pipe which forms the exit section of the nozzle.

The size of the nozzle is governed by the pumping capacity of the Booster Pumps. Data supplied by the manufacturer indicates a capacity of 2500 liters/sec. at a pressure of 100 microns for the two B-18 pumps. Making an allowance for entry losses the pumping speed was assumed to be 2000 liters/sec. giving a nozzle diameter of five inches for flow mach number of 0.50.

3.2 Instrumentation

3.2.1 The Impact Probe A view of the impact probe is shown in Figure 5. The probe was made of stainless steel in the shape of a wedge 2 3/4 inches long by 1 1/8 inches wide. The opening at the tip is 1.0 inches by 0.004 inches. This allows the flow to be sampled to within 0.002 inches of the model surface.

The wedge is connected by a four inch length of 1/8 inch inside diameter tubing to a temperature compensated NRC 801 thermocouple gauge (an analysis of the temperature dependence of thermocouple pressure gauges is given in Appendix B). A digital voltmeter was used to measure the output of the thermocouple gauge, giving a sensitivity of 30 microvolts per millitorr in the pressure range of 50 to 100 microns. Repeatability of this instrument was found to be excellent.

The thermocouple gauge was calibrated against a Granville Phillips capacitance manometer which has a sensitivity of 10^{-5} torr if the voltage response is measured by a digital voltmeter.

The probe was traversed through the boundary layer on a mechanism operated from outside the tunnel by means of a rotary feed through; the photograph in Figure 1 shows the traversing mechanism.

A dial indicator was used to determine the vertical position of the probe relative to the plate.

3.2.2 The Static Probe Static pressure was measured at a 1/8 inch diameter static tap located in the nozzle wall 1/2 inch from the exit (see Figure 3). An NRC 801 thermocouple gauge located outside the tunnel and connected to the static tap by a short length of stainless steel tubing was used to measure static pressure. The digital voltmeter was also used to measure the output of this gauge which was calibrated against the Granville Phillips Capacitance manometer at the same time as the impact pressure gauge. The calibration curves are included in Figure 7.

3.2.3 The Equilibrium Temperature Probe The equilibrium temperature probe is shown in Figure 3. It consists of a 0.003 inch iron-constantan thermocouple wire 14 inches long, supported by an aluminum arm. The ends of the arm are made of teflon so that the thermocouple wire is insulated from the metal. The thermocouple wire is held in tension by passing it through an insulated weak spring mounted on one of the arms (Figure 3). Iron-constantan extension wires were soldered to the ends of the fine wire and passed through the tunnel wall to a Leeds and Northrup millivolt potentiometer.

The thermocouple junction was obtained by spot welding a pair of crossed wires and then trimming the ends with a sharp razor blade under a microscope. The weld is about 0.004 inches in diameter which gives a spatial resolution compatible with that of the impact probe.

The Knudsen number for the equilibrium temperature probe

is about 5.3 at a pressure of 65 microns. A Knudsen number greater than five corresponds to the free molecular flow regime [30].

The temperature probe was mounted in the support provided for the impact probe and its position measured with the dial indicator (see Figure 4).

The plate wall temperature was measured by a thermocouple attached to the top of the plate, and stagnation temperature was measured by a thermocouple mounted in the stagnation chamber. Both of these thermocouples were made from 0.022 inch iron-constantan wire. All three thermocouple probes were read on the same potentiometer using a Honeywell thermocouple switch and an ice bath for a reference junction.

3.2.4 The Flat Plate Model A schematic diagram of the flat plate model is shown in Figure 8. Figure 3 and 4 show the model in the wind tunnel test section.

The plate was made of aluminum in the form of a sharp wedge. Two small compartments were milled out of the top of the wedge and two thin plates welded over the compartments in such a way that the compartments are flush with the top of the plate. Inlet and vent lines were provided for filling the plate with liquid nitrogen; a hole between compartments keeps the liquid level the same on both sides. Copper lines are used to carry the liquid nitrogen to the plate from outside the tunnel (Figure 4) and to take away the cold gas.

The bottom plate surface was polished smooth and the

leading edge brought to a sharp tip. The plate was placed in the tunnel test section with the bottom surface parallel to the axis of the nozzle and one inch above the nozzle centerline. Positioning of the plate was determined from previously conducted nozzle velocity profile surveys (Figures 9 and 10).

All tests were conducted on the bottom side of the plate as this insured liquid nitrogen contact with the test surface for the cold plate tests and hence less likelihood of temperature fluctuations.

CHAPTER IV

PROCEDURE

4.1 General Experimental Procedure

Experimental investigations were carried out at $P \approx 30$ microns and $P \approx 65$ microns. Two series of tests were made at 65 microns, one with an uncooled plate, and another series with the plate cooled to near 78°K (liquid nitrogen temperature).

Impact probe measurements were taken at five stations along the plate and up to 1.0 inch from the plate surface. The stations along the plate are: $x = 0.2, 0.4, 0.6, 0.8$, and 1.0 inches, measured from the leading edge. Probe measurements were obtained next at 11 wall positions starting at the leading edge, $x = 0$, and moving down the plate in 0.1 inch intervals. These results were used to obtain the slip profile.

The equilibrium temperature probe was mounted in the support used for the impact probe measurements, and T_c was obtained at the above mentioned stations.

Air taken into the tunnel was passed through a desiccant to remove water vapour which would have formed a frost on the cold plate. There was no visible build up of frost on the plate for the duration of any of the tests.

The cold plate temperature was maintained constant by filling with liquid nitrogen at frequent intervals (about 10

minutes). The temperature was monitored by a thermocouple mounted on the plate.

Since most of the tests required up to 16 hours to complete some fluctuations in conditions were encountered, especially in the cold plate test as the liquid nitrogen passing through the tunnel wall cooled the system over a period of hours. In order to reduce fluctuation errors most of the experiments were run at least twice and the results averaged.

4.2 Reduction of Experimental Data

If the flow in front of an impact probe is brought isentropically to rest the relation between P_t , P , and M is,

$$P_t = P \left(1 + \frac{\gamma-1}{2} M^2 \right)^{\frac{\gamma}{\gamma-1}} \quad 4.2-1$$

The speed ratio, S , defined in terms of mach number is,

$$S = \sqrt{\frac{\gamma}{2}} M \quad 4.2-2$$

Substituting 4.1-2 into 4.1-1 and re-arranging

$$S = \sqrt{\frac{\gamma}{\gamma-1} \left[\left(\frac{P_t}{P} \right)^{\frac{\gamma-1}{\gamma}} - 1 \right]} \quad 4.2-3$$

Speed ratio was determined from the measured values of P and P_t . Local temperature was obtained from equation 2.5-2 using the speed ratio calculated from the pressure measurements together with the wire temperature. Velocity can then be found from the definition of speed ratio,

$$U = \sqrt{2RT} S \quad 4.2-4$$

The calibration curve in Figure 7 was used to reduce P_t and P to microns pressure. T_c was reduced to $^{\circ}K$ using the tables in reference [31].

A simple computer program was set up to reduce all the experimental data.

4.2.1 Impact Probe Calibration P_t was obtained using a probe with a rectangular orifice, 0.004 inches high and 1.0 inches wide. It was felt that in order to obtain meaningful results good spatial resolution would be required, especially close to the wall where gradients are large. Calculations show, however, that the response time for a circular open ended probe of say 0.004 inches diameter is far too long to make measurements practical. Since theoretical calculations of response time in the transition regime may be inexact, small impact probes varying in diameter from 0.004 inches to almost .01 inches were made and tested in the wind tunnel at $P \approx 70$ microns. The response time of the smallest tube was of the order of 1/2 hour which was considered im-

practical for the large number of points to be measured.

In order to facilitate the reduction of the data it is useful to keep the probe in either free molecular flow or in continuum flow. At $P = 65$ microns, $\lambda \sim 0.03$ inches, which, if the crude criteria that the characteristic dimension must be $1/10$ of the gas mean free path for the free molecular probe is used, would require a circular probe of 0.003 inches diameter. A probe of this dimension would be impractical because of long response time. Another reason for rejecting a free molecular probe is that the theory used to reduce the data may not describe the flow adequately (see reference [32]). For these reasons it was decided to use a continuum probe for the measurements.

In order to insure fast response it was decided to use a probe one inch wide. The problem then is to determine for what pressure range the probe is in the continuum regime since it is not known what dimension should be taken as characteristic of the geometry. A. Sreekanth [33] has shown, however, that perhaps all dimensions of the probe should be considered in determining whether the probe is in the continuum flow regime or in transition flow. For this reason a test was conducted to find the continuum limit of the wedge. The impact pressure for static pressures ranging from 90 microns to 17 microns were measured and compared to results obtained with a circular probe with a 0.187 inch diameter orifice. The results are shown in Figure 11 with impact

pressures agreeing very well down to a static pressure of 50 microns. Below this pressure the wedge pressures are lower than the circular probe pressures. This would indicate that both probes are in the continuum down to 50 microns where it appears that the circular probe enters the transition regime. At some lower value of pressure the wedge probe will be in transition flow.

CHAPTER V

RESULTS AND DISCUSSION OF EXPERIMENTAL AND THEORETICAL INVESTIGATION

5.1 Slip and Temperature Jump Boundary Conditions

5.1.1 Results

5.1.1.1 Measurement of Slip Velocity on a Cold Plate Slip velocity as a function of distance from the leading edge was experimentally measured. These results are shown in Table 1 and plotted in Figure 12.

Five Theoretical determinations of slip velocity are shown in Figure 12 for comparison. The curves marked classical boundary conditions represent the end result of the iterative solution of the boundary layer equations using the classical slip condition and, where indicated, the temperature jump boundary condition given in Section 2.4.2. The boundary layer equations have been solved for a constant Prandtl number of 0.76. Summarizing the theoretical results, they include:

- (a) A solution of the classical slip condition with temperature jump, and with $\sigma = 0.9$, $\alpha = 1.0$.*
- (b) The Rayleigh solution discussed in Section 2.4.2

* Unless otherwise indicated the thermal accommodation coefficient will be taken to be 1.0.

- (c) A solution of the classical slip condition for no temperature jump, with $\sigma = 0.9$, and $\frac{U(0,0)}{U_\infty} = 0.5$.
- (d) A solution of the classical slip condition with no temperature jump; $\sigma = 0.9$ and $\frac{U(0,0)}{U_\infty} = 1.0$.
- (e) A solution with classical slip and temperature jump; $\sigma = 0.6$ and $\frac{U(0,0)}{U_\infty} = 1.0$.

5.1.1.2 Measurement of Slip and Temperature Jump on an Uncooled Plate at $P = 30.4$ Microns Figure 13 shows the experimental and theoretical results for slip over an uncooled plate at $P = 30.4$ microns, and Figure 14 shows the experimental and theoretical results for temperature jump. The experimental data for slip and temperature jump is summarized in Table 2.

The theoretical slip profiles obtained from a solution of the boundary layer equations for a constant Prandtl number of 0.71 include:

- (a) A solution of the classical slip condition with temperature jump; $\sigma = 0.9$ and $\frac{U(0,0)}{U_\infty} = 1.0$.
- (b) A solution of the classical slip condition with no temperature jump; $\sigma = 0.9$ and $\frac{U(0,0)}{U_\infty} = 1.0$.
- (c) A solution of the classical slip condition with temperature jump; $\sigma = 0.7$ and $\frac{U(0,0)}{U_\infty} = 1.0$.
- (d) The Rayleigh solution.

The theoretical temperature jump curve in Figure 14 is the curve obtained in conjunction with the solution in (a).

5.1.1.3 Measurement of Slip and Temperature Jump on an Uncooled Plate at P = 65.0 Microns A test similar to the one in Section 5.1.1.2 was conducted at P = 65.0 microns. Slip profiles are shown in Figure 15 and temperature jump curves in Figure 16. The experimental data is tabulated in Table 3.

The theoretical slip profiles include:

- (a) A classical slip profile with temperature jump effects;
 $\frac{U(0,0)}{U_\infty} = 1.0$ and $\sigma = 0.6$.
- (b) A classical slip profile with no temperature jump effect;
 $\frac{U(0,0)}{U_\infty} = 0.5$ and $\sigma = 0.9$.
- (c) Classical slip with no temperature jump effect; $\frac{U(0,0)}{U_\infty} = 1.0$ and $\sigma = 0.9$.
- (d) Classical slip with temperature jump effects; $\frac{U(0,0)}{U_\infty} = 1.0$ and $\sigma = 0.9$.
- (e) The Rayleigh solution.

The theoretical temperature jump profile in Figure 16 is obtained in conjunction with the solution in (d).

5.1.2 Discussion

5.1.2.1 Experimental Results Examination of the slip profiles show an apparent leveling off of the curves at approximately 0.3 inches in the cold plate test, and at 0.6 to 0.7 inches in the uncooled plate tests. Values of slip velocity after 1.0 inch are $\frac{U}{U_\infty} = 0.279$ and $\frac{U}{U_\infty} = 0.336$ for the uncooled plate at 30.4 microns and 65.0 microns respec-

tively, and $\frac{U}{U_\infty} = 0.356$ for the cooled plate at 65.0 microns.

These values are somewhat higher than the theory predicts. Some higher order terms which are important near the leading edge have been neglected in the theory and inclusion of these would tend to increase the theoretical values somewhat.

Small changes in static pressure would have a large influence on the experimental slip values, particularly when the slip velocities are small as can be seen from equation 4.2-3. For example, an increase of static pressure of 0.5 microns in the run at 30.5 microns, and 1.6 microns in the run at 65.0 microns, is enough to make the experiments coincide with theory. Experimental curves have been calculated with these changes in static pressure and are shown in Figures 13 and 15.

Static pressure was assumed to be constant over the plate and equal to the static pressure measured 1/2 inch from the nozzle exit. An increase in static pressure could occur due to such effects as spreading of the free jet and influence of the model and impact probe in the stream. Any one of these could account for the small pressure change needed to account for the difference between experiment and theory. It is interesting to note that in the uncooled tests, the measured value of $\frac{U}{U_\infty}$ is 0.903 at $x = 0$ when $P = 30.4$ microns, and $\frac{U}{U_\infty} = 0.893$ at $P = 65.0$ microns. These values are somewhat higher than some theories predict. For example references [26], [34] and [35] obtain $\frac{U}{U_\infty} = 0.5$ at the leading edge when

$$\sigma = 1.0$$

The experimental temperature jump profiles level off after approximately 0.2 inches from the leading edge and differ with theory by less than 1% at $x = 1.0$ inch. The data clearly indicates that non adiabatic wall conditions exist in the test region; for example, $T_w = 301.4^\circ\text{K}$ and $T_1 = 291.8^\circ\text{K}$ for the $P = 30.4$ micron case, and $T_w = 300.5^\circ\text{K}$ and $T_1 = 296.5^\circ\text{K}$ at $P = 65.0$ microns.

5.1.2.2 Theoretical Results Comparison of the theoretical profiles with experiment shows that theory predicts lower values of slip and that the best correlation occurs for the solutions having lower values of accommodation.

E. Merlic [12] measured the tangential accommodation of air on an aluminum cylinder and found that $\sigma = 0.9$ on a surface left in a chamber at 0.01 microns for one to three days before carrying out tests. He found, however, that if the chamber was maintained at 250 microns for six days before tests, a value of $\sigma = 0.6$ was obtained. This was thought to be due to the adsorption of an oil film on the aluminum surface, caused by back migration from the diffusion pump. The oil film is more "specular" than the metal surface and hence lowers the value of the accommodation coefficient. This condition of the surface is similar to that of the aluminum plate in the low density wind tunnel; the plate was cleaned after mounting but the tunnel was pumped for a few days before actual tests began. Furthermore, the physical size of the

test section makes it necessary to mount the model near the opening to one of the diffusion pumps, increasing the possibility of oil contamination. Baffles placed on the opening to the diffusion pumps reduce the problem but do not completely eliminate it.

Oil contamination of the surface was increased in the cold plate tests where the plate acts as a very effective cold trap. After the cold plate tests a slight oil film could be detected by running a finger over the plate surface.

Theoretical solutions of classical slip with no temperature jump have been obtained with starting values of $\frac{U}{U_{\infty}} = 1.0$ and 0.5 at the leading edge to observe the change in the slip profiles caused by varying the starting values. A very important observation is that at $P = 65.0$ microns the uncooled plate slip velocities are almost the same after 0.15 inches from the leading edge for both starting conditions. The same effect is observed in the cold plate profiles with both curves merging at approximately $X = 0.25$ inches.

Another interesting point is that inclusion of the temperature jump boundary condition does not have a very significant affect on the slip profiles. As expected, however, the addition of this boundary condition becomes more important at lower pressures. This can be seen by comparing Figure 14 and Figure 16.

The Rayleigh solution included in the theory compares well with classical theory for an uncooled plate if the

accommodation coefficient, σ , is assumed to be 0.9. Since the Rayleigh solution starts with $\frac{U}{U_\infty} = 0.5$ at the leading edge it will compare best with the classical solution having $\frac{U}{U_\infty} = 0.5$ at $x = 0$ (see Figure 15). The Rayleigh solution does not compare as well with the classical theory for flow over a very cold plate (see Figure 12).

5.2 Velocity and Temperature Profiles

5.2.1 Results

5.2.1.1 Velocity and Temperature Profiles on a Cold Plate Velocity and temperature profiles for flow over a cold flat plate are summarized in Tables 4-8 with velocity versus distance from the plate surface at five different plate positions plotted in Figures 17 to 21. Temperature profiles are shown in Figures 22 to 26. Two sets of theoretical curves, one using as starting values the previously mentioned experimental slip and temperature jump profiles with corrections for small changes in P , U_∞ , and T_∞ , and one using the classical boundary conditions ($\sigma = 0.90$) are included for comparison with the experimental curves. The plate wall temperature is considered constant at 82.7°K and the value of the free stream Mach number is 0.63.

5.2.1.2 Velocity and Temperature Profiles on an Uncooled Plate Results for experiments at $P = 29.0$ microns and $P = 64.0$ microns are tabulated in Tables 9-13 and 14-18

respectively. Velocity profiles are shown in Figures 27 to 30 and Figures 35 to 39, and temperature profiles in Figures 31 to 34, and Figures 40 to 44. Two theoretical determinations using the boundary conditions mentioned in 5.2.1.1 have been included.

5.2.2 Discussion A general observation of velocity and temperature profiles indicates a large discrepancy between theory and experiment at $x = 0.2$ inches with considerable improvement in the correlation after 1.0 inches in the uncooled plate tests. At 1.0 inches $Re_x \approx 11$ for $P = 30.4$ microns and $Re_x \approx 24$ for $P = 65.0$ microns. Good agreement would not be expected in the region near the leading edge considering that the order of magnitude analysis on the governing theoretical equations in Chapter II assumed $Re_L \gg 0(1)$.

5.3 Error Analysis

5.3.1 Experimental Accuracy

5.3.1.1 Resolution of the Static and Impact Probes

The instrument used to measure impact and static pressures has a resolution of 0.3 microns which results in an error of $\pm 0.3\%$ to $\pm 1\%$ in the pressure data. This error has been reduced by taking more than one pressure reading and averaging the results. Since the error caused by the resolution of the instrument will be larger at lower pressures, the error

in equation 4.2-3 has been calculated for $P \approx 30$ microns and $P_t \approx P$. The static pressures have been arrived at by averaging up to 10 pressure readings and if they can be considered correct, the maximum error in equation 4.2-3 is 6.5%. The magnitude of the error, however, will be much less than this for most of the tests.

5.3.1.2 Accuracy of Temperature Measurements

The accuracy of the equilibrium wire temperature measurements vary from 0.33°C to 0.20°C depending on the magnitude of the temperature. For example, at temperature of the order -109°C the tables in reference [31] can be read to 0.33°C . This is considered to be acceptable when taking into account other approximations.

Values of local temperature are obtained from expression 2.5-2. A calculation shows that the effect of radiation is negligible and therefore it has not been considered in the calculations (see Appendix A).

The maximum error in speed ratio was calculated in the previous section to be 6.5%. Using typical values of $T_c = 301^\circ\text{K}$ and $S = 0.10$ the error in T calculated from equation 2.5-2 is 0.07%.

5.3.1.3 Error in Reading the Dial Indicator Read-

ings were taken at various positions in the boundary layer with a dial indicator capable of being read to 0.001 inches. However, errors could result from a certain amount of back lash in the spring of the traversing mechanism (see Chapter III).

5.3.1.4 Other Possible Sources of Error Other possible sources of error not previously mentioned are the spreading of the nozzle jet and the influence of the model on the flow. It is necessary to treat these effects simultaneously.

S. Gordon [32] investigated the flow of gas over a two inch flat plate lying one inch in front of the nozzle exit. He observed that the plate influenced the flow up to approximately 10 mean free paths in front of the leading edge. To complicate matters he also noted that the centerline speed ratio had dropped by 12% three inches from the nozzle exit which he attributed to the spreading of the nozzle jet. From Gordon's observations it would seem necessary to place the model far enough from the nozzle exit so as not to disturb the flow in the nozzle, and at the same time, close enough to minimize the spreading of the nozzle jet on the area of the plate tested. For the present tests the model was placed 0.22 inches from the nozzle exit which corresponds to about eight mean free paths at 65.0 microns. There was no measureable drop in centerline velocity for the region studied. Undoubtedly the presence of the model influenced the flow in front of the leading edge but its affect has not been estimated.

5.3.2 Accuracy of the Numerical Analysis The errors involved in using the integration and finite difference formulas are summarized in Appendix C. The accuracy of the numerical technique for the compressible boundary layer without slip has been analyzed in reference [22].

The solution at a station is obtained by getting three solutions that extend all the way to η_∞ within the bounds of $\phi'(\eta_\infty) \pm K'$ where K' has been taken as 1.0 in the analysis. This bound was checked by running a program with $K' = 0.95$ which showed a negligible change in the results. The step size in the x direction was taken to be 0.02 for the first 0.1 inches and then increased to 0.04 for the remaining stations. The error in the results are not necessarily decreased by taking smaller step sizes in the x direction as the important parameter is $\frac{x}{\Delta x}$. Oscillations in the curves can be prevented by keeping $\frac{x}{\Delta x} \leq 25$ [21]. This criterion was proven to be correct as it was found that oscillations began to appear for $\frac{x}{\Delta x} \approx 28$.

The change in η was chosen to be 0.1 and $\eta_\infty = 5.2$. These values are governed largely by computer storage space; however, it was found that an increase to $\eta_\infty = 5.7$ only affected the fourth or fifth decimal place in the velocity results. Since the analysis is accurate to the third or fourth decimal place this difference is not significant.

The Prandtl number was taken to be 0.71 for the uncooled tests and 0.76 for the cooled test. The effect of Prandtl number on the results was checked by changing the value from 0.76 to 0.73 in the cold plate theory. This caused the boundary layer thickness to vary by 0.0006 inches at $x = 0.02$ inches and 0.0045 inches at $x = 1.0$ inches.

CHAPTER VI

SUMMARY AND CONCLUSIONS

A theoretical and experimental study has been conducted in the transition flow regime. The conclusions from the investigation are listed as follows:

(a) The numerical analysis of the compressible boundary layer on an uncooled plate with experimentally determined boundary conditions indicates that the boundary layer equations are valid for $x \geq 1.0$ inches and $Kn \sim 0.11$. At $x = 1.0$ inches and $P \approx 30$ microns the value of the local Reynolds number is approximately 11.

(b) Theory predicts lower values of slip than were experimentally determined.

(c) Experimental results give a value of $\frac{U}{U_\infty} \approx 0.9$ at the leading edge, contrary to some theories which obtain $\frac{U}{U_\infty} = 0.5$ for diffuse reflection. The starting value for $\frac{U}{U_\infty}$ at the leading edge does not significantly affect the slip profiles after approximately three mean free paths from the leading edge.

(d) The classical slip condition as determined from an iterative solution of the boundary layer equations has been compared to Cercignani and Sernagiotto's time variant solution of the Boltzmann equation, transformed to a two-dimensional steady problem. The theories agree very well for a tangential accommodation of 0.9 in the classical theory.

(e) For $Kn \sim 0.6$ the inclusion of the temperature jump boundary condition does not change the slip velocity profile appreciably; for $Kn \sim 0.11$ the change is more significant but still small.

(f) The use of a rectangular shaped impact probe gives better resolution and can measure total pressures closer to the wall than a circular orifice having a similar response time.

(g) A low density wind tunnel has been designed and instrumentated which enables the study of transition flows. The tunnel operates under stable conditions with very little evidence of oil back migration.

BIBLIOGRAPHY

1. A. Cemal Eringen, "Mechanics of Continua", John Wiley and Sons, Inc., New York, London, Sydney, 1967.
2. M. Reiner, "Rheology", Handbuck der Physik (Edited by S. Flügge), Springer-Verlag, Berlin, 1958, Vol. 6, p. 447.
3. J.A. Owczarek, "Fundamentals of Gas Dynamics", International Textbook Company, Scranton, Pennsylvania, 1964, p. 542.
4. A.M. Kuethe and J.D. Schetzer, "Foundations of Aerodynamics", John Wiley and Sons, Inc., New York, London, Sydney, second edition, 1965, p. 379.
5. S. Dushman, "Foundations of Vacuum Technique", John Wiley and Sons, Inc., New York, London, Sydney, second edition, 1962, p. 81.
6. K.S. Van Dyke, "The Coefficients of Viscosity and of Slip of Air and of Carbon Dioxide by the Rotating Cylinder Method", Phys. Rev. 21, 250 (1923).
7. E. Kennard, "Kinetic Theory of Gases", McGraw-Hill Book Company, Inc., New York and London, 1938, p. 292.
8. J. Maxwell, "On Stresses in Rarefied Gases", Phil. Trans, Roy, Soc. Part 1, 1879; The Scientific Papers of James Clerk Maxwell, Vol. 2, Dover Publications, Inc., New York.
9. R.A. Millikan, "Coefficients of Slip in Gases and the Law of Reflection of Molecules from the Surfaces of Solids and Liquids", Phys. Rev. 21, 217 (1923).
10. E. Kennard, "Kinetic Theory of Gases", McGraw-Hill Book Company, Inc., New York and London, 1938, pp. 295-296.
11. F.C. Hurlbut, "On the Molecular Interactions between Gases and Solids", University of California Technical Report HE-150-208, 1962.
12. E. Merlic, "An Experimental Determination of Reflection Coefficients for Air on Aluminum", University of California Engineering Project Report HE-150-141, 1956.

13. S. Schaaf and P. Chambré, "Flow of Rarefied Gases", Princeton University Press, 1958, pp. 34-35.
14. E. Kennard, "Kinetic Theory of Gases", McGraw-Hill Book Company, Inc., New York and London, 1938, p. 311.
15. E. Kennard, "Kinetic Theory of Gases", McGraw-Hill Book Company, Inc., New York and London, 1938, p. 312.
16. R. Street, "A Study of Boundary Conditions in Slip-Flow Aerodynamics", Rarefied Gas Dynamics, 1960, pp. 276-292.
17. G.N. Patterson, "Molecular Flow of Gases", John Wiley and Sons, Inc., New York, 1956, Chapter 5.
18. H. Schlichting, "Boundary Layer Theory", McGraw-Hill Book Company, Inc., New York, Toronto, London, 4th edition (1960), p. 51.
19. J.A. Owczarek, "Fundamentals of Gas Dynamics", International Textbook Company, Scranton, Pennsylvania, 1964, pp. 537-542.
20. S. Maslen, "Second Approximation to Laminar Compressible Boundary Layer on Flat Plate in Slip Flow", NACA TN 2818, 1952.
21. D. Clutter and A. Smith, "Solution of the General Boundary Layer Equations for Compressible Laminar Flow, Including, Transverse Curvature", Douglas Aircraft Co., Inc., Report No. LB 31088, 1963.
22. R. Street, "A Study of Boundary Conditions in Slip-Flow Aerodynamics", Rarefied Gas Dynamics, 1960, p. 279.
23. S. Schaaf and P. Chambré, "Flow of Rarefied Gases", Princeton University Press, 1958, p. 35.
24. R. Street, "A Study of Boundary Conditions in Slip-Flow Aerodynamics", Rarefied Gas Dynamics, 1960, p. 282.
25. L. Rosenhead, "Laminar Boundary Layers", Oxford University Press, 1963, p. 137.
26. C. Cercignani and F. Sernagiotto, "Rayleigh's Problem at Low Mach Numbers According to Kinetic Theory", Rarefied Gas Dynamics, Vol. 1, 1965, pp. 332-353.
27. A. Huang and D. Hartley, "Nonlinear, Rarefied Rayleigh's Problem", AIAA Journal, Vol. 6, No. 10, p. 2023.

28. J. Stalder, G. Goodwin, and M. Creager, "A Comparison of Theory and Experiment for High-Speed Free-Molecule Flow", NACA TN 2244, 1950.
29. W. MacDermott, "Preliminary Experimental Results of the Reduction of Viscous Effects in a Low-Density Supersonic Nozzle by Wall Cryopumping", AEDC-TN-6J-71, 1961.
30. S. Schaaf and P. Chambré, "Flow of Rarefied Gases", Princeton University Press, 1958, p. 44.
31. Conversion Tables for Thermocouples, Leeds and Northrup Company, Issue 4.
32. S. Gordon, "Flow of Low Density Air over a Heated Flat Plate at Mach No. 0.5", UTIAS Report No. 92, 1964.
33. A.K. Sreekanth, "Drag Measurements on Circular Cylinders and Spheres in the Transition Regime at a Mach Number of 2", UTIA Report No. 74, 1961.
34. H. Yang and L. Lees, "Rayleighs Problem at Low Mach Number According to the Kinetic Theory of Gases", Journal of Math and Physics 35, No. 3, 1956.
35. A. Huang and D. Hartley, "Kinetic Theory of the Sharp Leading Edge Problem in Supersonic Flow", Physics of Fluids, Vol. 12, No. 1, 1969, p. 96.
36. M. Abramowitz and L. Stegun, "Handbook of Mathematical Functions", National Bureau of Standards, Applied Mathematics Series, 55, 1966.
37. C. Van Atta, "Vacuum Science and Engineering", McGraw-Hill Book Company, New York, Toronto, London, 1965, p. 81.
38. H. Allsopp, F.J. Bradshaw, R. Stanford, and N. Wadsworth, "A Sensitive Constant Resistance Pirani Gauge with a Fast Response Time", Vacuum, Vol. 19, No. 2, 1968, p. 61.

APPENDIX A

THEORY OF THE EQUILIBRIUM TEMPERATURE PROBE

The basic assumption in the derivation of the solution for heat transfer between a gas and a transverse cylinder in free molecular flow is that the impinging molecules have a classical Maxwellian velocity distribution superimposed on a uniform mass velocity.

For a monatomic gas the translational molecular energy incident on an element of area dA inclined at an angle θ with respect to the stream mass velocity U is,

$$dE_t = n\left(\frac{mU^2}{2} + \psi kT\right)dA \quad A-1$$

where k = Boltzmann constant, and,

$$\psi = 1 + \frac{1 + \frac{3\sqrt{\pi}}{2} s \sin \theta [1 + \operatorname{erf}(s \sin \theta)] e^{s^2 \sin^2 \theta}}{1 + \sqrt{\pi} s \sin \theta [1 + \operatorname{erf}(s \sin \theta)] e^{s^2 \sin^2 \theta}} \quad A-2$$

n is the number of molecules striking a unit surface area per unit time and can be expressed by

$$n = \frac{NV_m \chi}{2\sqrt{\pi}} \quad A-3$$

The energy incident from the opposite side is given by

$$dE_t' = n' \left(\frac{mU^2}{2} + \psi' kT \right) dA \quad A-4$$

with

$$n' = \frac{NV_m \chi'}{2\sqrt{\pi}} \quad A-5$$

and

$$\psi' = 1 + \frac{1 - \frac{3\sqrt{\pi}}{2} s \sin \theta [1 - \operatorname{erf}(s \sin \theta)] e^{s^2 \sin^2 \theta}}{1 - \sqrt{\pi} s \sin \theta [1 - \operatorname{erf}(s \sin \theta)] e^{s^2 \sin^2 \theta}} \quad A-6$$

For a diatomic gas the rotational component of the molecular internal energy must be added to the translational component. Considering a diatomic molecule whose structure is assumed to be that of a dumbbell

$$E_R = kT \quad A-7$$

The total molecular energy becomes

$$dE_1 = n \left[\frac{mU^2}{2} + (\psi+1)kT \right] dA \quad A-8$$

$$dE_1' = n' \left[\frac{mU^2}{2} + (\psi'+1)kT \right] dA \quad A-9$$

Now,

$$\alpha = \frac{E_i - E_r}{E_i - E_w} \quad \text{A-10}$$

where α is defined as the thermal accommodation coefficient and E_w is the rate of re-emitted molecular energy carried by the scattered stream if it is in equilibrium with the surface temperature T_w .

The rate of re-emitted energy for a diatomic gas is given by,

$$dE_w = 3nkT_w dA \quad \text{A-11}$$

Combining A-10 and A-11 the energy transported from the front of the element by re-emitted molecules becomes

$$dE_r = (dE_t + nkTdA) (1-\alpha) + 3\alpha nkT_c dA \quad \text{A-12}$$

where T_c is the surface temperature of the cylinder.

Similarly the energy transported from the rear side of dA is given by

$$dE_r' = (dE_t' + n'kTdA) (1-\alpha) + 3\alpha n'kT_c dA \quad \text{A-13}$$

For a cylinder of length L and radius r the elemental area is

$$dA = rLd\theta$$

The energy balance is

$$2\alpha rL \left\{ \int_0^{\frac{\pi}{2}} n \left[\frac{mU^2}{2} + (\psi+1)kT \right] d\theta + \int_0^{\frac{\pi}{2}} n' \left[\frac{mU^2}{2} + (\psi'+1)kT \right] d\theta \right\} \\ - 6\alpha rLkT_c \left(\int_0^{\frac{\pi}{2}} n d\theta + \int_0^{\frac{\pi}{2}} n' d\theta \right) \quad A-14$$

$$+ 2\pi rL [Q - \epsilon\sigma(T_c^4 - T_t^4)] = 0$$

where Q is the internal energy input to the cylinder per unit area and it has been assumed gray body radiation occurs between the cylinder and the surroundings. T_t is the effective temperature of the surroundings.

The integrals in equation A-14 have been solved in [28]. The solution then becomes

$$3\frac{T_c}{T}(Z_1+Z_2) - [Z_1(s^2+3) + Z_2(s^2+\frac{7}{2})]$$

A-15

$$+ \frac{2\pi^{3/2}}{PV_m\alpha} [\epsilon\sigma(T_c^4 - T_t^4) - Q] = 0$$

where

$$z_1 = \pi e^{-\frac{s^2}{2}} I_0\left(\frac{s^2}{2}\right)$$

and

$$z_2 = \pi s^2 e^{-\frac{s^2}{2}} \left[I_0\left(\frac{s^2}{2}\right) + I_1\left(\frac{s^2}{2}\right) \right]$$

I_0 and I_1 denote modified Bessel functions of the first kind and zero and first order respectively.

[36] gives a series expansion of the modified Bessel function for small arguments. Both series may be truncated after the second term as the error in I_0 and I_1 introduced by neglecting higher order terms is 0.36% and 0.03% respectively for a speed ratio of 1.0. Since the maximum speed ratio is about 0.7 this error is reduced considerably further.

A.1 Radiation Effects

To analyze the magnitude of the radiation term in A-15 a simple calculation is carried out.

Assuming:

$$S = 0.70$$

$$T_c = 30^\circ$$

$$T_t = -190^\circ$$

$$P = 0.0056 \text{ lb/in}^2 \quad (\sim 30 \text{ microns})$$

$$\epsilon = 0.3$$

$$\alpha = 1$$

$$V_m = 238 \text{ ft/sec}$$

substituting these values into A-15 gives

$$3 \frac{T_c}{T} (3.76) - 10.06 + 0.5 = 0$$

For $T_c = 30^\circ\text{C}$,

$$T = 34.1^\circ\text{C}.$$

Neglecting radiation effects gives

$$T = 34.0^\circ\text{C}$$

This gives an error of .29% which is less than the other errors involved in measuring temperature.

Therefore neglecting radiation effects the final equation becomes

$$3 \frac{T_c}{T} (Z_1 + Z_2) - [Z_1 (s^2 + 3) + Z_2 (s^2 + \frac{7}{2})] = 0 \quad \text{A-16}$$

APPENDIX B

PRESSURE RESPONSE TO THERMOCOUPLE WALL TEMPERATURE VARIATION

The thermocouple gauge works on the principle that the heat loss to a hot wire in free molecular flow is proportional to the pressure in the thermocouple head.

Since the important modes of heat transfer are conduction by gas molecules and radiation, the energy balance will consist of the addition of these effects. However, radiation effects only become important at low pressures [37]; for example, at $P = 0.01$ torr with a filament temperature of 100°C and wall temperature at 20°C , the heat transfer due to conduction is 8.87×10^{-3} watts/cm² and, that due to radiation is 6.80×10^{-4} watts/cm². As the tests conducted at $P \approx 30$ microns will have a still larger relative heat transfer by conduction, radiation will be neglected in this simple analysis.

Therefore,

$$E_t = PK_0 \alpha \left(\frac{273}{T_{\text{gas}}} \right)^{1/2} (T_c - T_{\text{gas}})$$

where K_0 is the free molecular conductivity of air and

$$T_{\text{gas}} = T_w$$

To obtain the expression for response due to temperature change, assume two different sets of values of T_w and P which give the same value for E_t .

Equating and re-arranging,

$$\frac{P_1}{P_2} = \left(\frac{T_{w1}}{T_{w2}}\right)^{1/2} \frac{(T_c - T_{w2})}{T_c - T_{w1}}$$

Substituting $T_c = 150^\circ\text{C}$, $T_{w2} = 20^\circ\text{C}$, $P_2 = 30$ microns, $T_{w1} = 10^\circ\text{C}$, the value for P_1 is 27.4 microns. This represents an error of 8.66% which is significant. When dealing with the cooled plate, a temperature change of this magnitude could easily occur. Because of the difficulty in maintaining constant thermocouple wall temperature it was deemed necessary to have a temperature compensated thermocouple gauge for the experiments. The National Research Corporation have a thermocouple gauge which is temperature compensated, and it was decided to use the NRC 801 thermocouple gauge.

The outline of a design of a sensitive pirani gauge is given in reference [39]. This gauge has a sensitivity of 40 millivolts per millitorr and should give better resolution than the thermocouple gauge used. However, it is not readily available and may require special corrections for temperature variations.

APPENDIX C

ERROR IN NUMERICAL EXPRESSIONS

The errors involved in the various expressions in the numerical analysis are listed here.

C.1 Finite Difference Representations

Two Points:

$$\frac{\partial \phi_M}{\partial x} = \frac{\phi_M - \phi_{M-1}}{X_M - X_{M-1}}$$

The error is,

$$\frac{(X_M - X_{M-1})}{2} \frac{\partial^2 \phi(\xi)}{\partial x^2}$$

where ξ is some value of x in the interval $X_M - X_{M-1}$.

Three Points:

$$\begin{aligned} \frac{\partial \phi_M}{\partial x} = & \left[\frac{1}{(X_M - X_{M-1})} + \frac{1}{(X_M - X_{M-2})} \right] \phi_M \\ & - \frac{(X_M - X_{M-2})}{(X_M - X_{M-1})(X_{M-1} - X_{M-2})} \phi_{M-1} \\ & + \frac{(X_M - X_{M-1})}{(X_M - X_{M-2})(X_{M-1} - X_{M-2})} \phi_{M-2} \end{aligned}$$

The error is,

$$\frac{(X_M - X_{M-1})(X_M - X_{M-2})}{6} \frac{\partial^3 \phi(\xi)}{\partial x^3}$$

C.2 Integration Expressions

C.2.1 Extrapolation Formulas

$$\begin{aligned} (C\phi'')_{N)E} &= (C\phi'')_{N-1} + \frac{\Delta\eta}{24} [55(C\phi'')'_{N-1} \\ &\quad - 59(C\phi'')'_{N-2} + 37(C\phi'')'_{N-3} - 9(C\phi'')'_{N-4}] \end{aligned}$$

where $\Delta\eta$ is the step size and subscript E denotes extrapolation.

The error is

$$E_1 \leq + \frac{251}{720} (\Delta\eta)^5 [C\phi''(\xi)]^V$$

The formulas for ϕ' and ϕ are:

$$\phi'_{N)E} = \phi'_{N-1} + \frac{\Delta\eta}{24} [55\phi''_{N-1} - 59\phi''_{N-2} + 37\phi''_{N-3} - 9\phi''_{N-4}]$$

$$E_2 \leq + \frac{251}{720} (\Delta\eta)^5 \phi^{VI}(\xi)$$

and,

$$\phi_N)_E = \phi_{N-1} + \Delta\eta\phi'_{N-1}$$

$$+ \frac{(\Delta\eta)^2}{360} [323\phi''_{N-1} - 264\phi''_{N-2} + 159\phi''_{N-3} - 38\phi''_{N-4}]$$

$$E_3 \leq \frac{3}{32} (\Delta\eta)^6 \phi^{VI}(\xi)$$

Values of $[C\phi'']$ can now be determined at station N using the momentum equation and the extrapolated values of ϕ'' , ϕ' , ϕ .

C.2.2 Interpolation Formulas

$$\begin{aligned} (C\phi'')_N &= (C\phi'')_{N-1} + \frac{\Delta\eta}{24} [9(C\phi'')'_N)_E + 19(C\phi'')'_{N-1} \\ &\quad - 5(C\phi'')'_{N-2} + (C\phi'')'_{N-3}] \end{aligned}$$

with an error of

$$E_4 \leq -\frac{19}{720} (\Delta\eta)^5 [C\phi''(\xi)]^V$$

also,

$$\phi'_N = \phi'_{N-1} + \frac{\Delta\eta}{24} [9\phi''_N + 19\phi''_{N-1} - 5\phi''_{N-2} + \phi''_{N-3}]$$

$$E_5 \leq - \frac{19}{720} (\Delta\eta)^5 \phi^{VI}(\xi)$$

and,

$$\phi_N = \phi_{N-1} + \Delta\eta \phi'_{N-1}$$

$$+ \frac{(\Delta\eta)^2}{360} [38\phi''_N + 171\phi''_{N-1} - 36\phi''_{N-2} + 7\phi''_{N-3}]$$

$$E_6 \leq - \frac{17}{1440} (\Delta\eta)^6 \phi^{VI}(\xi)$$

As can be seen the error in the interpolation formulas are much less than the error in the extrapolation formulas. Since the errors are of opposite sign, the exact values must be within the bounds of the extrapolated and interpolated values. The solution can be made more exact by choosing smaller values of $\Delta\eta$.

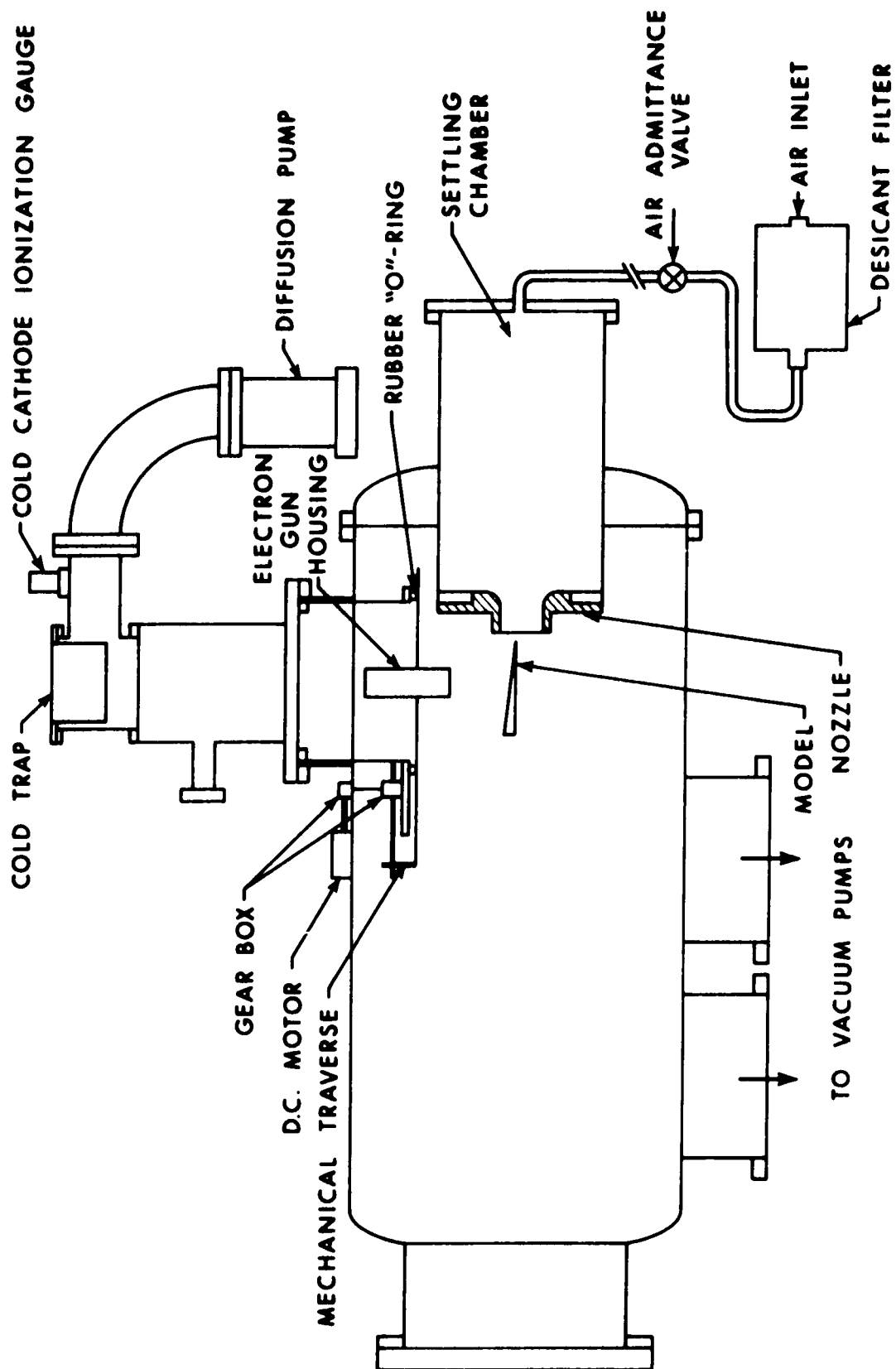


FIGURE 1 SCHEMATIC DIAGRAM OF LOW DENSITY WIND TUNNEL

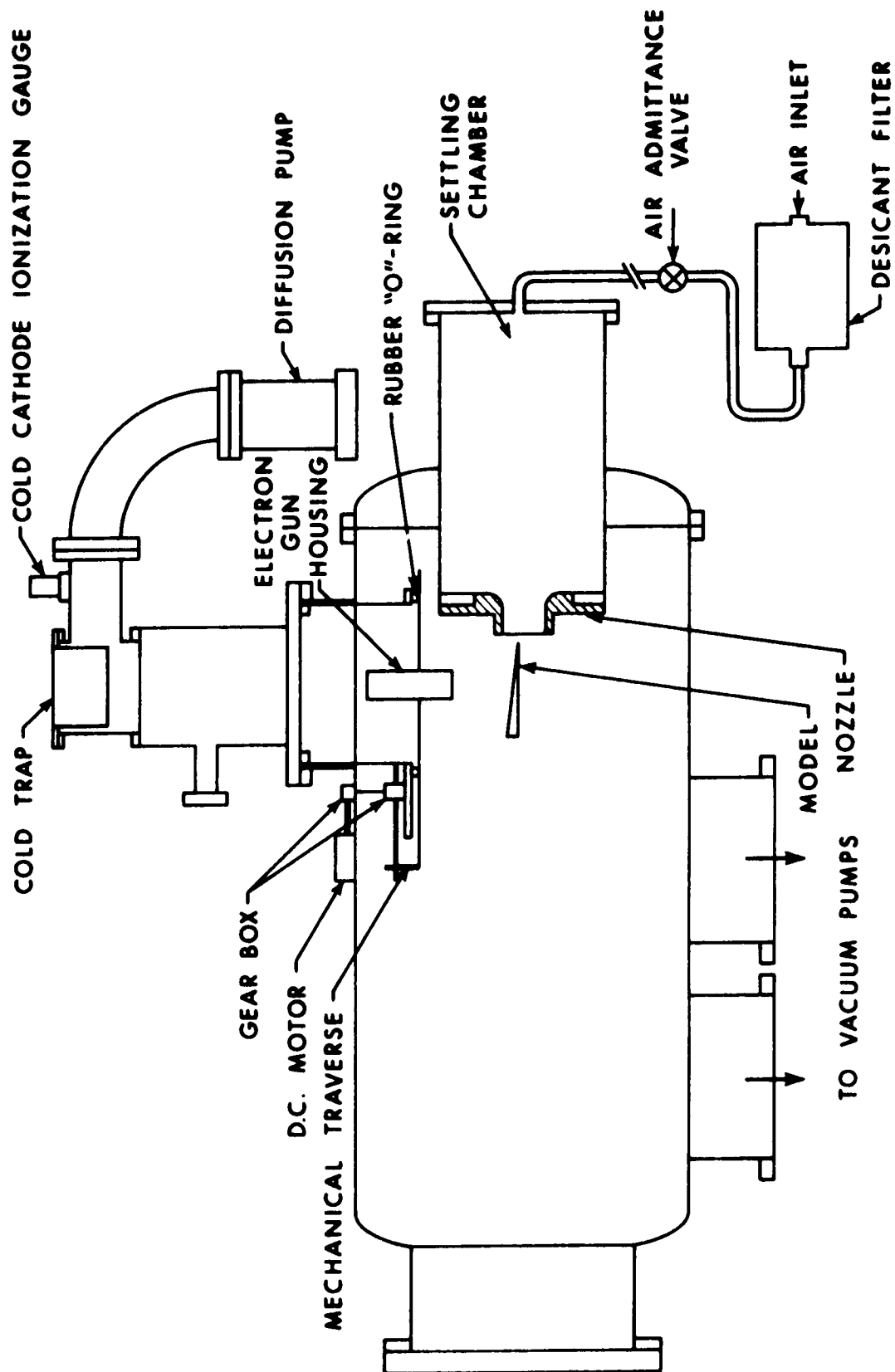
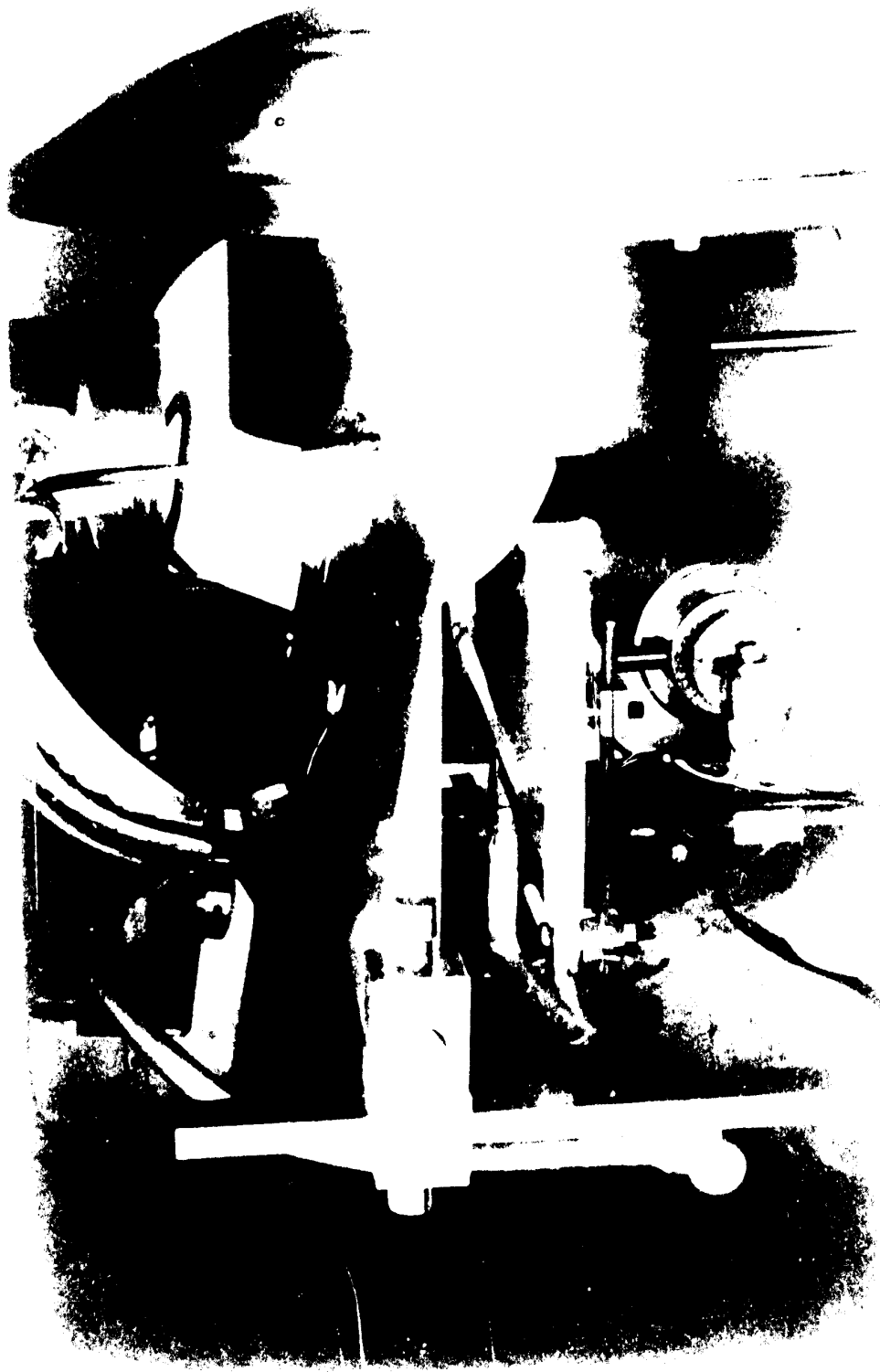


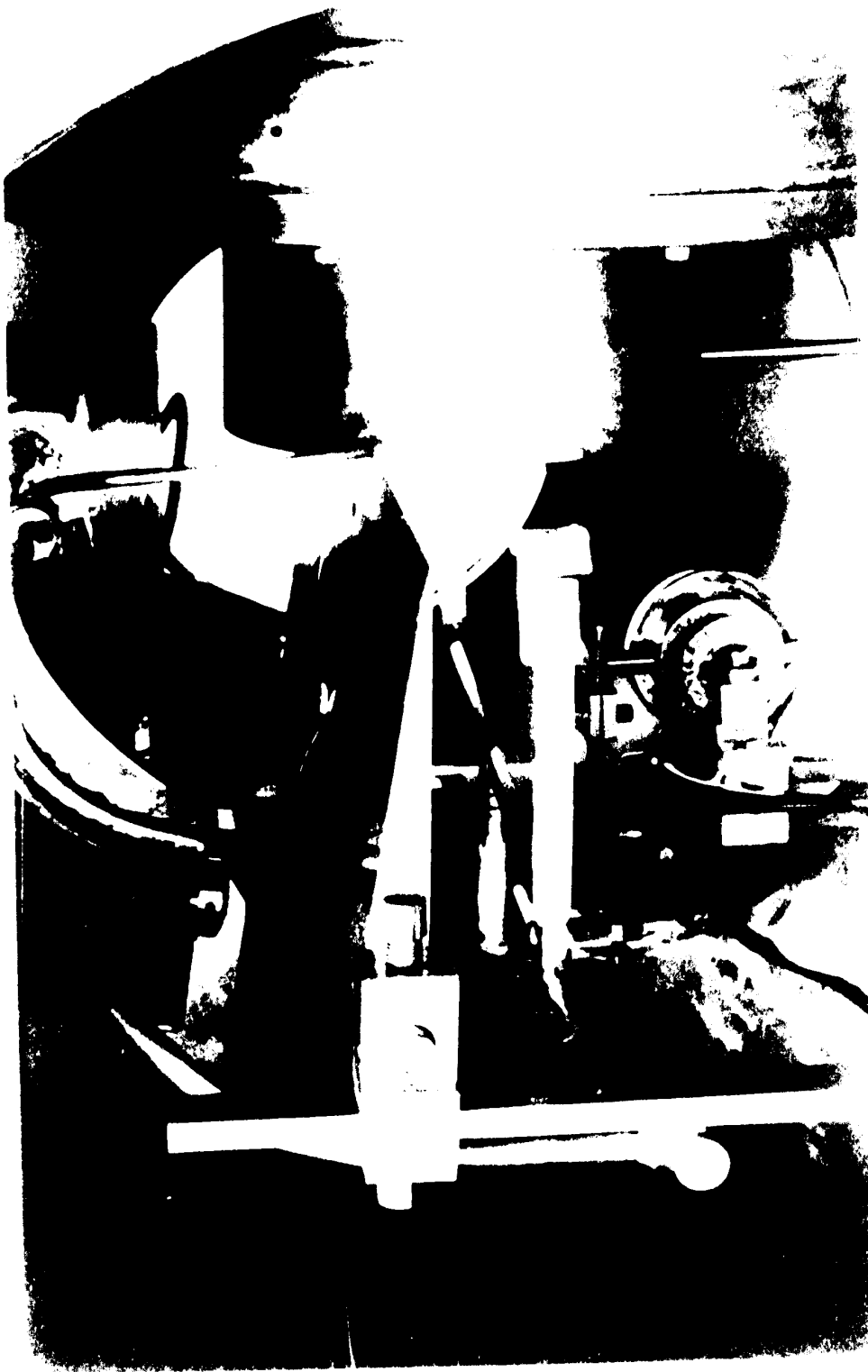
FIGURE 1 SCHEMATIC DIAGRAM OF LOW DENSITY WIND TUNNEL



FIGURE 2 PHOTOGRAPH OF LOW DENSITY WIND TUNNEL







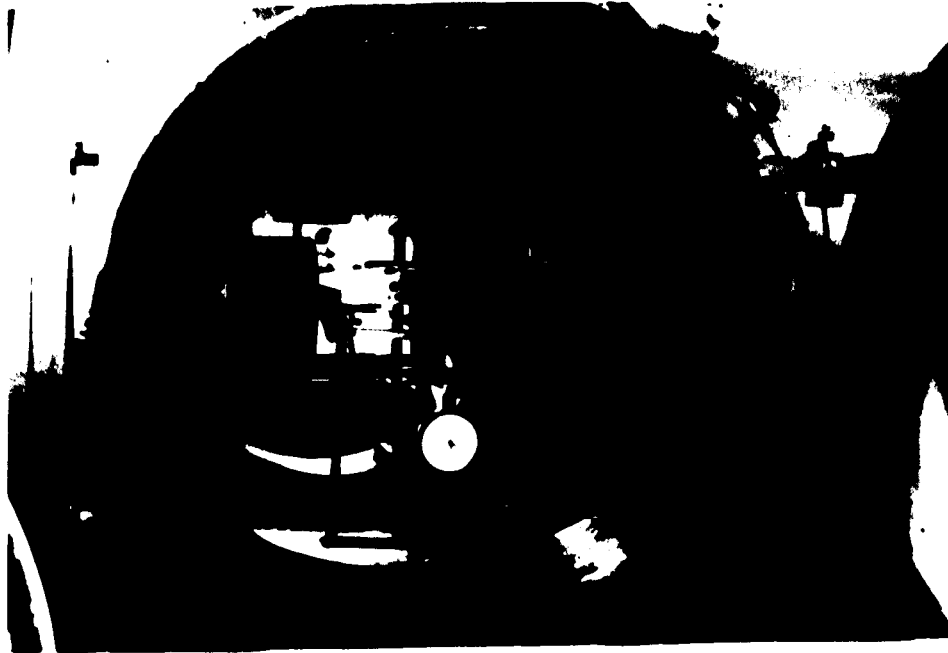


FIGURE 4 PHOTOGRAPH OF TEST SECTION
SHOWING TRAVERSING MECHANISM

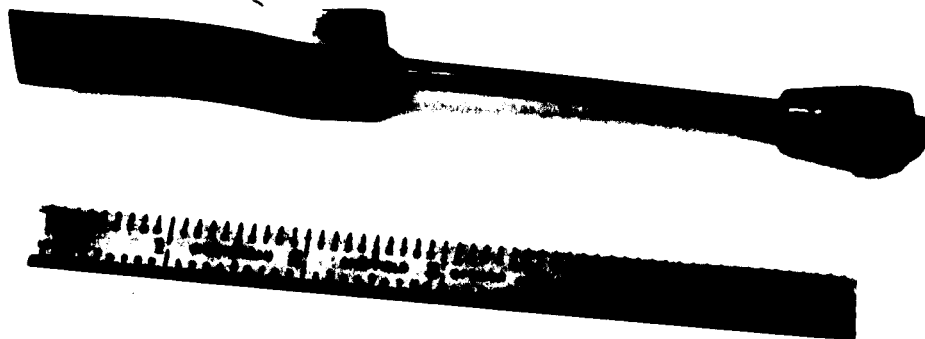


FIGURE 5 PHOTOGRAPH OF IMPACT PROBE

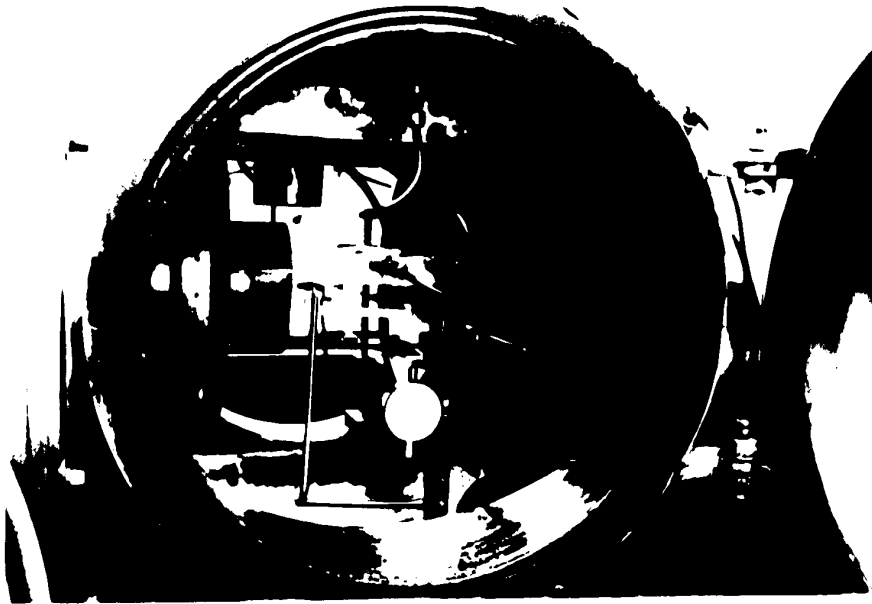
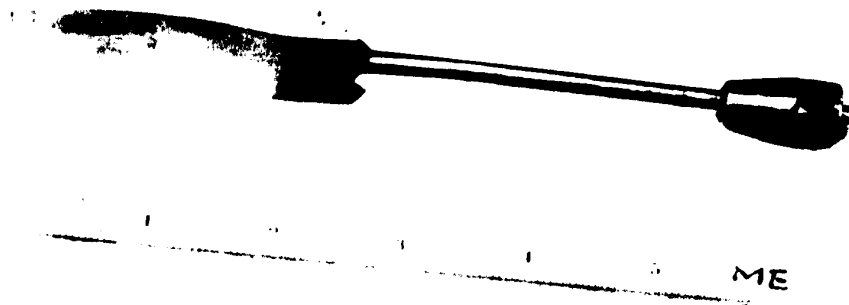


Figure 1. The mechanical device shown in Figure 1 is a mechanical device used for the purpose of the study.



ME

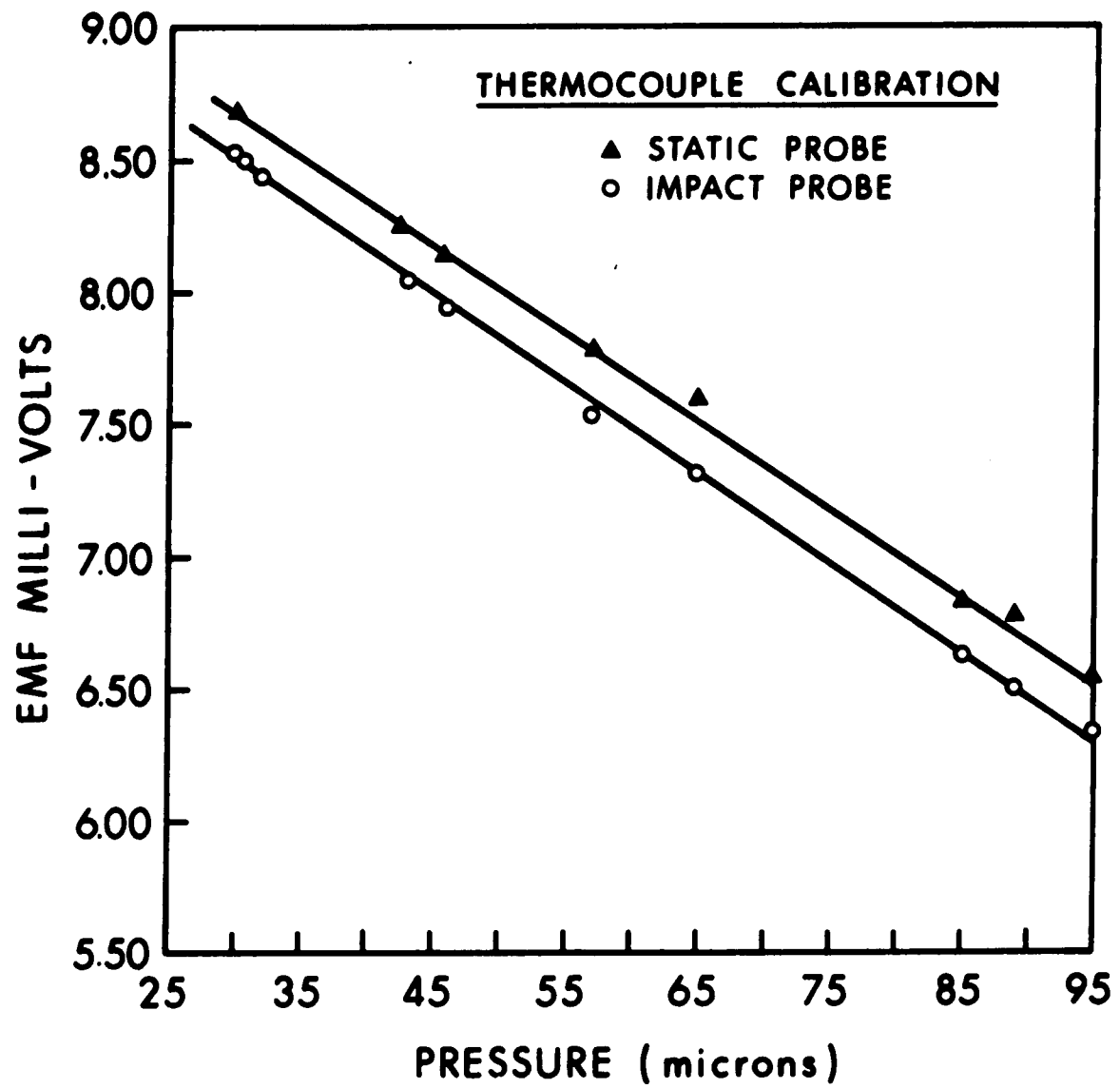
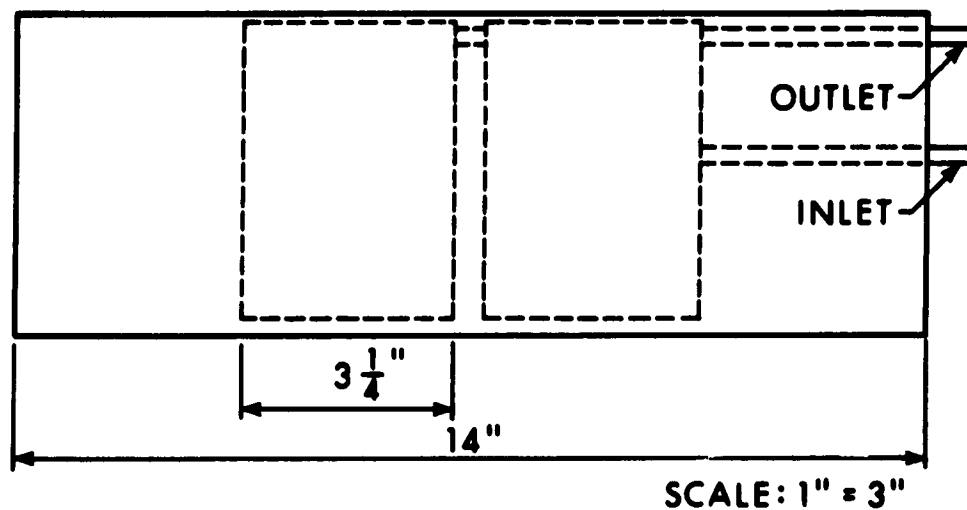
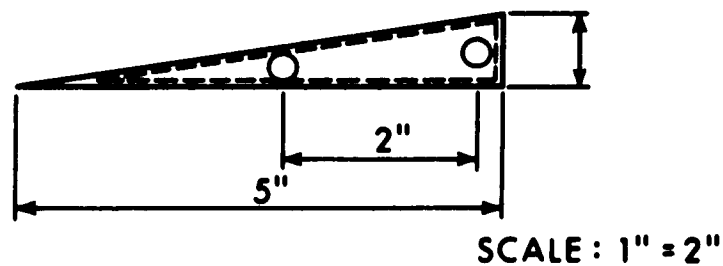


FIGURE 7 THERMOCOUPLE CALIBRATION CURVE



TOP VIEW



SIDE VIEW

NOTE:

1. All materials are aluminum. The plates covering the milled out compartments are welded to the top of the plate.
2. The inlet and outlet tubes are 1/4" aluminium tubing.
3. The bottom plate surface is polished to a very smooth finish and the front of the plate is machined to a sharp tip.

FIGURE 8 SCHEMATIC DIAGRAM OF PLATE MODEL

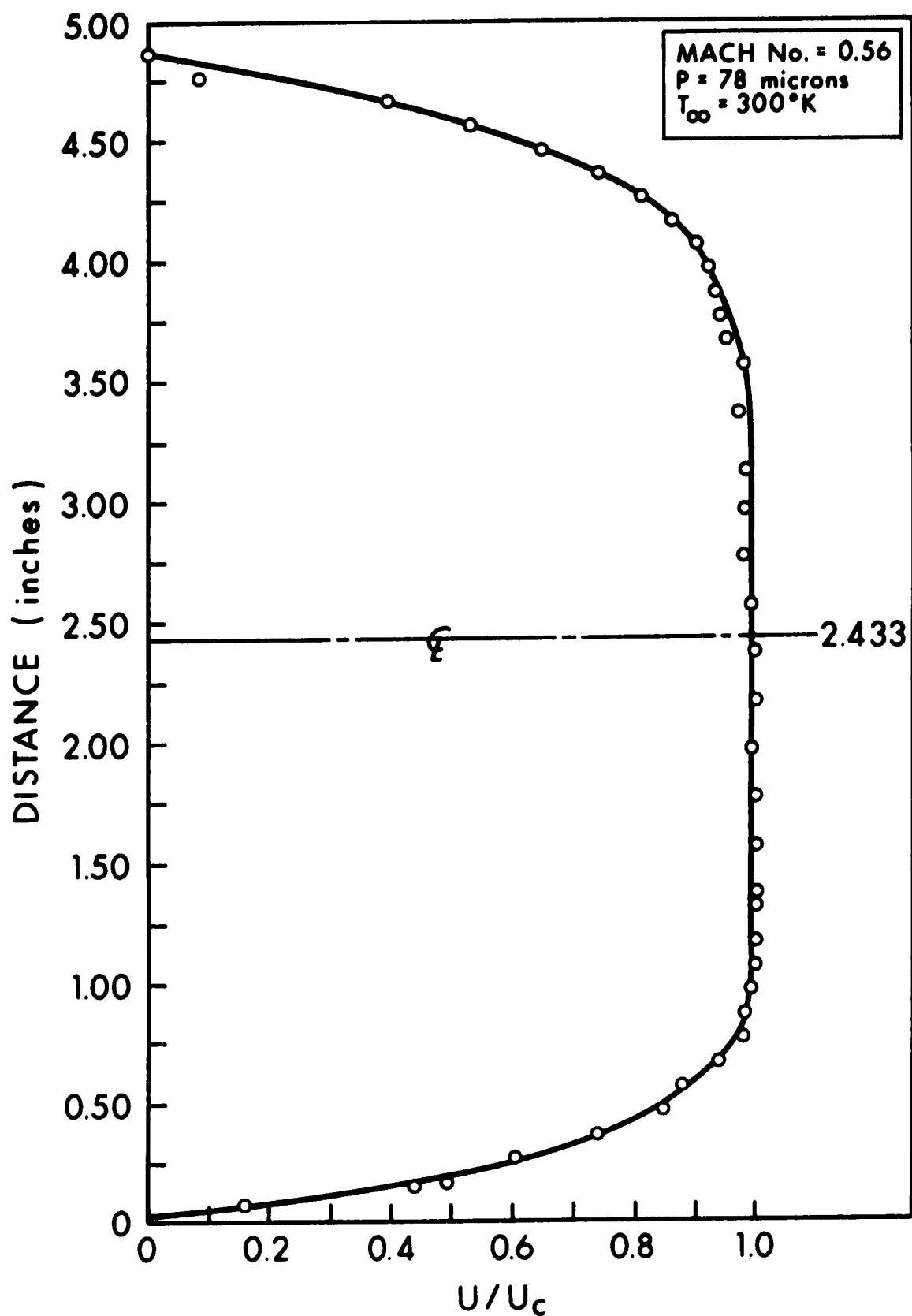


FIGURE 9 VELOCITY PROFILE AT NOZZLE EXIT:
P = 78 MICRONS

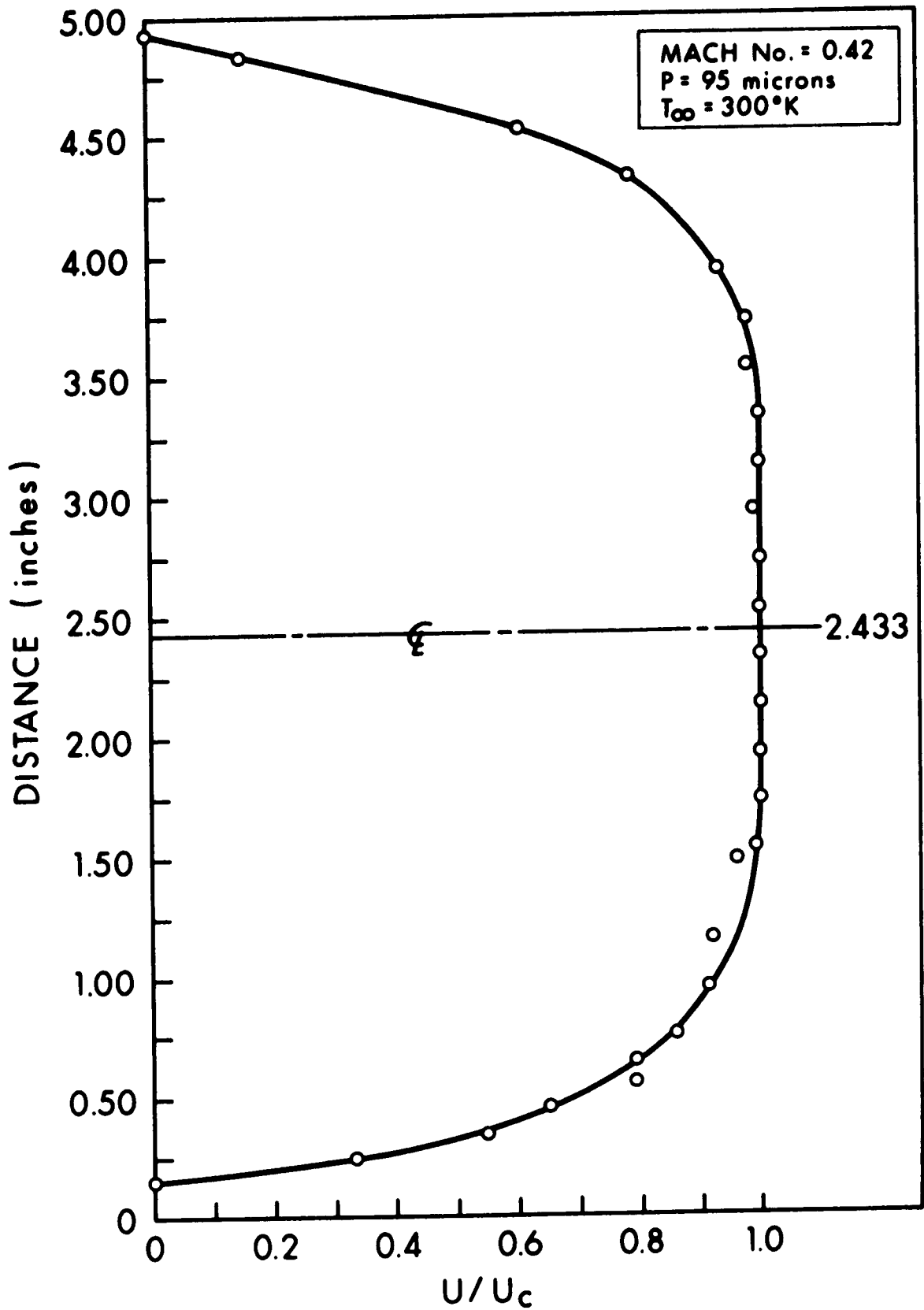


FIGURE 10 VELOCITY PROFILE AT NOZZLE EXIT:

P = 95 MICRONS

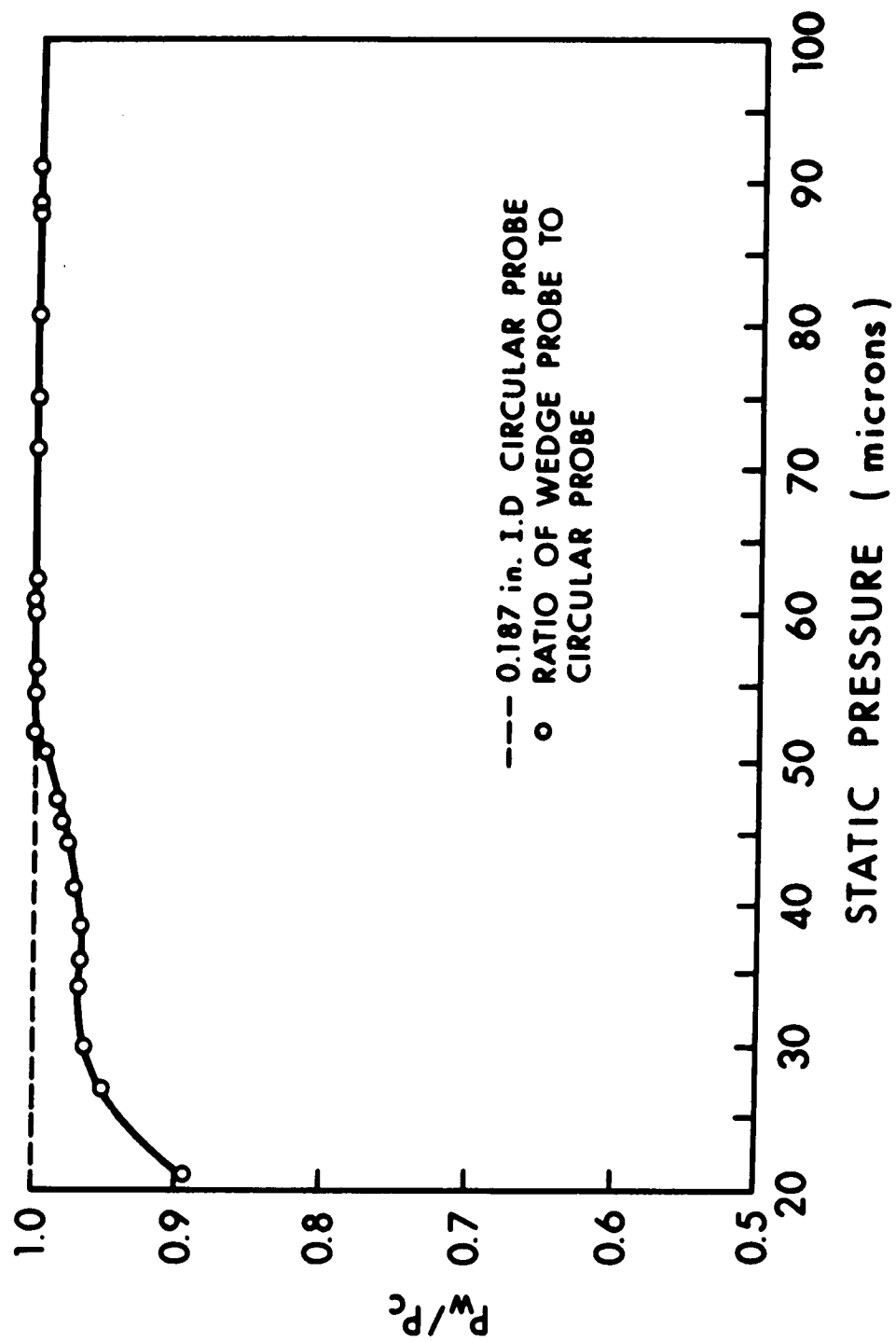


FIGURE 11 IMPACT PROBE CALIBRATION

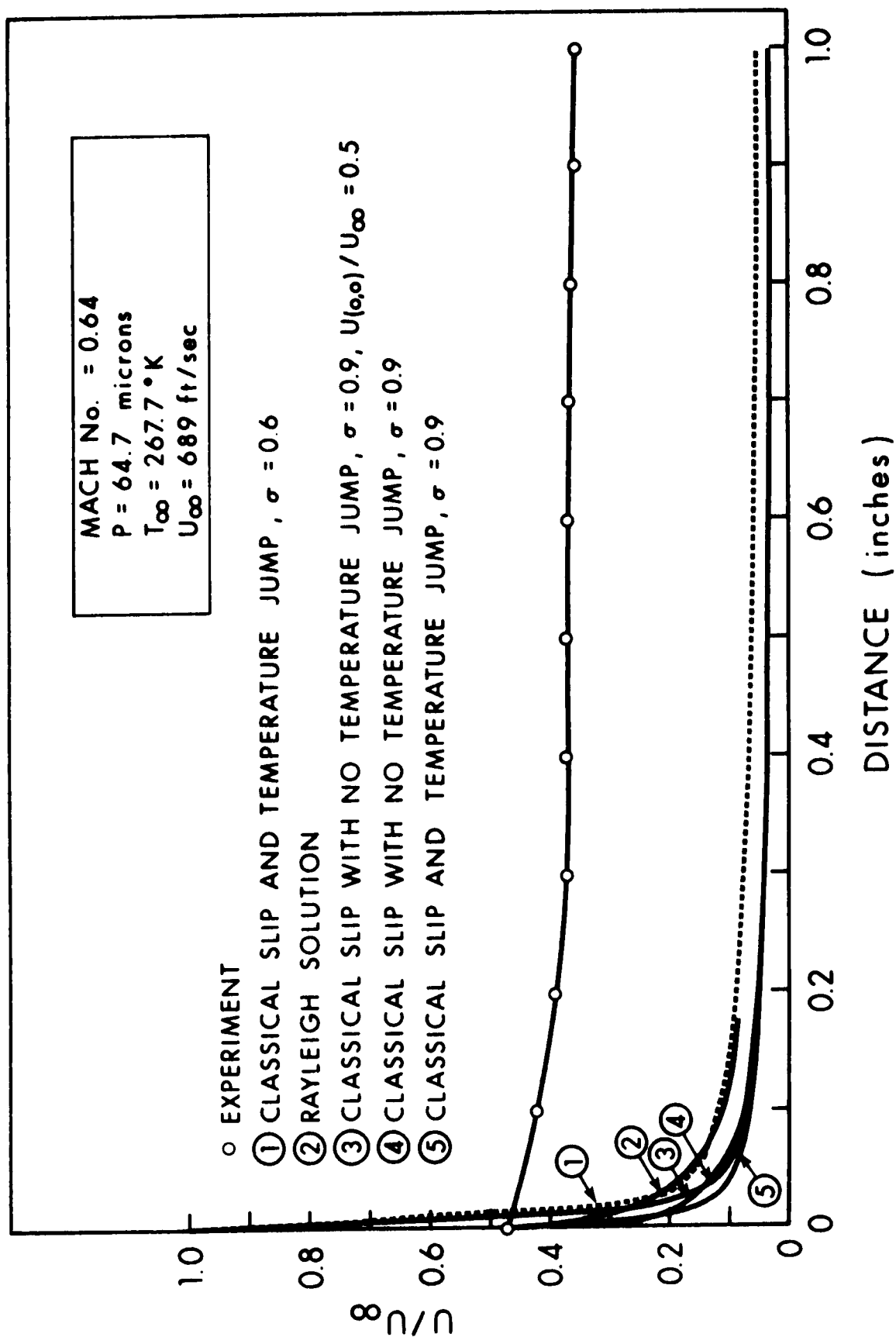


FIGURE 12 SLIP ALONG A COLD FLAT PLATE

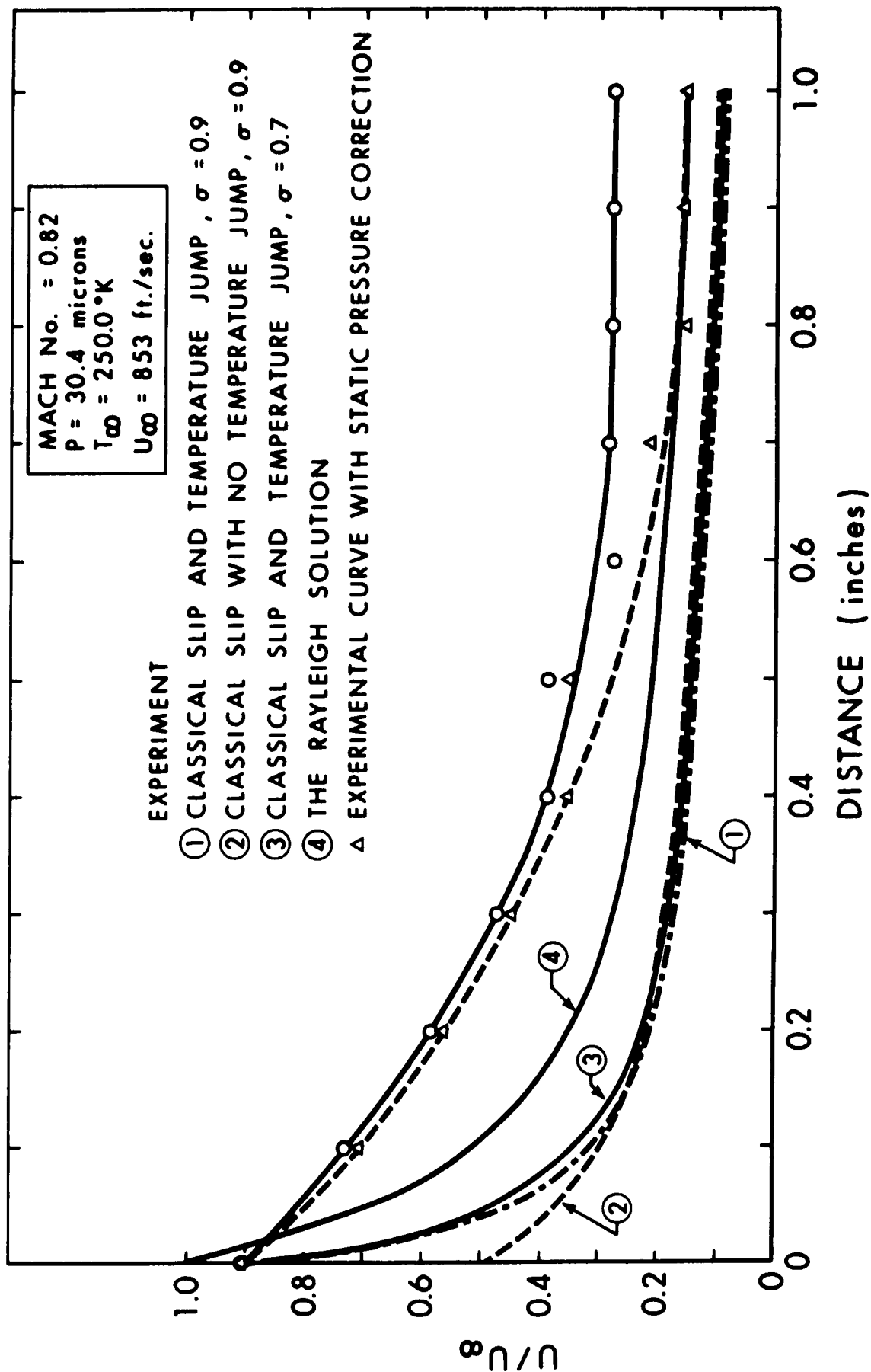


FIGURE 13 SLIP ALONG A FLAT PLATE:
 $P = 30.4$ MICRONS

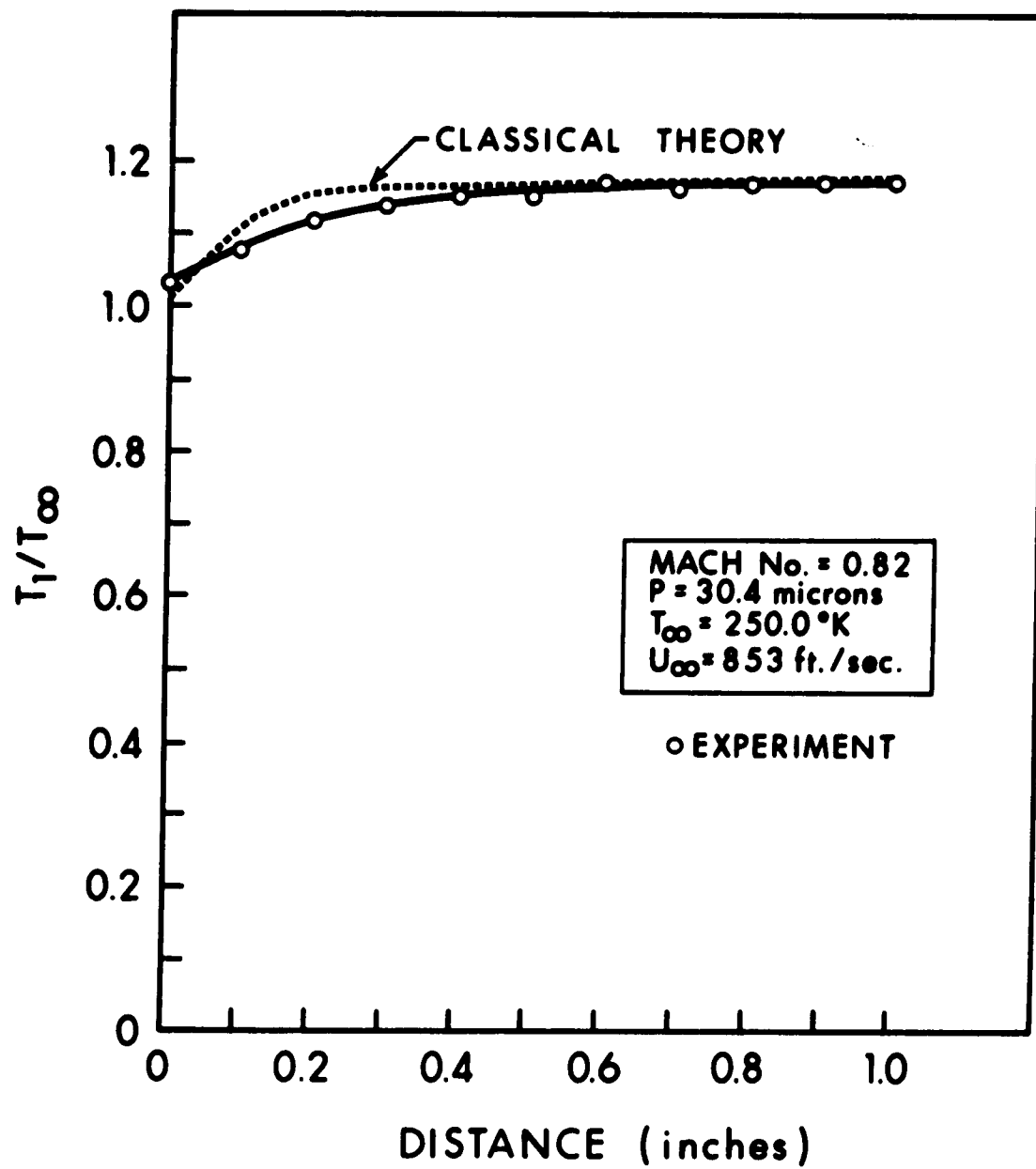


FIGURE 14 TEMPERATURE JUMP ALONG A FLAT PLATE:
P = 30.4 MICRONS

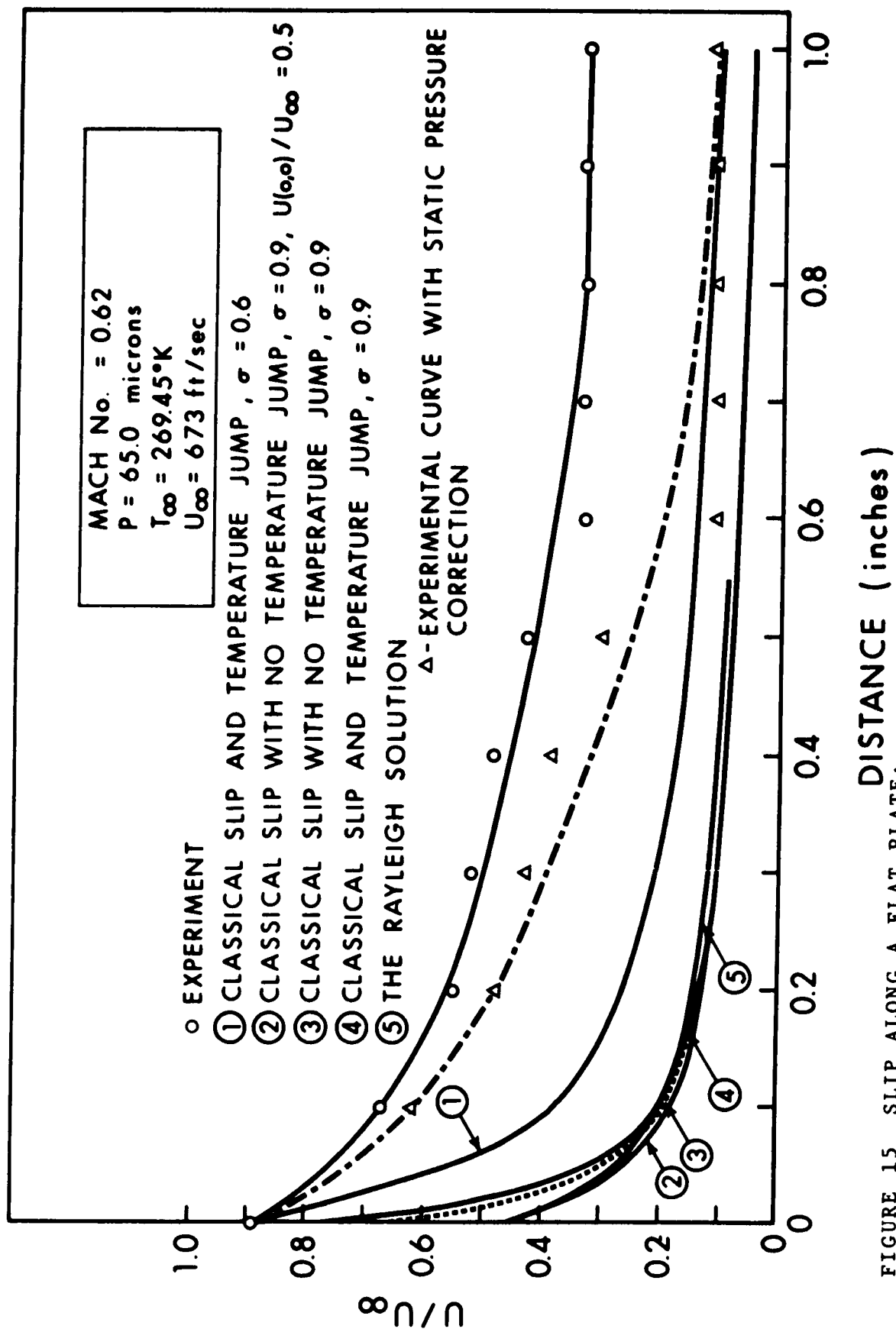


FIGURE 15 SLIP ALONG A FLAT PLATE:

P = 65.0 MICRONS

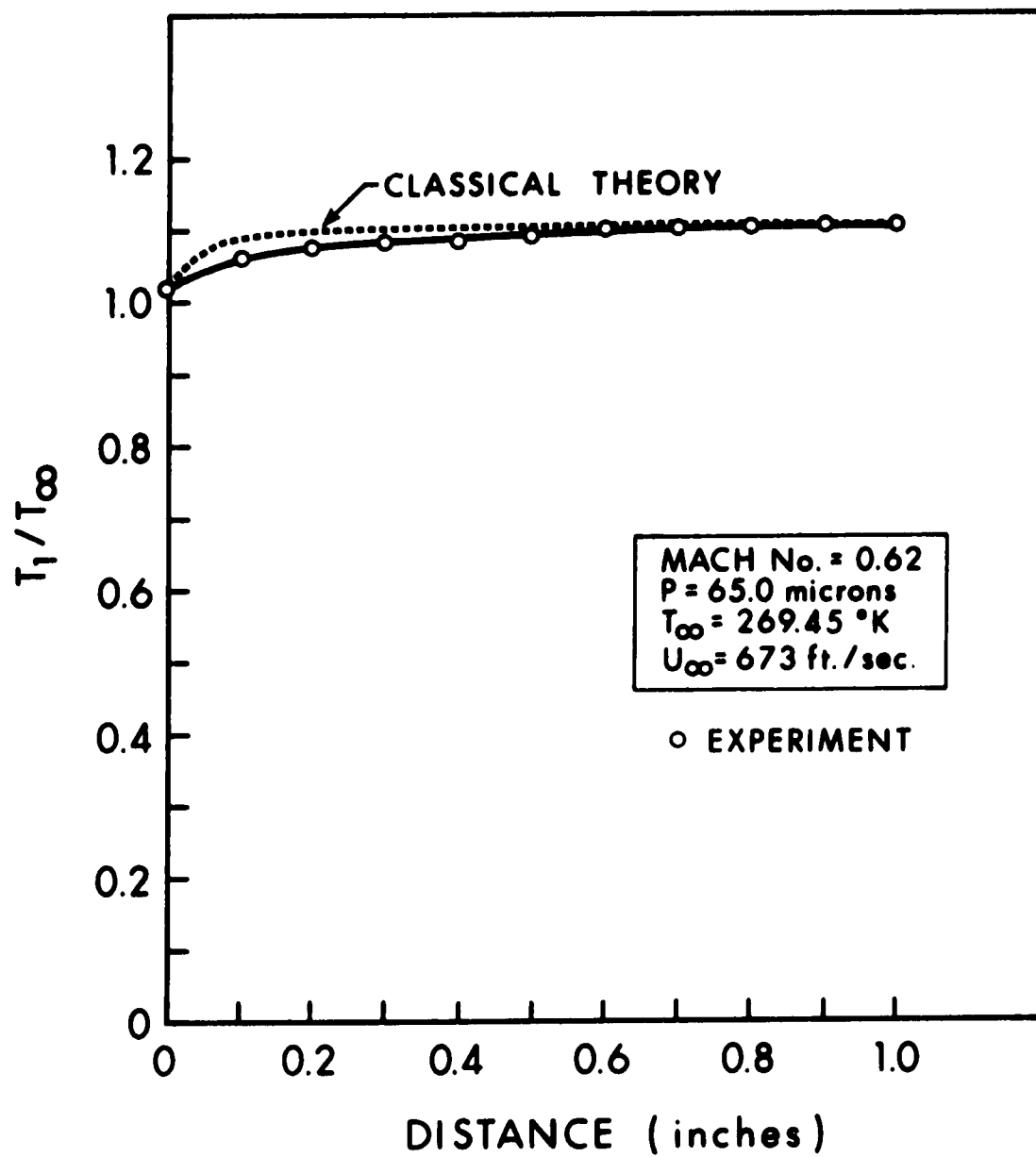


FIGURE 16 TEMPERATURE JUMP ALONG A FLAT PLATE:
P = 65.0 MICRONS

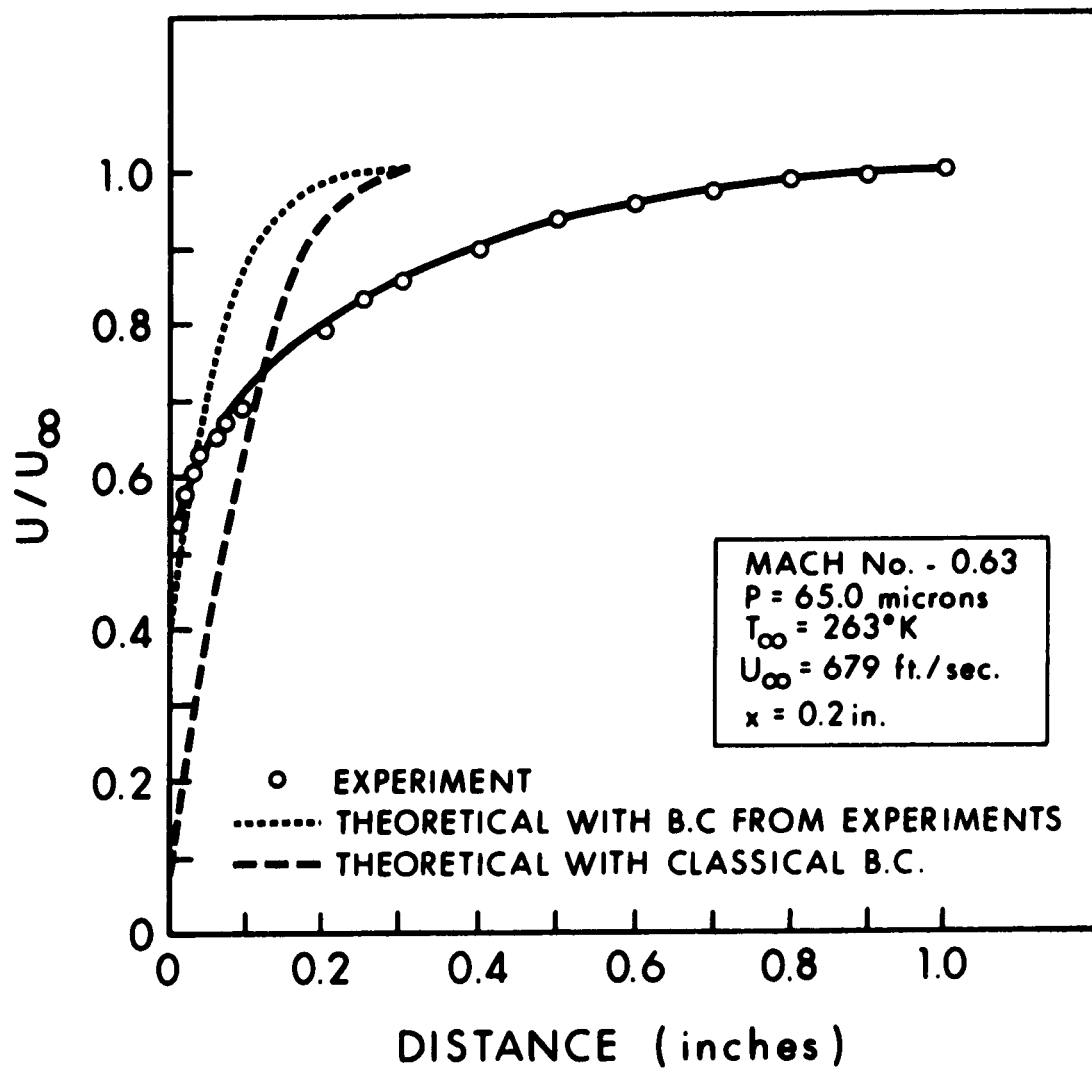


FIGURE 17 VELOCITY PROFILE ON A COLD FLAT PLATE:
 $x = 0.2 \text{ INCHES}$

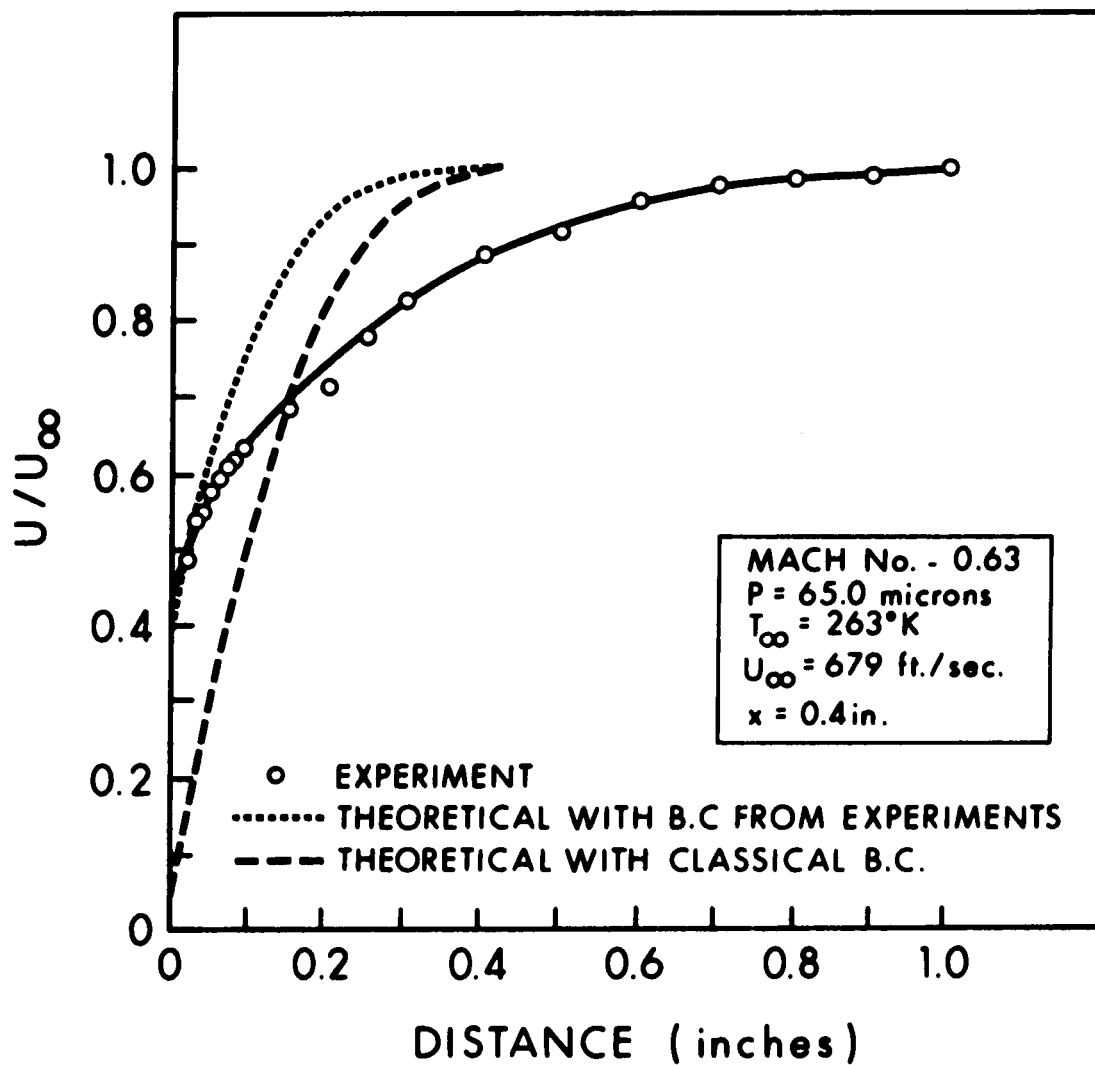


FIGURE 18 VELOCITY PROFILE ON A COLD FLAT PLATE:
 $x = 0.4$ INCHES

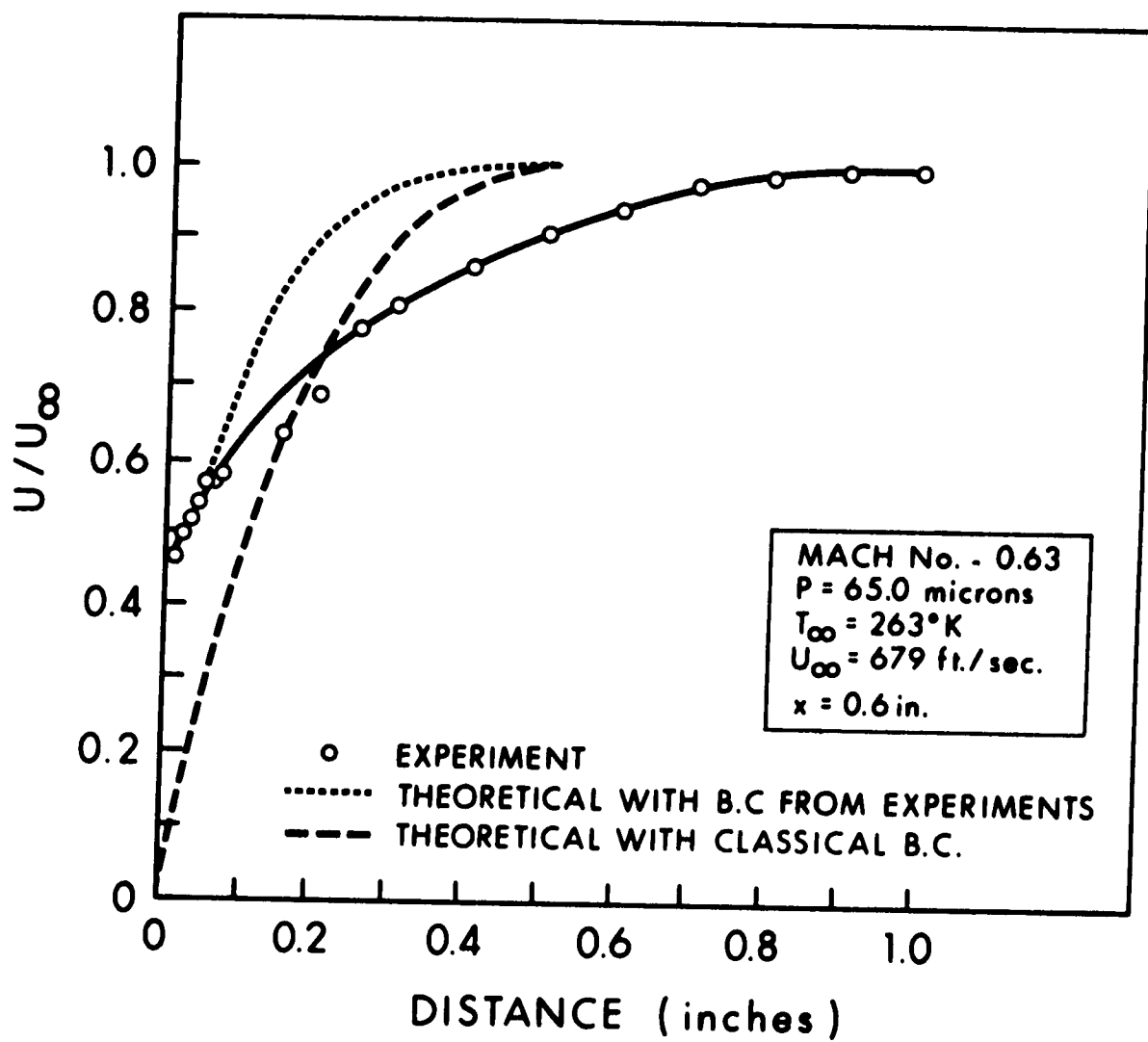


FIGURE 19 VELOCITY PROFILE ON A COLD FLAT PLATE:
x = 0.6 INCHES

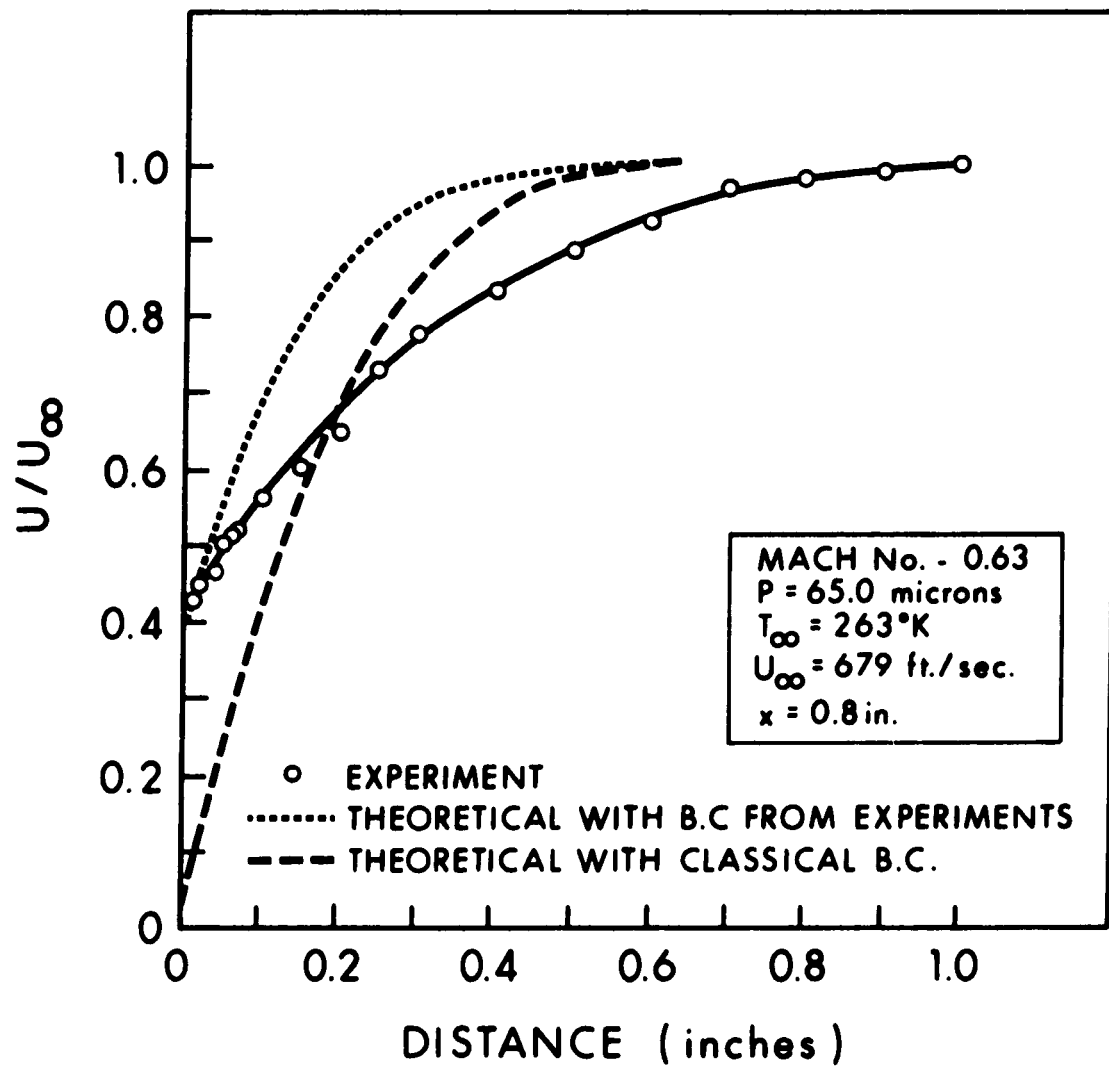


FIGURE 20 VELOCITY PROFILE ON A COLD FLAT PLATE:
x = 0.8 INCHES

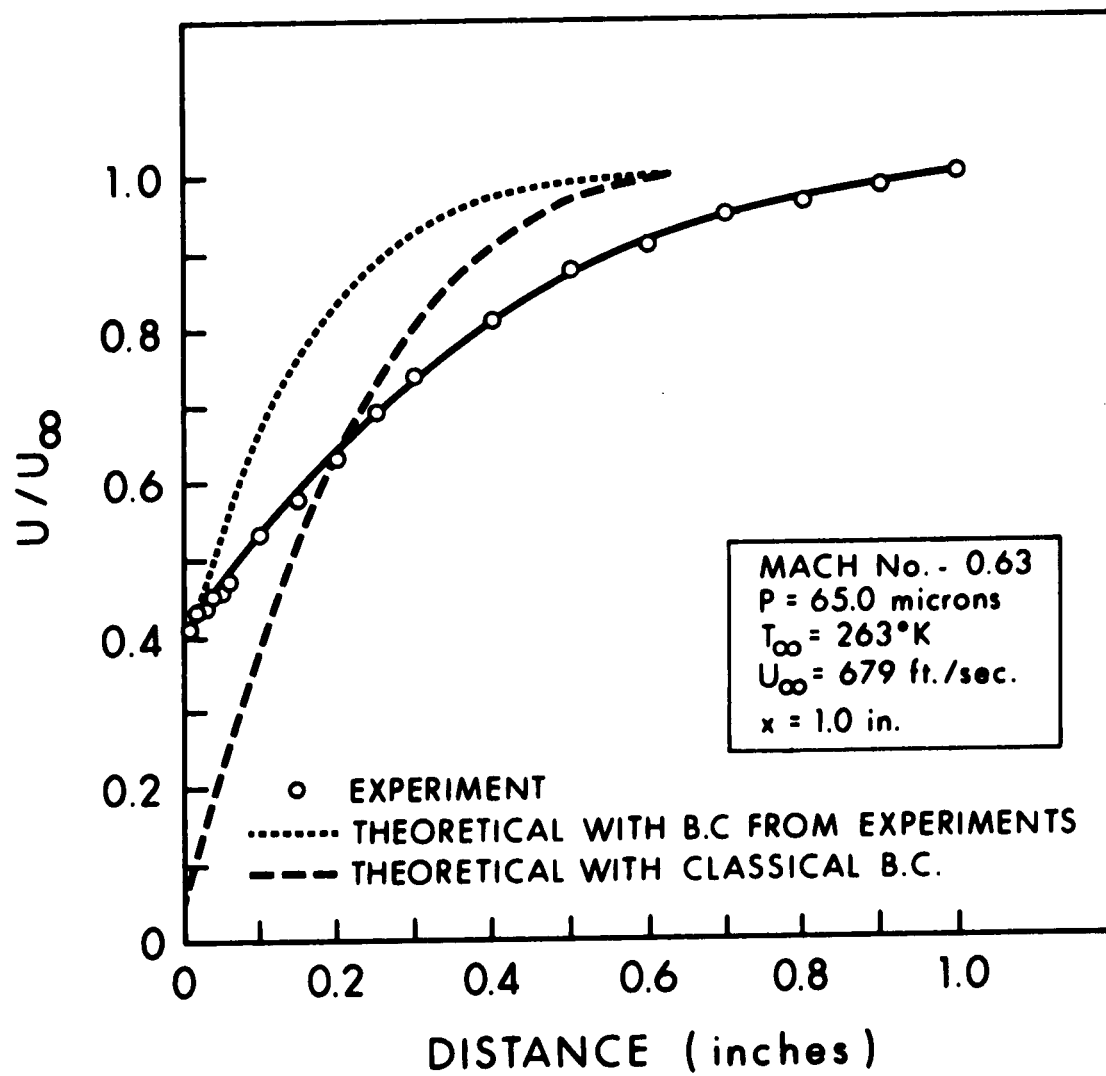


FIGURE 21 VELOCITY PROFILE ON A COLD FLAT PLATE:
x = 1.0 INCHES

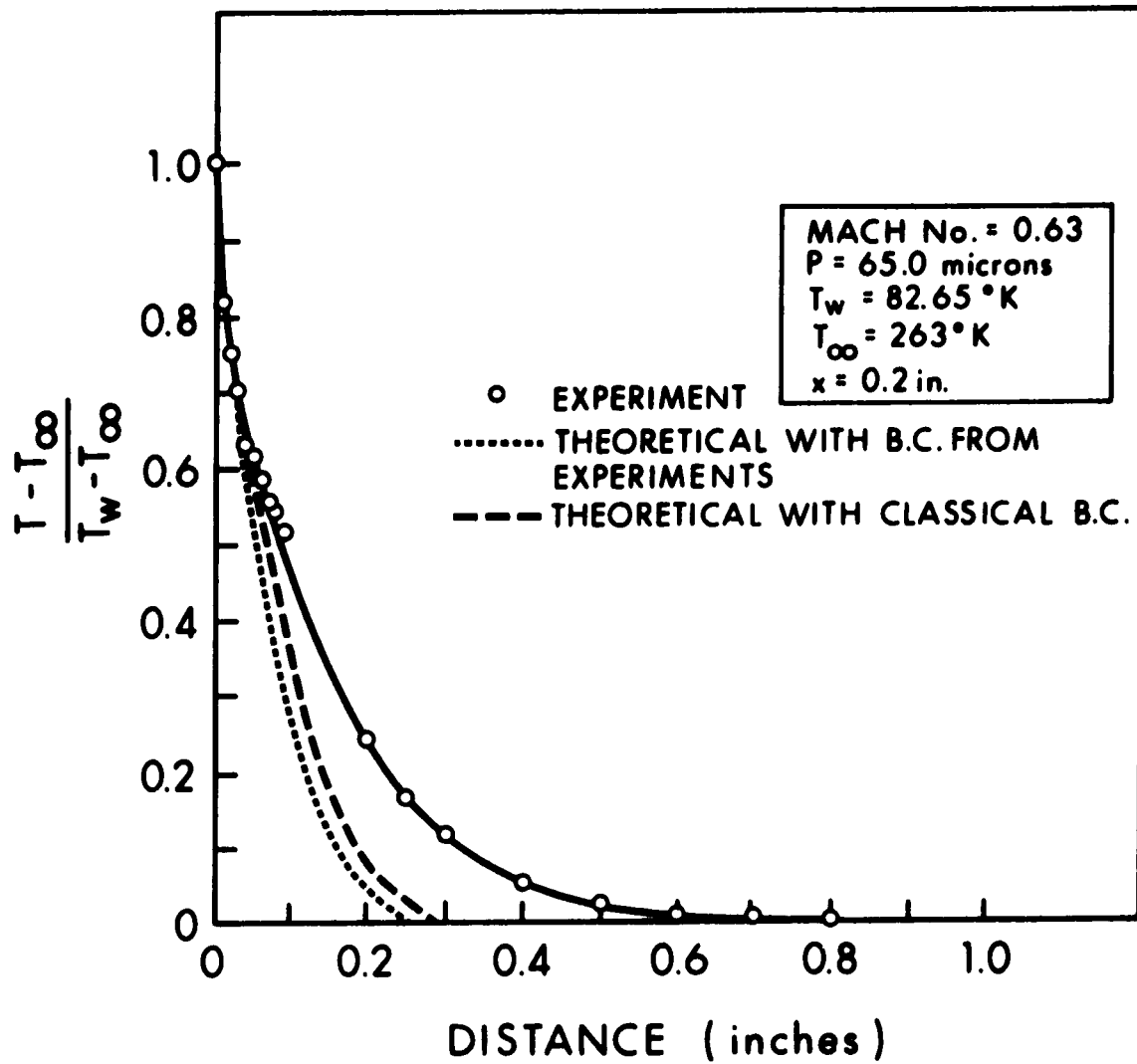


FIGURE 22 TEMPERATURE PROFILE ON A COLD FLAT PLATE:
 $x = 0.2 \text{ INCHES}$

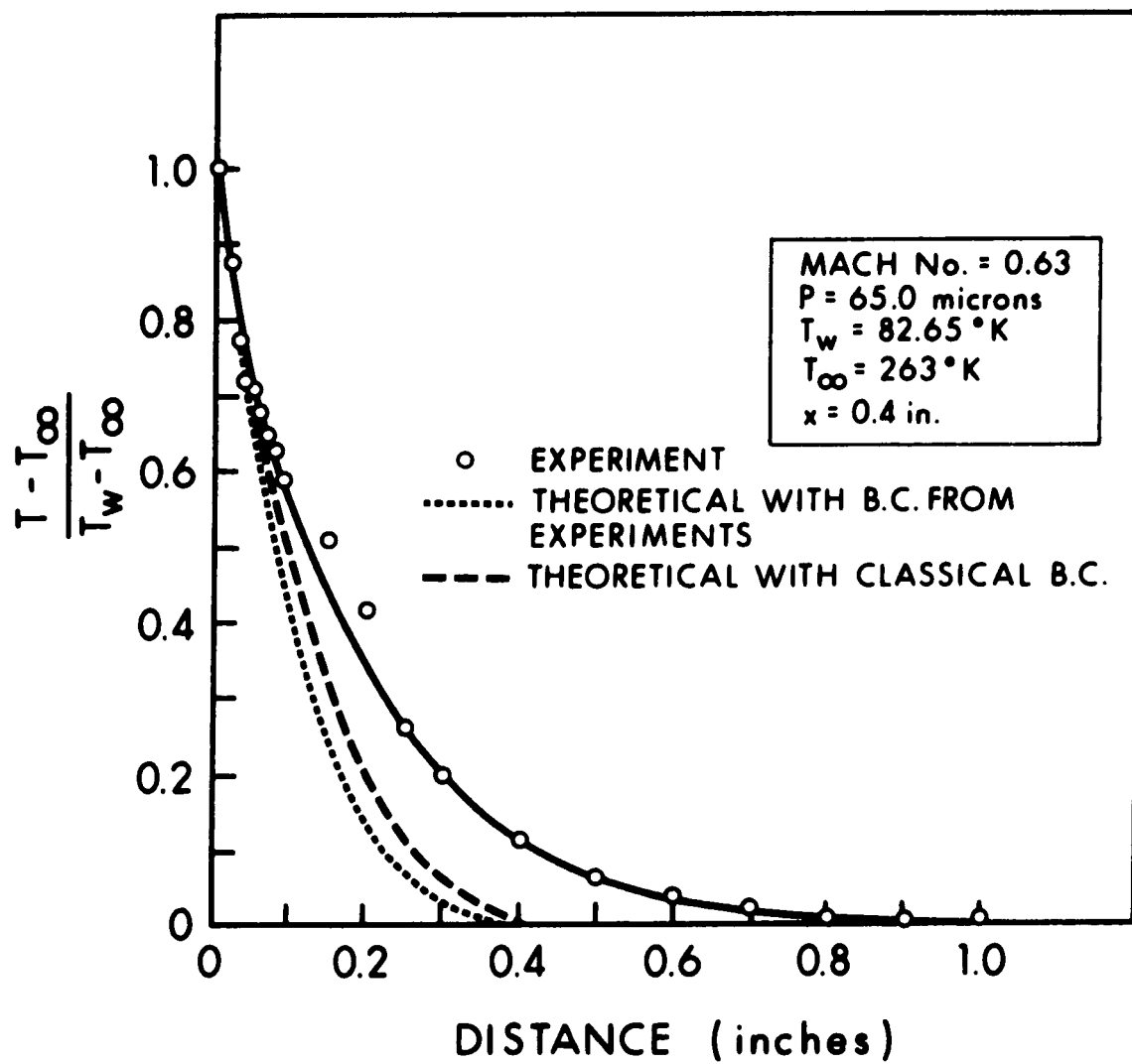


FIGURE 23 TEMPERATURE PROFILE ON A COLD FLAT PLATE:
x = 0.4 INCHES

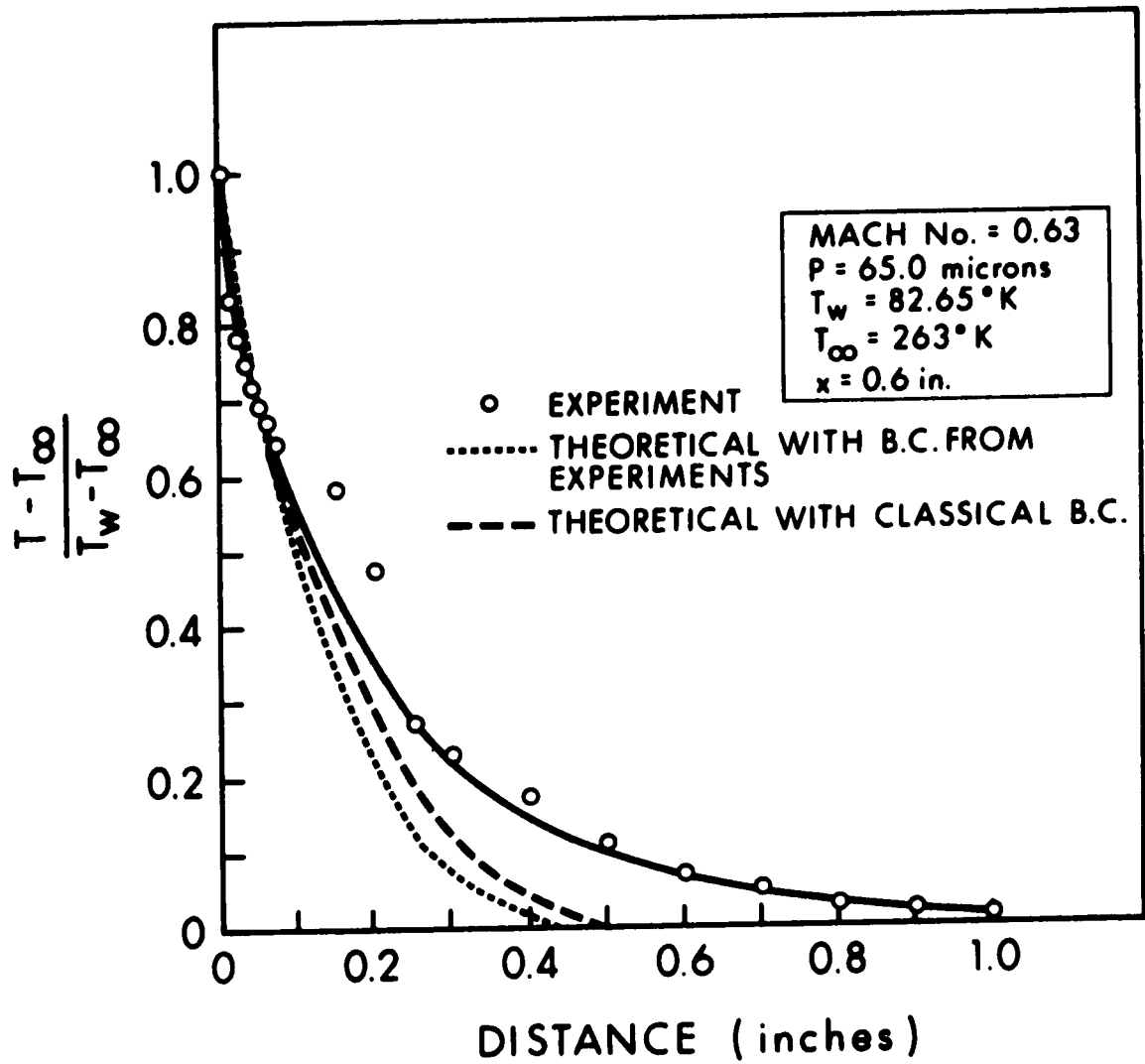


FIGURE 24 TEMPERATURE PROFILE ON A COLD FLAT PLATE:
 $x = 0.6$ INCHES

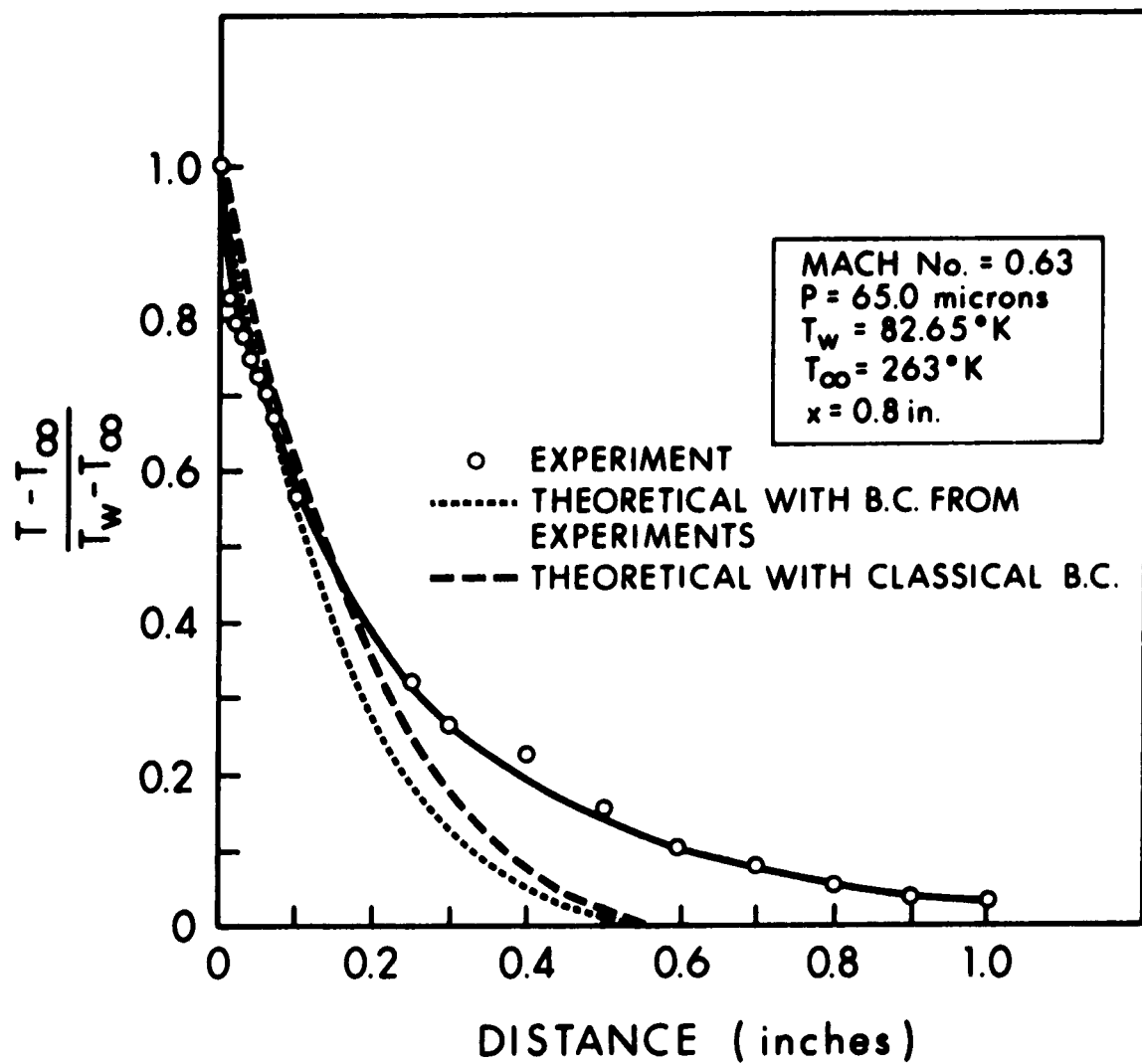


FIGURE 25 TEMPERATURE PROFILE ON A COLD FLAT PLATE:
x = 0.8 INCHES

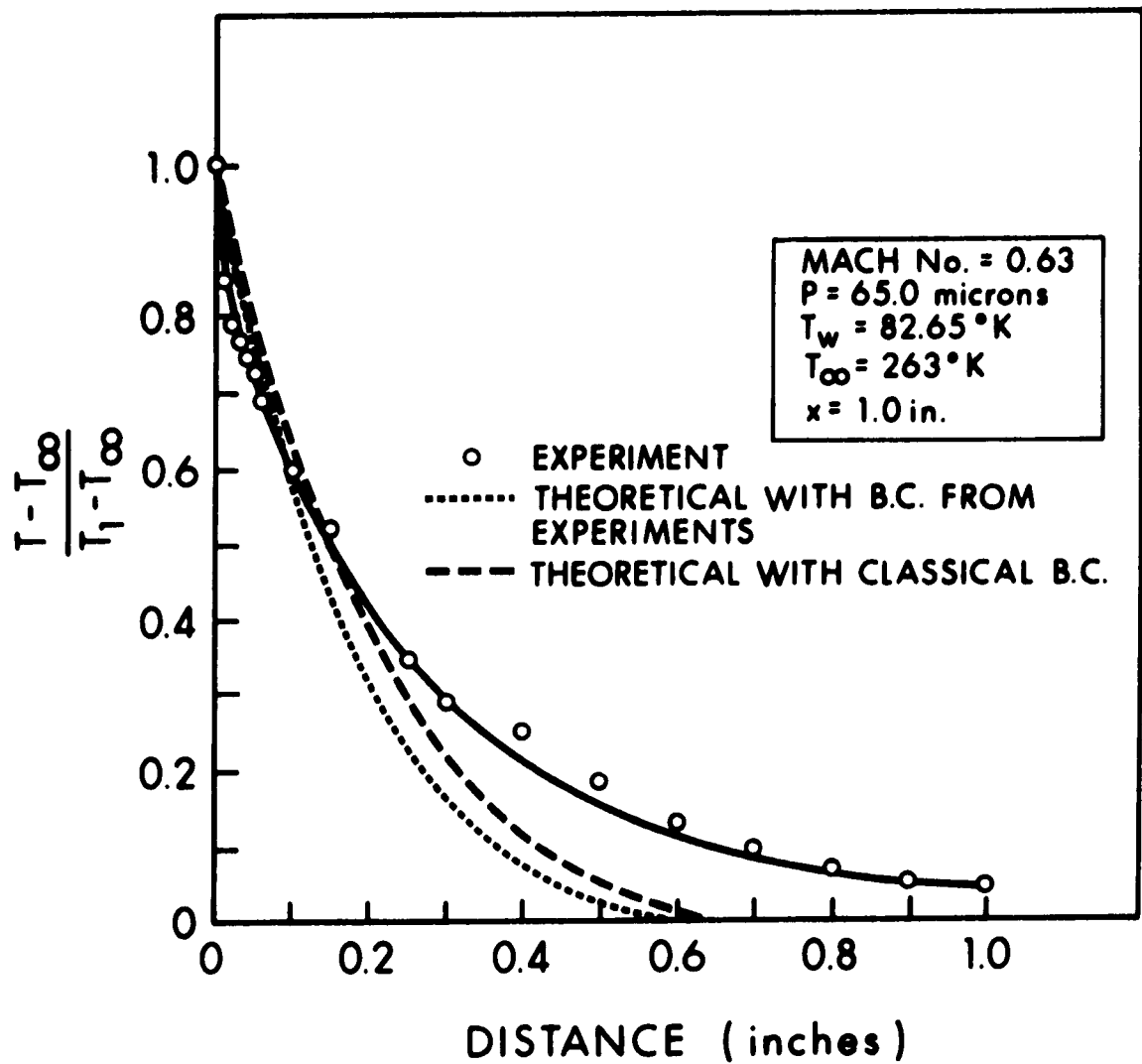


FIGURE 26 TEMPERATURE PROFILE ON A COLD FLAT PLATE:
 $x = 1.0\text{ INCHES}$

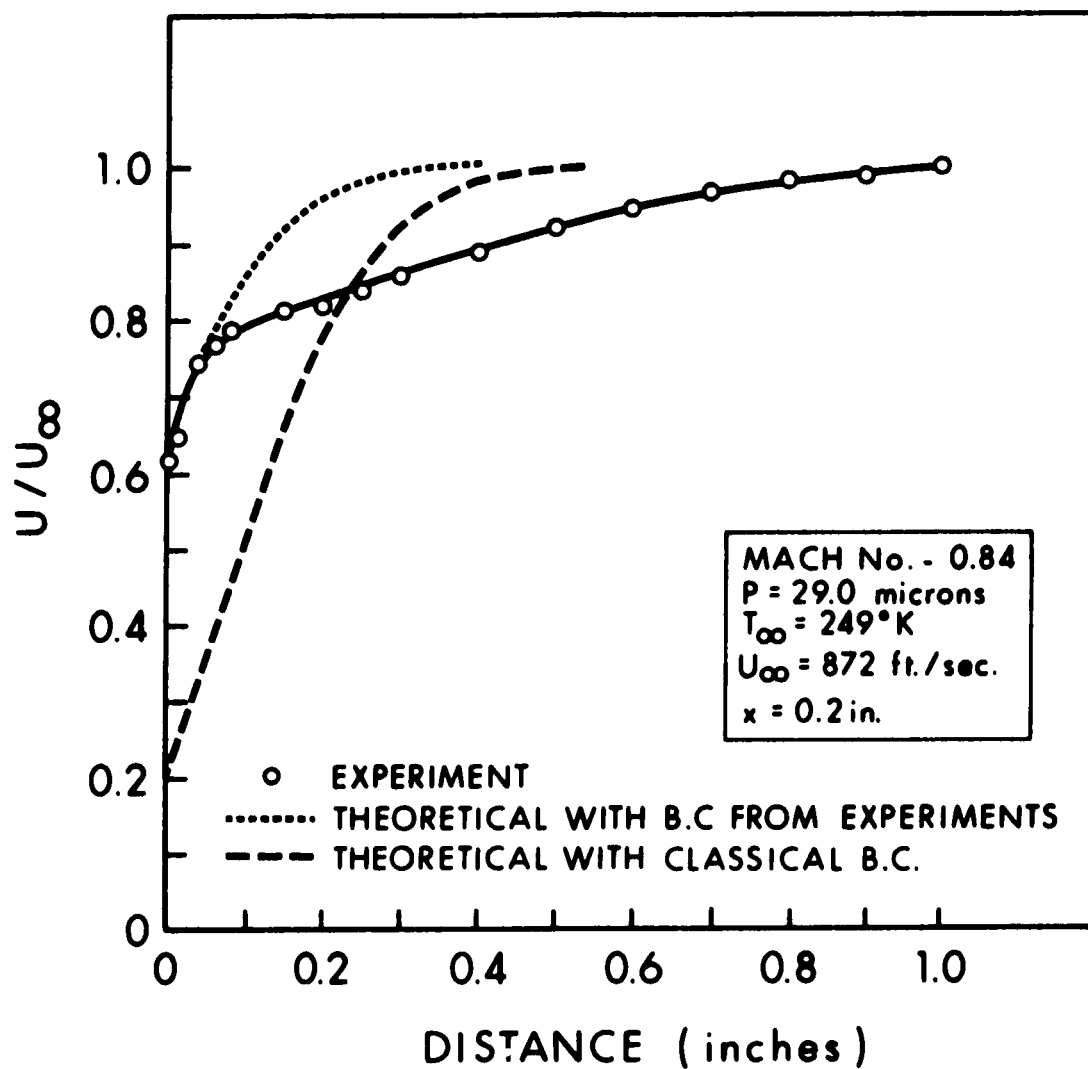


FIGURE 27 VELOCITY PROFILE ON A FLAT PLATE:
P = 29.0 MICRONS x = 0.2 INCHES

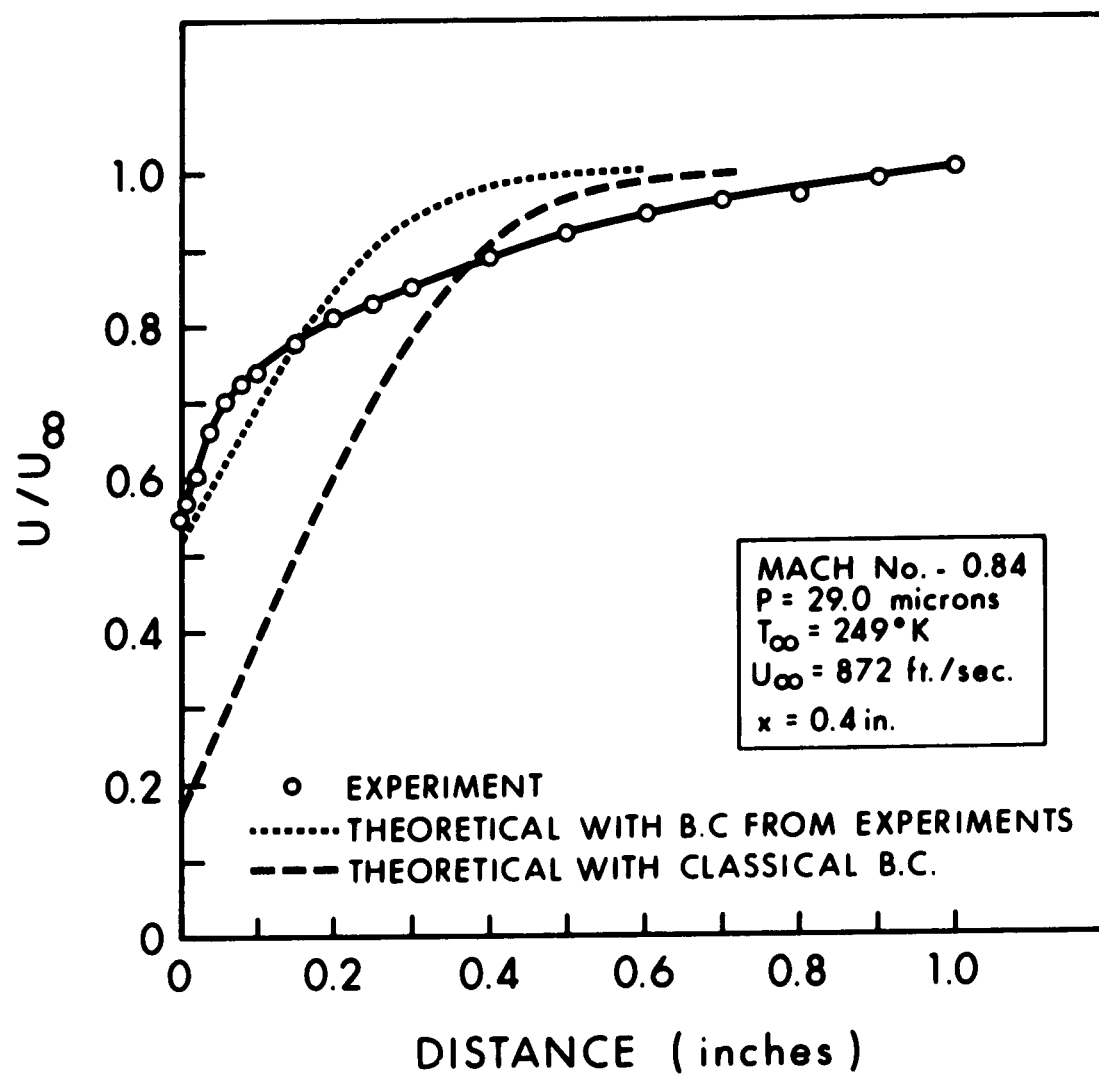


FIGURE 28 VELOCITY PROFILE ON A FLAT PLATE:
P = 29.0 MICRONS x = 0.4 INCHES

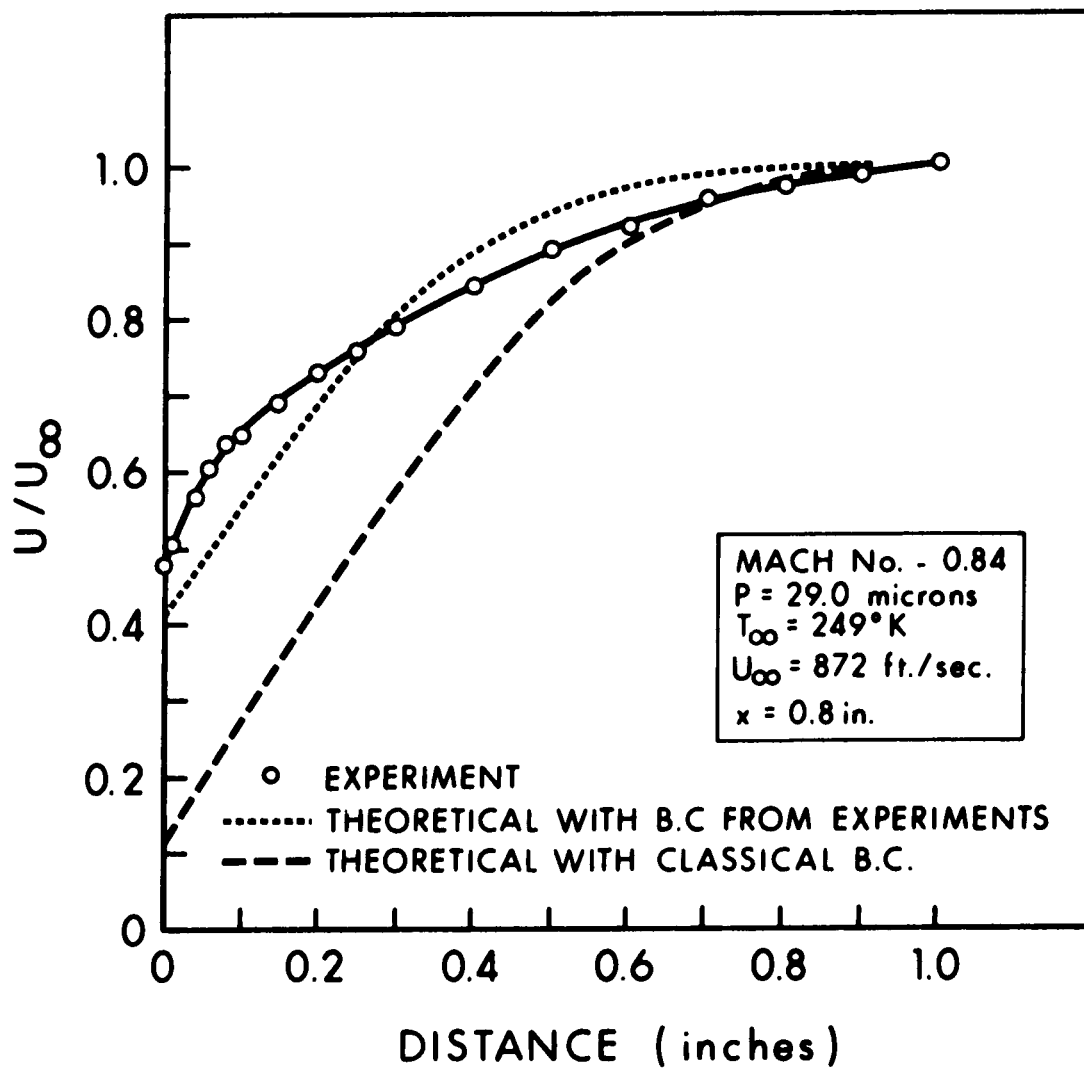


FIGURE 29 VELOCITY PROFILE ON A FLAT PLATE:
 P = 29.0 MICRONS x = 0.8 INCHES

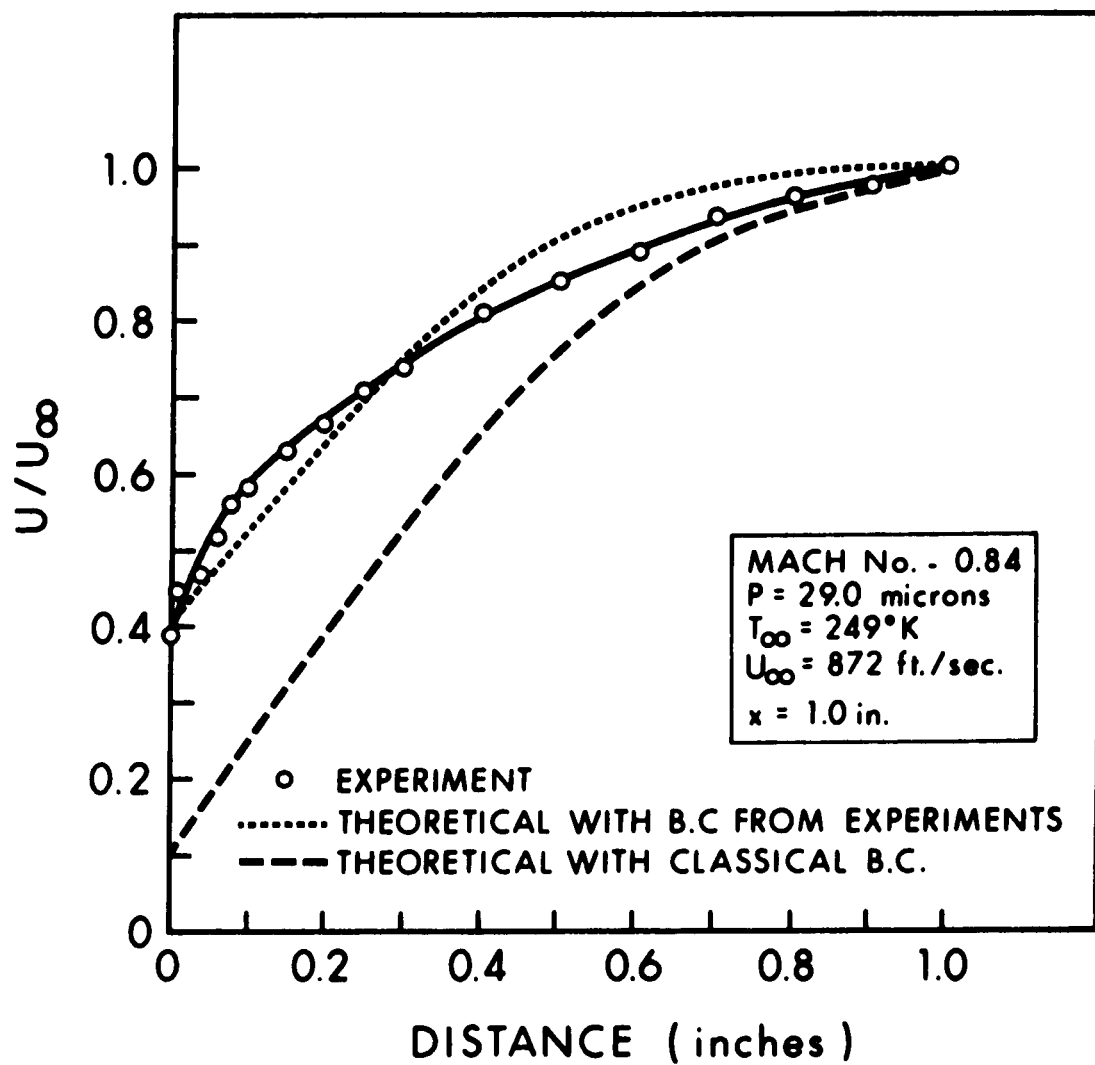


FIGURE 30 VELOCITY PROFILE ON A FLAT PLATE:
P = 29.0 MICRONS $x = 1.0$ INCHES

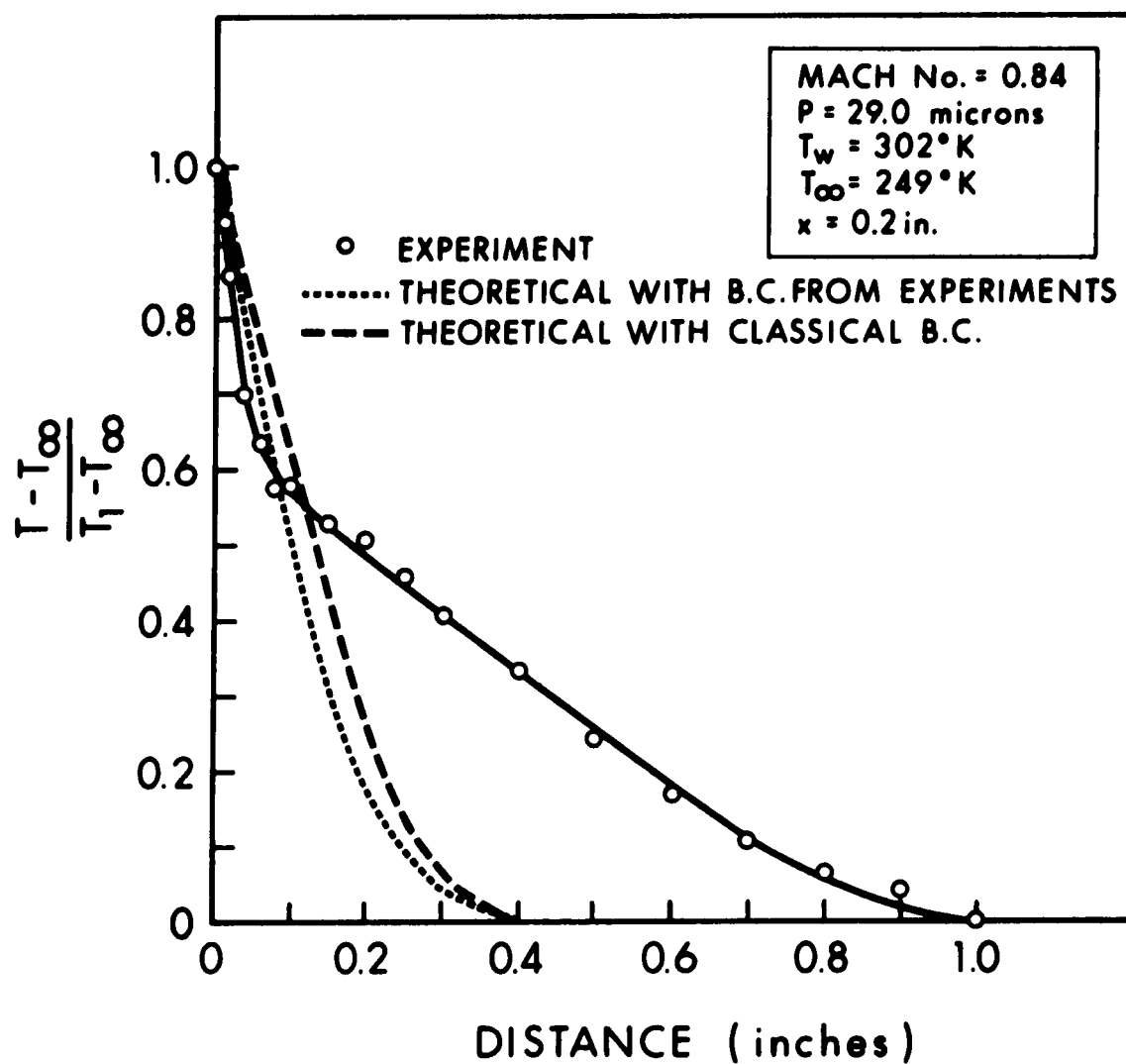


FIGURE 31 TEMPERATURE PROFILE ON A FLAT PLATE:
 P = 29.0 MICRONS $x = 0.2$ INCHES

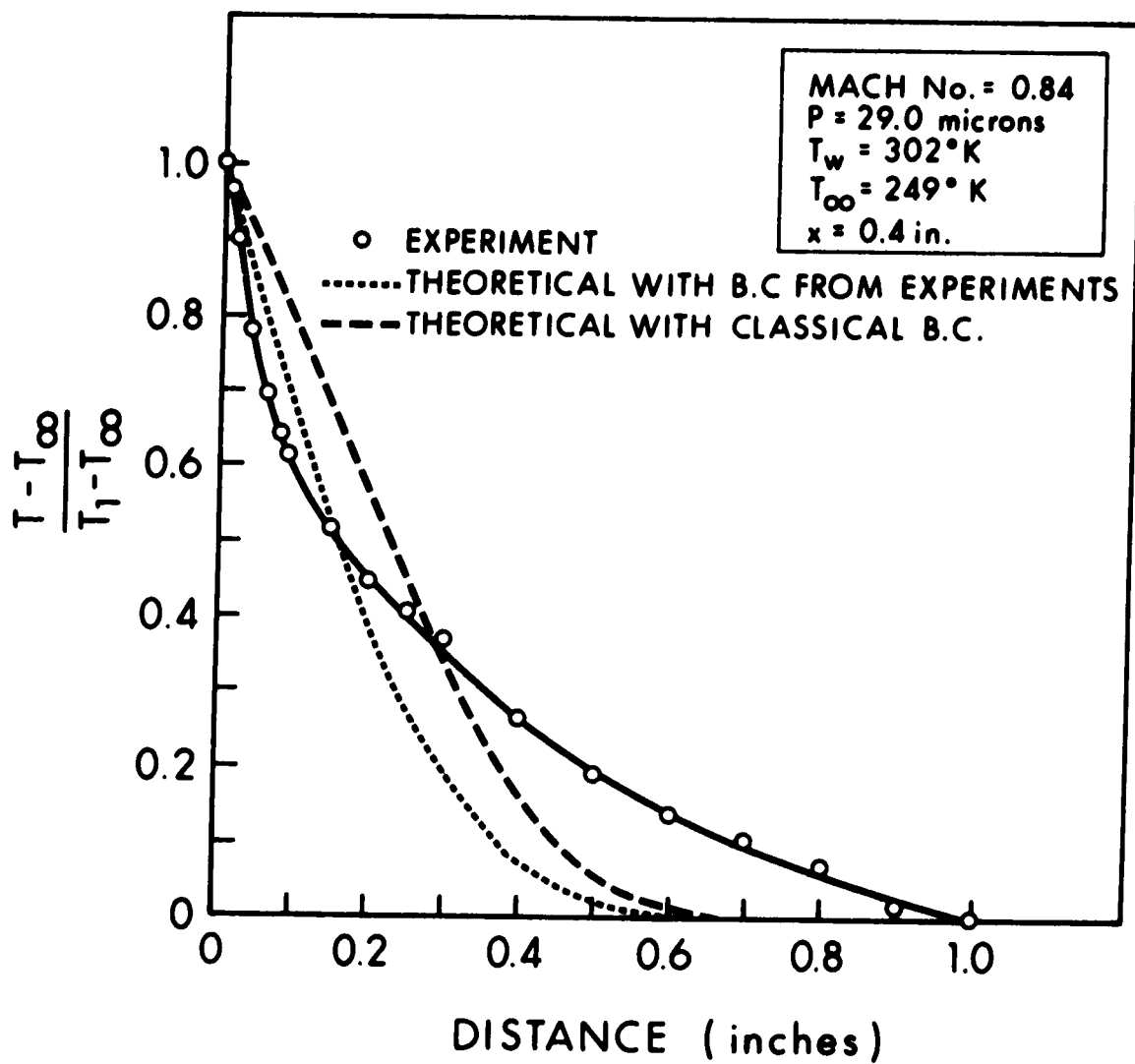


FIGURE 32 TEMPERATURE PROFILE ON A FLAT PLATE:
P = 29.0 MICRONS x = 0.4 INCHES

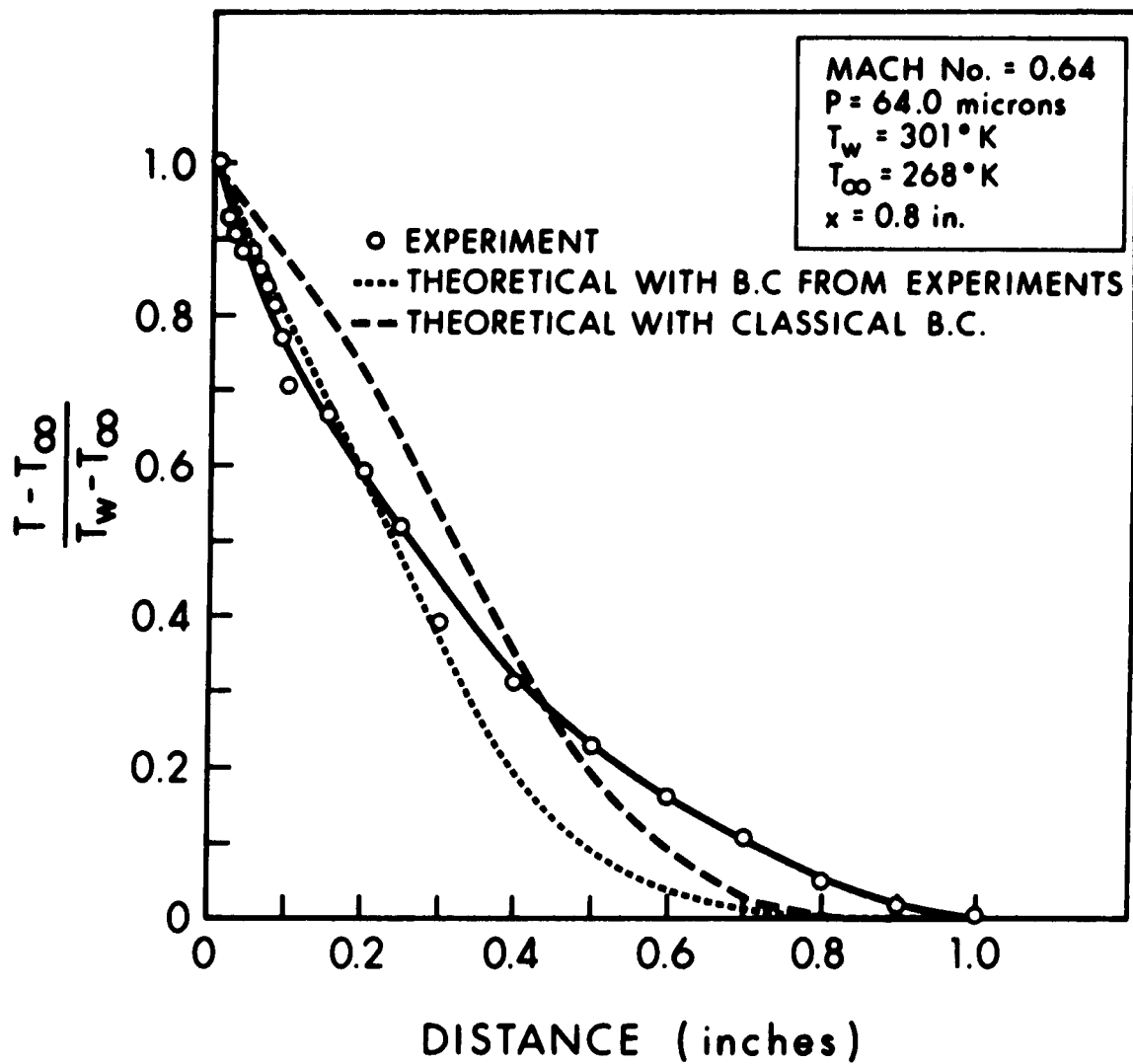


FIGURE 33 TEMPERATURE PROFILE ON A FLAT PLATE:
 P = 29.0 MICRONS x = 0.8 INCHES

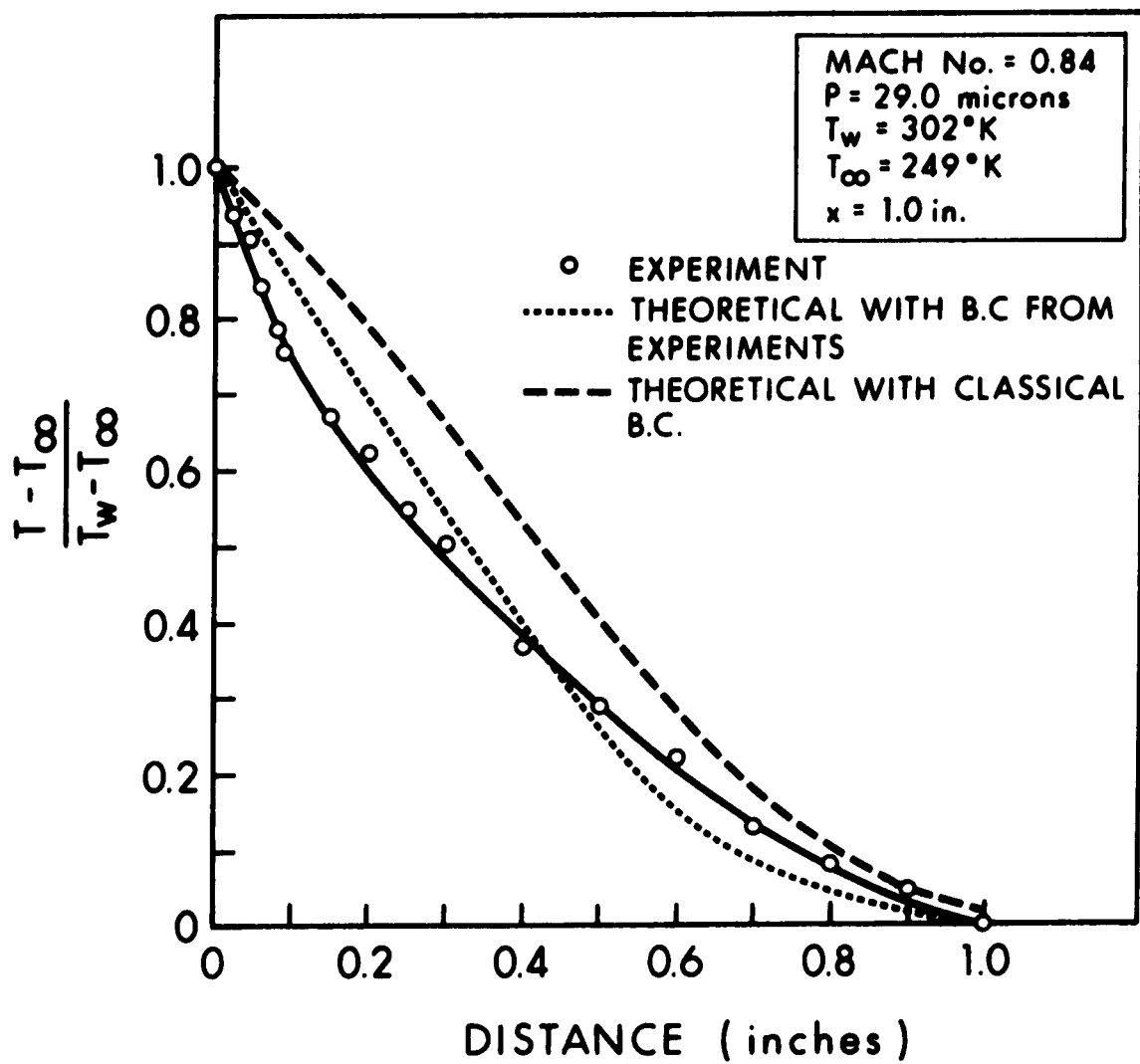


FIGURE 34 TEMPERATURE PROFILE ON A FLAT PLATE:
P = 29.0 MICRONS x = 1.0 INCHES

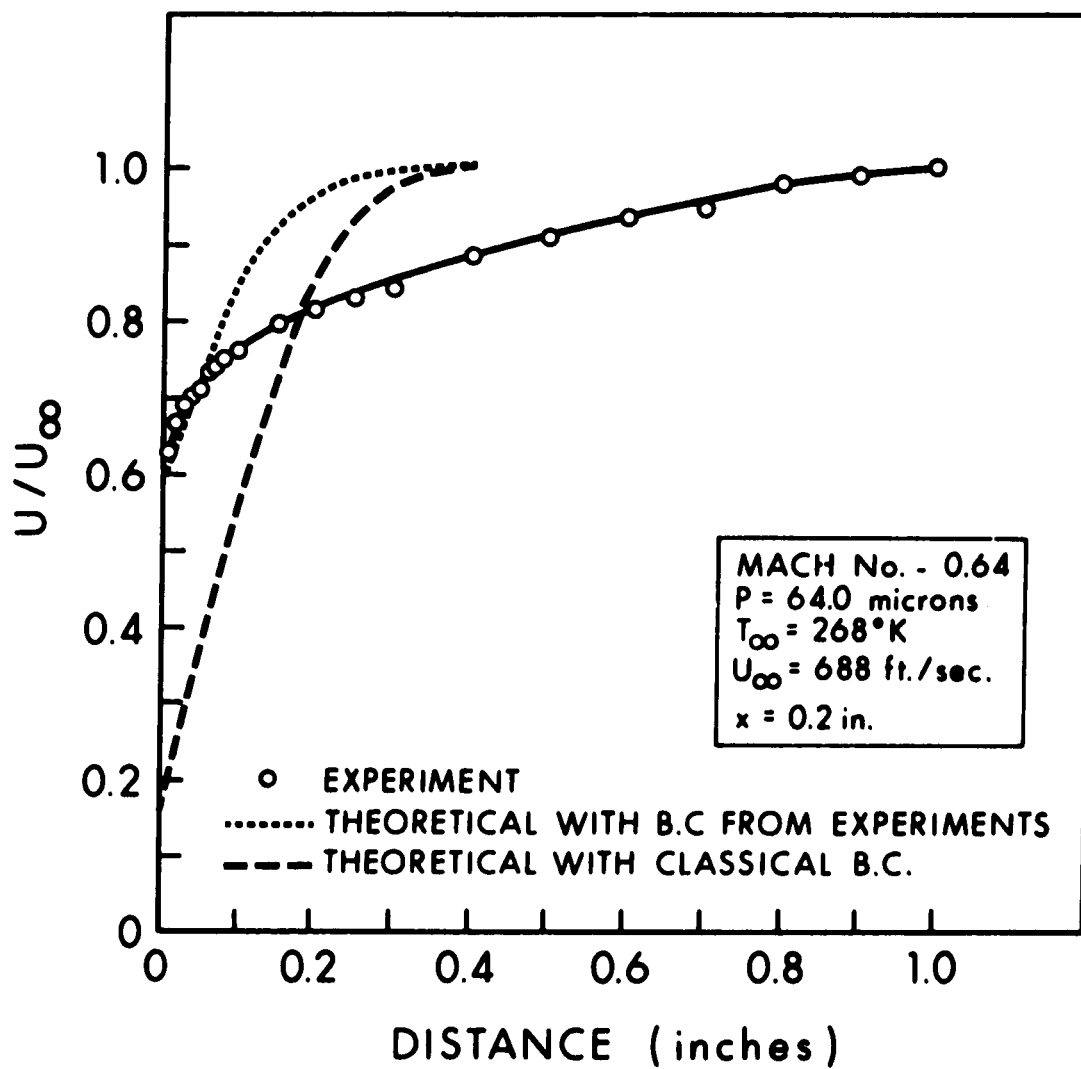


FIGURE 35 VELOCITY PROFILE ON A FLAT PLATE:
 $P = 64.0$ MICRONS $x = 0.2$ INCHES

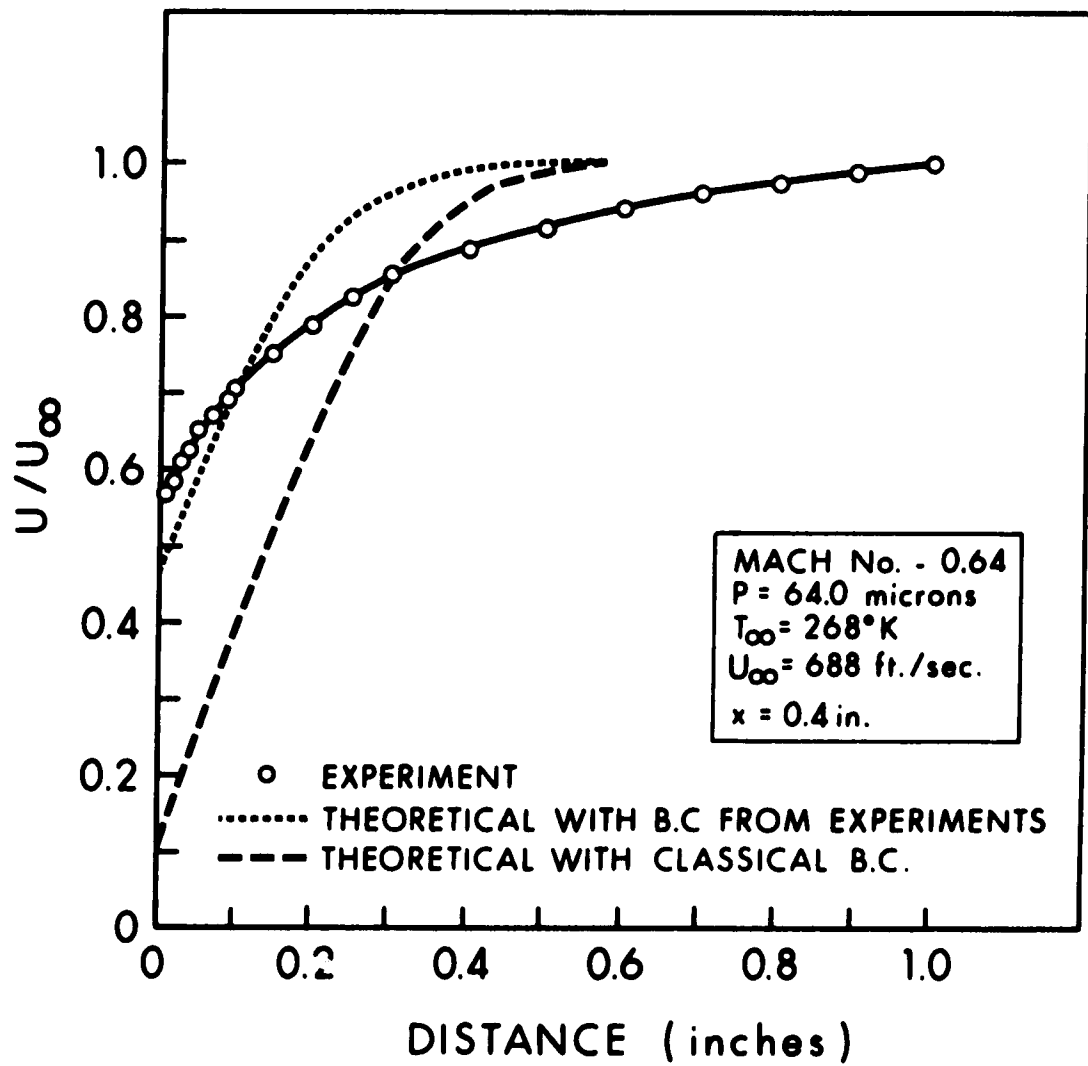


FIGURE 36 VELOCITY PROFILE ON A FLAT PLATE:
 $P = 64.0$ MICRONS $x = 0.4$ INCHES

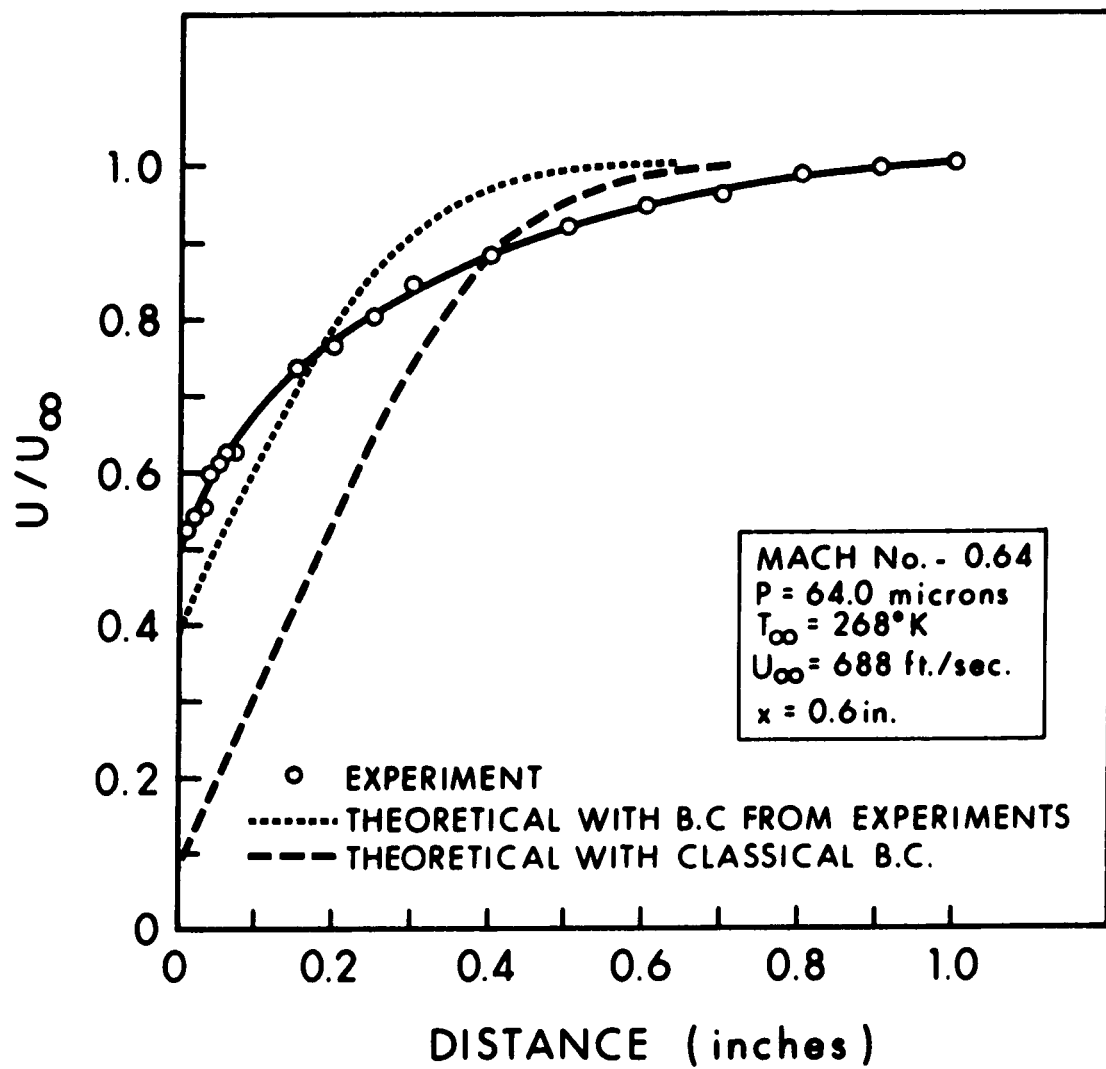


FIGURE 37 VELOCITY PROFILE ON A FLAT PLATE:
 $P = 64.0$ MICRONS $x = 0.6$ INCHES

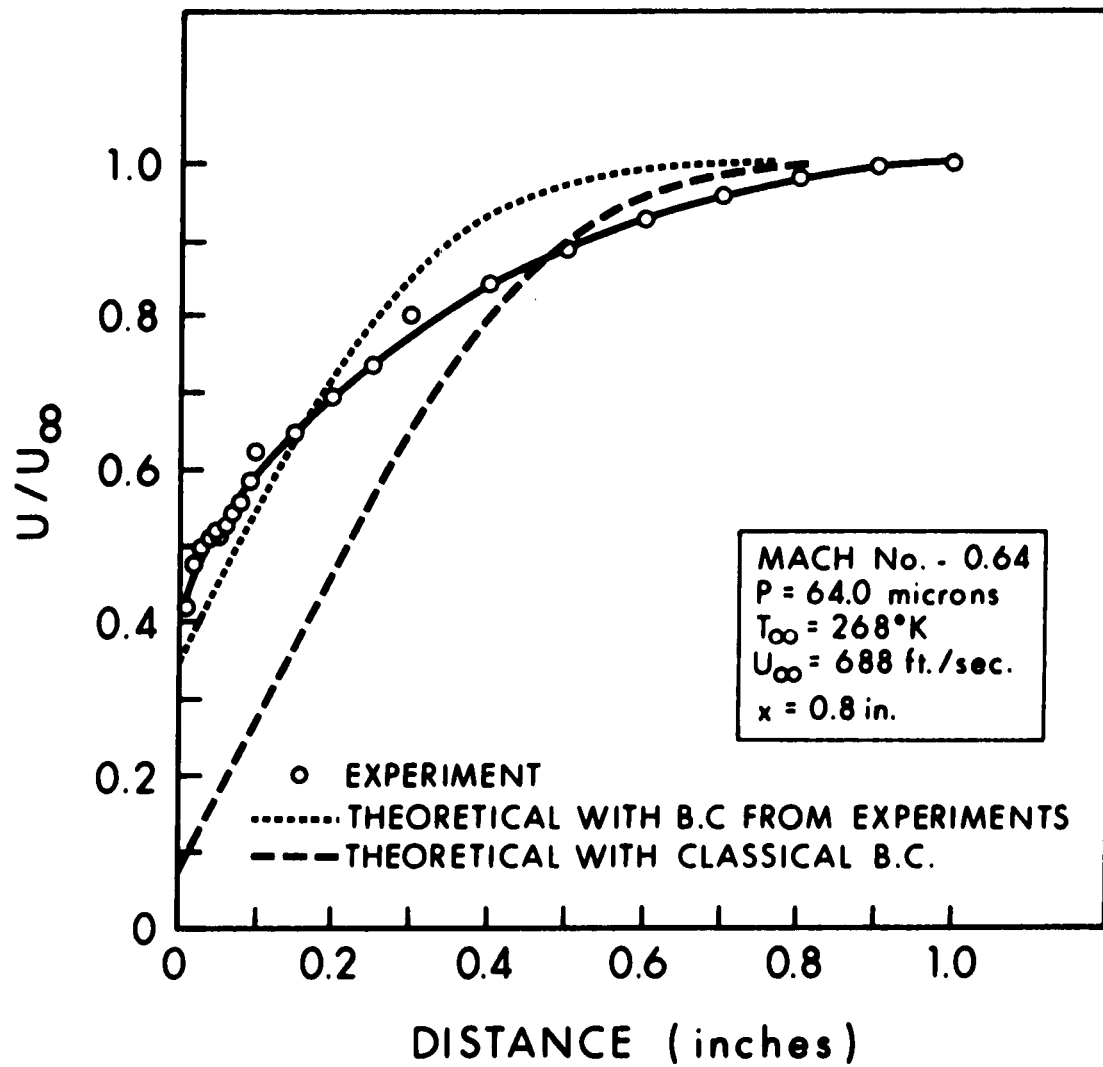


FIGURE 38 VELOCITY PROFILE ON A FLAT PLATE:
 $P = 64.0$ MICRONS $x = 0.8$ INCHES

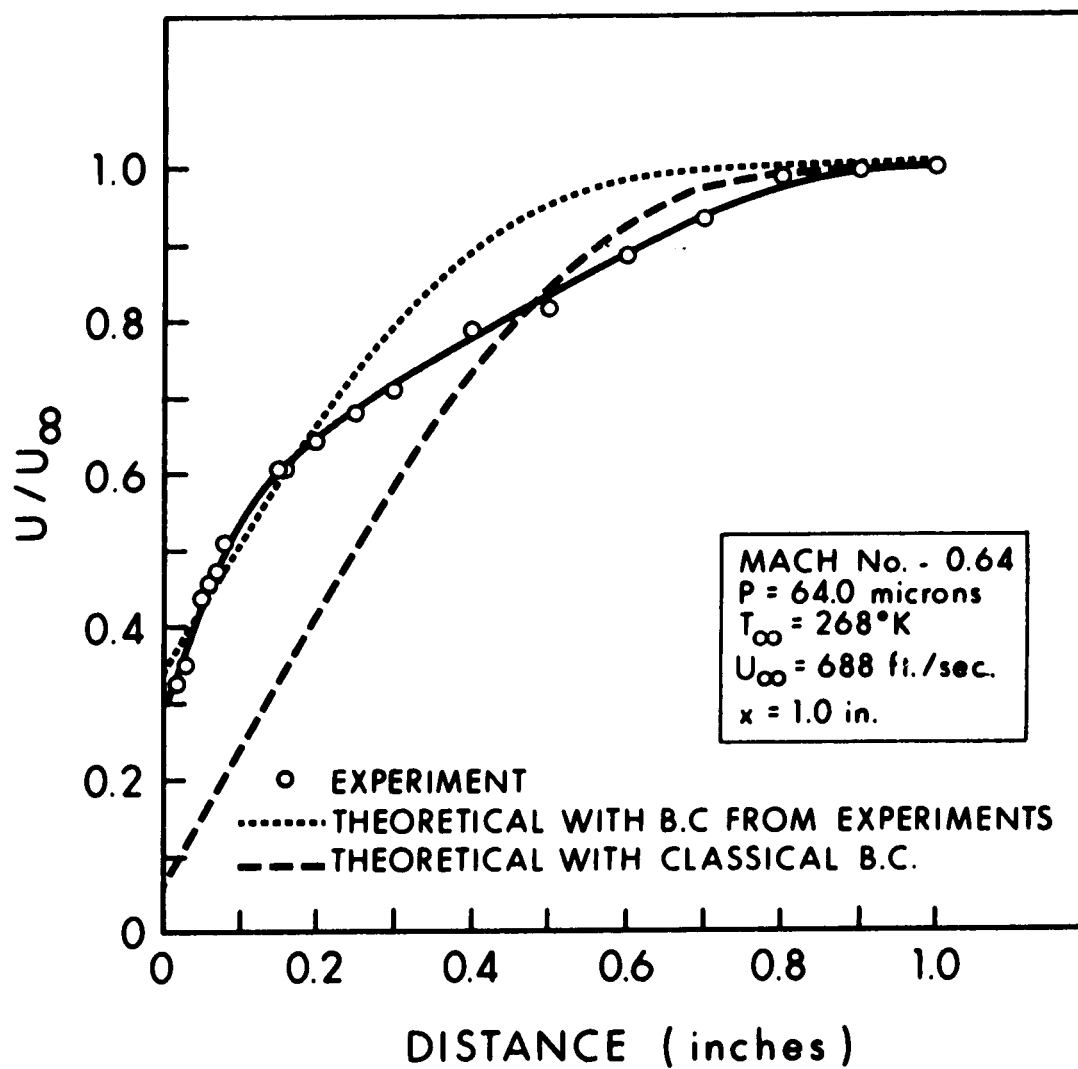


FIGURE 39 VELOCITY PROFILE ON A FLAT PLATE:
 $P = 64.0$ MICRONS $x = 1.0$ INCHES

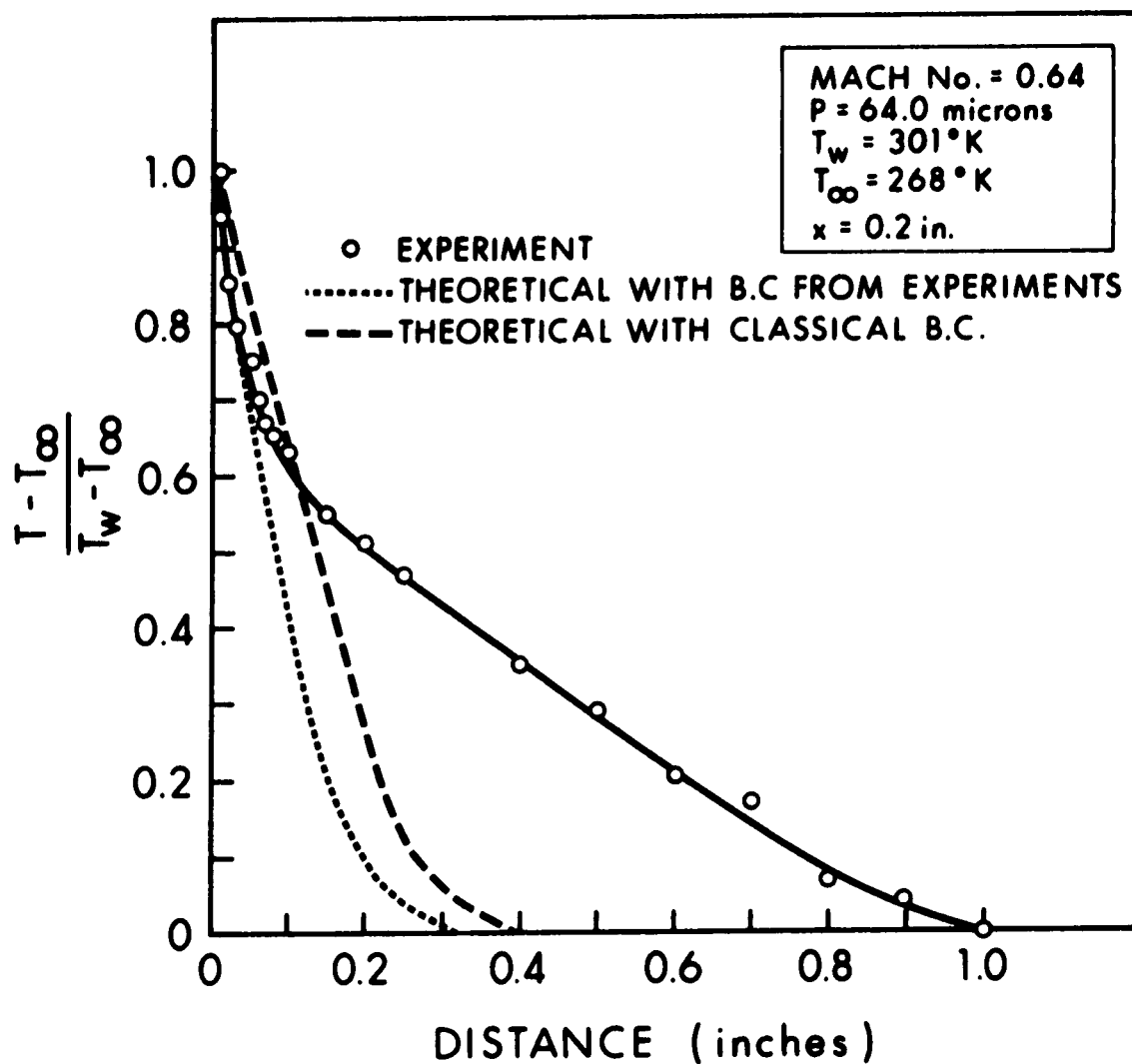


FIGURE 40 TEMPERATURE PROFILE ON A FLAT PLATE:
 P = 64.0 MICRONS x = 0.2 INCHES

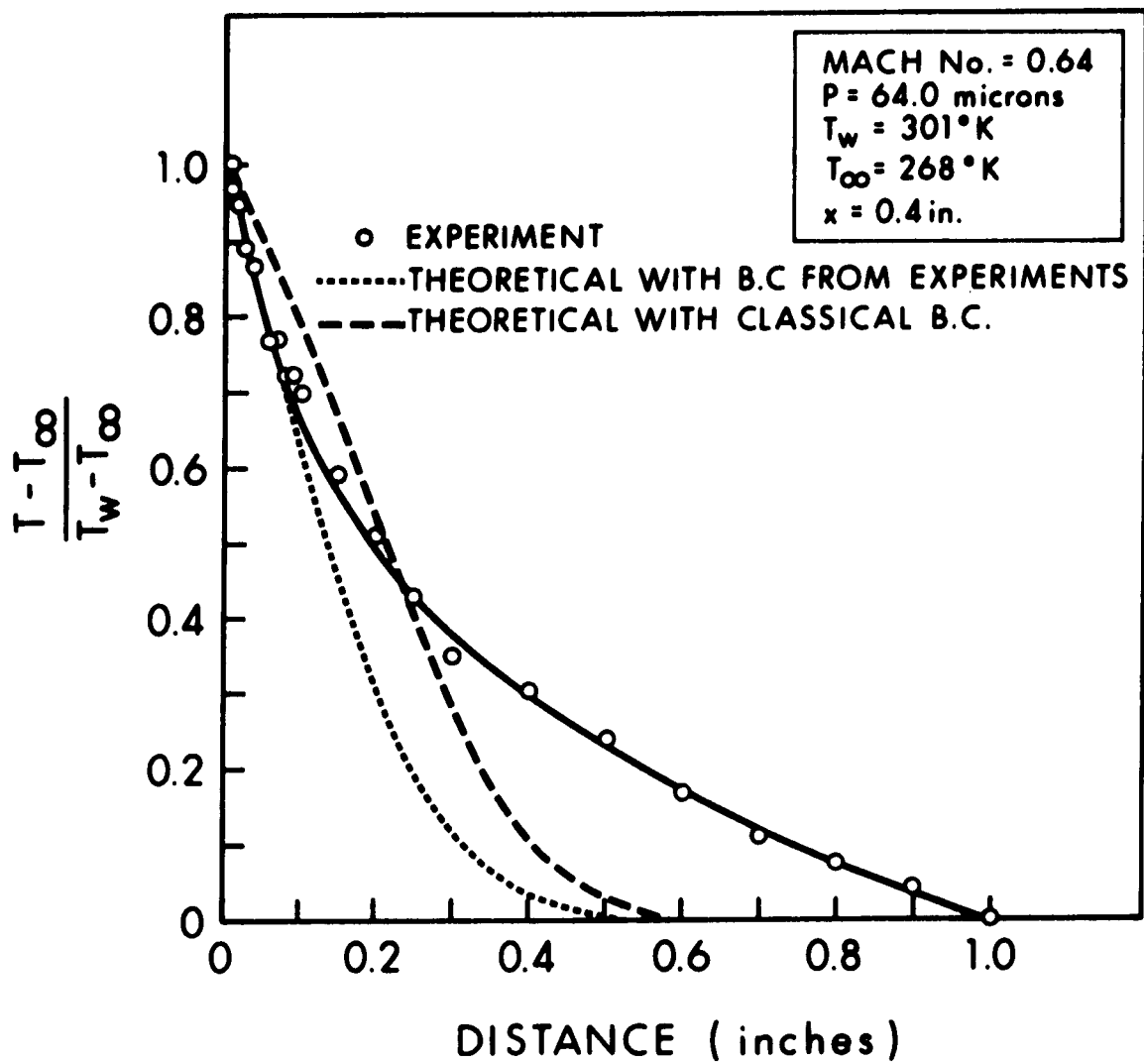


FIGURE 41 TEMPERATURE PROFILE ON A FLAT PLATE:
P = 64.0 MICRONS x = 0.4 INCHES

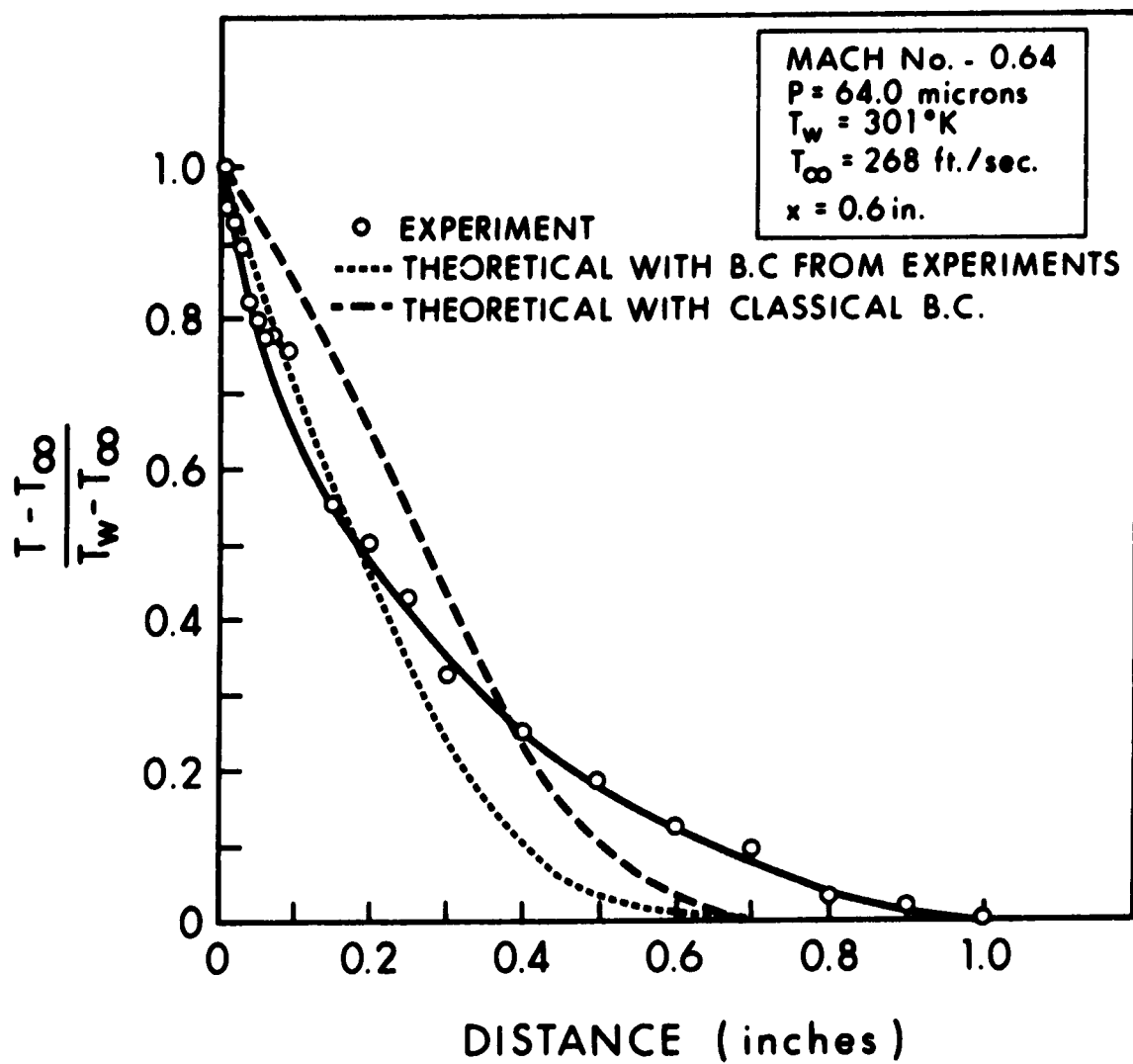


FIGURE 42 TEMPERATURE PROFILE ON A FLAT PLATE:
P = 64.0 MICRONS x = 0.6 INCHES

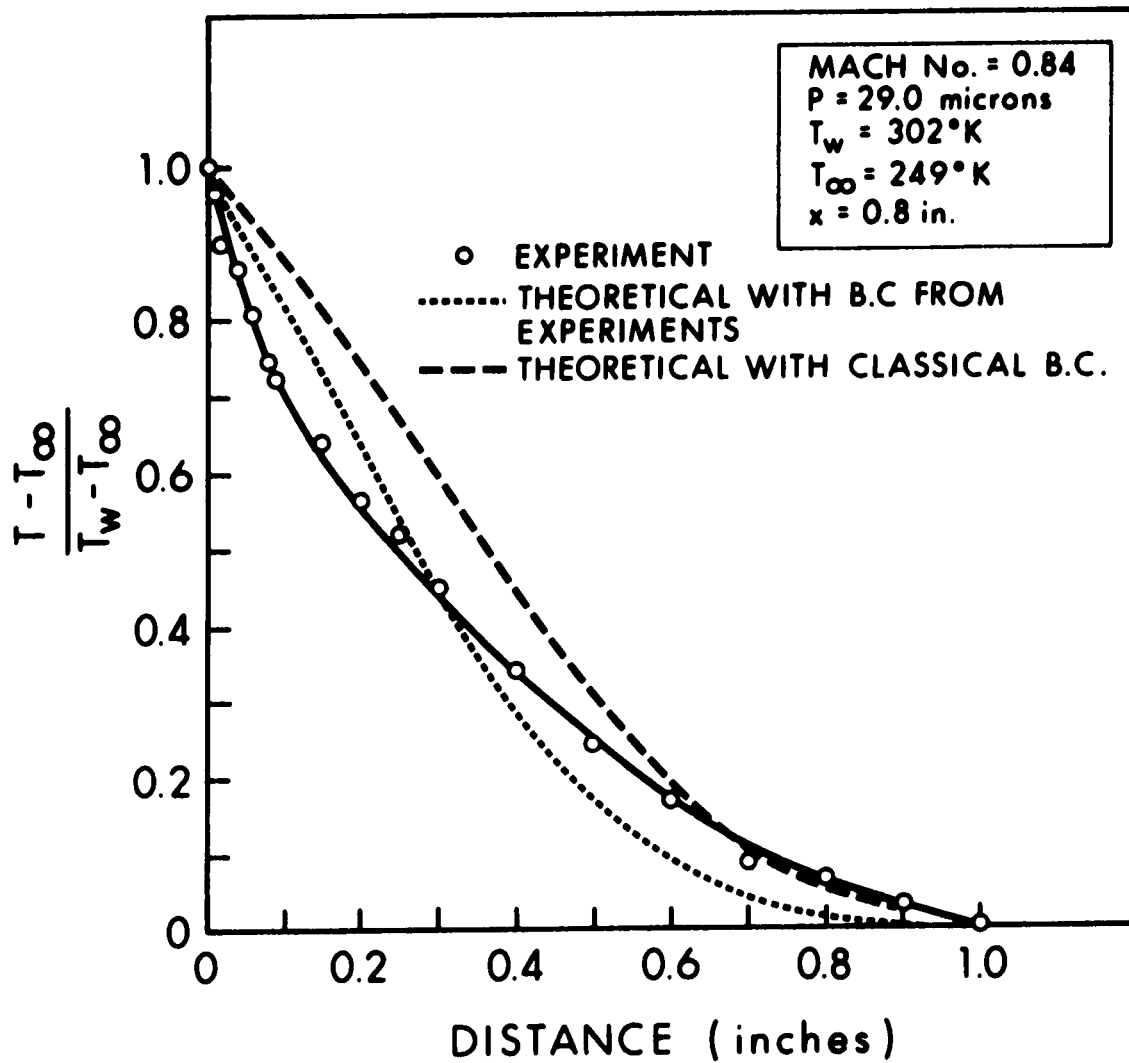


FIGURE 43 TEMPERATURE PROFILE ON A FLAT PLATE:
 $P = 64.0$ MICRONS $x = 0.8$ INCHES

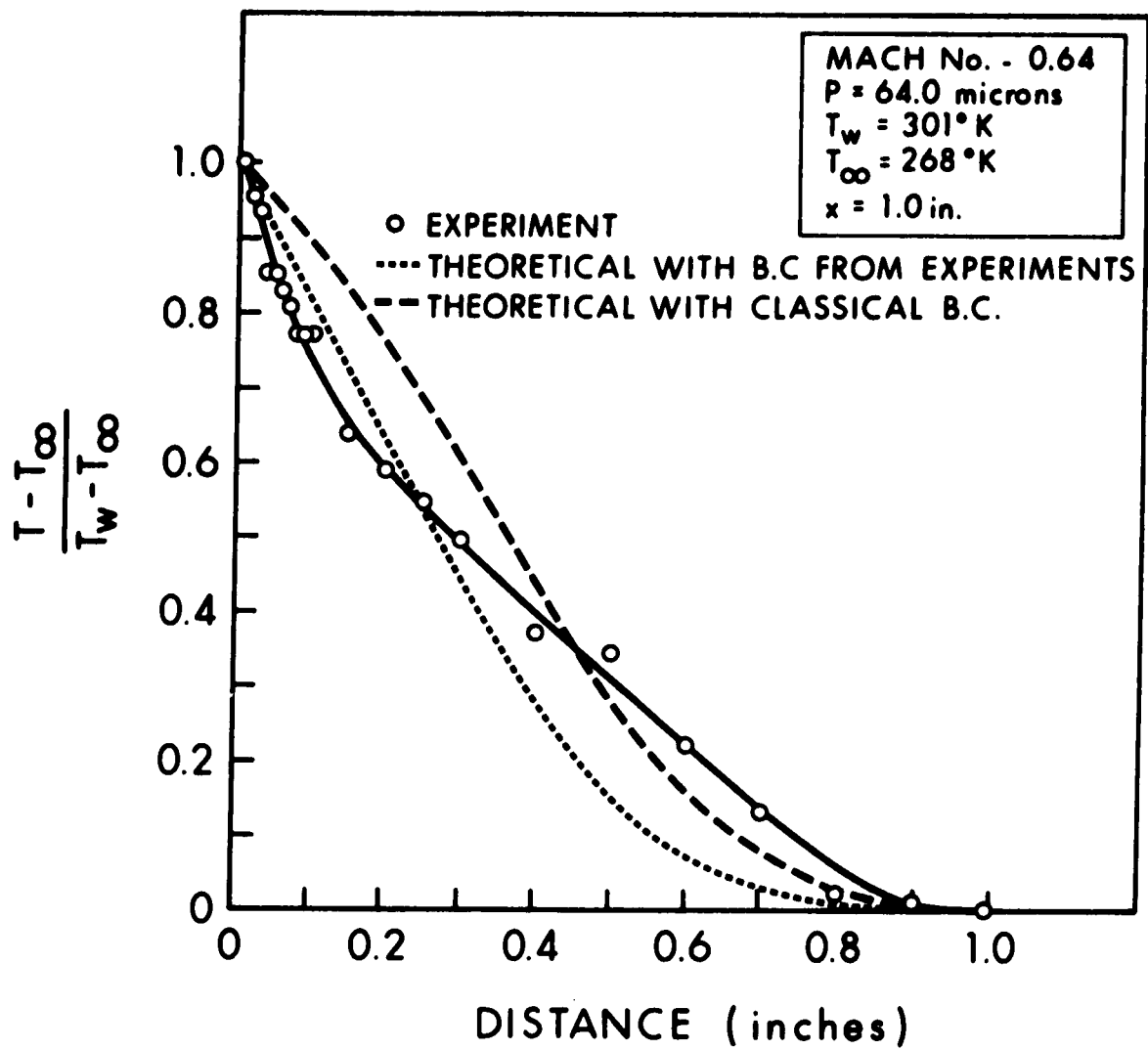


FIGURE 44 TEMPERATURE PROFILE ON A FLAT PLATE:
P = 64.0 MICRONS x = 1.0 INCHES

TABLE 1

EXPERIMENTAL DATA AT THE WALL (COOLED PLATE)

$P = 64.7$ microns $T_{\infty} = 267.9^{\circ}\text{K}$
 $U_{\infty} = 689$ ft/sec $T_w = 82.1^{\circ}\text{K}$

Distance from Leading Edge inches	P_t microns	$\frac{U}{U_{\infty}}$	T_c $^{\circ}\text{K}$	$\frac{T_1}{T_{\infty}}$
0.0	80.5	0.470	83.1	-
0.1	77.0	0.421	83.1	-
0.2	75.2	0.393	83.1	-
0.3	74.0	0.372	83.1	-
0.4	74.0	0.372	83.1	-
0.5	73.7	0.367	83.1	-
0.6	73.7	0.367	83.1	-
0.7	73.4	0.361	83.1	-
0.8	73.4	0.361	83.1	-
0.9	73.4	0.361	83.1	-
1.0	73.1	0.356	83.1	-

TABLE 2

EXPERIMENTAL DATA AT THE WALL (UNCOOLED PLATE)

$P = 30.4$ microns $T_{\infty} = 250.0^{\circ}\text{K}$

$U_{\infty} = 819$ ft/sec $T_w = 301.4^{\circ}\text{K}$

Distance from Leading Edge inches	P_t microns	$\frac{U}{U_{\infty}}$	T_c $^{\circ}\text{K}$	$\frac{T_1}{T_{\infty}}$
0.0	42.1	0.903	302.1	1.027
0.1	37.0	0.729	301.5	1.078
0.2	34.7	0.583	301.3	1.114
0.3	33.2	0.475	301.3	1.137
0.4	32.3	0.392	301.3	1.151
0.5	32.3	0.392	301.3	1.151
0.6	32.0	0.279	301.3	1.167
0.7	31.4	0.322	301.3	1.161
0.8	31.1	0.279	301.3	1.167
0.9	31.1	0.279	301.3	1.167
1.0	31.1	0.279	301.4	1.167

TABLE 3

EXPERIMENTAL DATA AT THE WALL (UNCOOLED PLATE)

$P = 65.0$ microns $T_{\infty} = 269.5^{\circ}\text{K}$
 $U_{\infty} = 673$ ft/sec $T_w = 300.5^{\circ}\text{K}$

Distance from Leading Edge inches	P_t microns	$\frac{U}{U_{\infty}}$	T_c $^{\circ}\text{K}$	$\frac{T_1}{T_{\infty}}$
0.0	79.9	0.893	301.6	1.016
0.1	72.8	0.669	300.8	1.057
0.2	70.1	0.550	300.7	1.075
0.3	69.5	0.518	300.6	1.080
0.4	68.9	0.485	300.6	1.084
0.5	68.0	0.428	300.6	1.091
0.6	66.8	0.336	300.6	1.100
0.7	66.8	0.336	300.6	1.100
0.8	66.8	0.336	300.6	1.100
0.9	66.8	0.336	300.6	1.100
1.0	66.8	0.336	300.6	1.101

TABLE 4

EXPERIMENTAL DATA AT P = 65.0 MICRONS (COOLED PLATE)

x = 0.2 inches $T_{\infty} = 263^{\circ}\text{K}$ $U_{\infty} = 664 \text{ ft/sec}$ $T_w = 82.7^{\circ}\text{K}$

Distance inches	P_t microns	$\frac{U}{U_{\infty}}$	T_c $^{\circ}\text{K}$	$\frac{T-T_{\infty}}{T_w-T_{\infty}}$
.004	76.7	0.503	117.7	0.855
.005	76.7	0.508	120.1	0.843
.006	76.7	0.509	120.5	0.841
.007	76.7	0.511	121.5	0.836
.008	76.7	0.515	123.0	0.828
.009	77.0	0.522	124.0	0.824
.01	77.6	0.536	125.6	0.819
.02	78.2	0.576	139.2	0.751
.03	78.5	0.603	149.6	7.000
.04	78.5	0.629	162.9	0.632
.05	78.5	0.635	166.1	0.616
.06	78.8	0.653	172.5	0.585
.07	79.0	0.670	178.5	0.556
.08	79.3	0.683	182.1	0.539
.09	79.3	0.692	186.8	0.516
.15	79.3	0.706	194.6	0.476
.20	79.6	0.794	241.7	0.240
.25	80.2	0.832	257.2	0.166
.30	80.5	0.856	267.9	0.115
.40	81.4	0.898	281.6	0.053
.50	82.6	0.936	288.7	0.026
.60	83.2	0.955	292.7	0.011
.70	83.8	0.971	295.0	0.004
.80	84.4	0.986	296.3	0.002
.90	84.7	0.993	297.1	0.003
1.00	85.0	1.000	297.6	0.000

TABLE 5

EXPERIMENTAL DATA AT P = 65.0 MICRONS (COOLED PLATE)

$x = 0.4$ inches $T_{\infty} = 263$ °K

$U_{\infty} = 664$ ft/sec $T_w = 82.7$ °K

Distance inches	P_t microns	$\frac{U}{U_{\infty}}$	T_c °K	$\frac{T - T_{\infty}}{T_w - T_{\infty}}$
.004	74.6	0.433	104.3	0.917
.005	74.6	0.435	105.1	0.912
.006	74.6	0.437	105.9	0.908
.007	74.6	0.443	109.0	0.892
.020	76.1	0.482	113.3	0.875
.030	76.7	0.535	113.5	0.773
.040	77.0	0.565	145.6	0.713
.050	77.3	0.574	147.2	0.706
.060	77.6	0.591	152.8	0.678
.070	77.6	0.604	159.5	0.644
.080	77.9	0.618	163.9	0.623
.090	77.9	0.632	171.0	0.586
.150	78.8	0.681	187.5	0.507
.200	78.8	0.713	205.8	0.414
.250	79.3	0.779	236.7	0.261
.300	80.2	0.822	250.3	0.199
.400	81.7	0.886	269.2	0.114
.500	82.3	0.918	280.5	0.062
.600	83.5	0.955	287.2	0.038
.700	84.1	0.974	291.1	0.023
.800	84.4	0.984	293.5	0.013
.900	84.7	0.992	295.0	0.008
1.000	85.0	1.000	295.8	0.006

TABLE 6

EXPERIMENTAL DATA AT P = 65.0 MICRONS (COOLED PLATE)

$$x = 0.6 \text{ inches} \quad T_{\infty} = 263 \text{ }^{\circ}\text{K}$$

$$U_{\infty} = 664 \text{ ft/sec} \quad T_w = 82.7^{\circ}\text{K}$$

Distance inches	P _t microns	$\frac{U}{U_{\infty}}$	T _c °K	$\frac{T-T_{\infty}}{T_w-T_{\infty}}$
.004	74.0	0.416	103.1	0.920
.005	74.0	0.423	106.3	0.903
.006	74.3	0.437	110.1	0.884
.007	74.3	0.445	114.1	0.863
.008	74.3	0.446	114.9	0.859
.009	74.3	0.452	117.7	0.844
.010	74.6	0.464	120.7	0.830
.020	75.2	0.497	130.9	0.779
.030	75.5	0.517	137.9	0.744
.040	75.8	0.534	143.5	0.716
.050	75.8	0.543	148.5	0.690
.060	76.4	0.565	153.1	0.669
.070	76.4	0.576	159.1	0.639
.150	77.9	0.633	172.0	0.580
.200	78.5	0.685	193.2	0.475
.250	79.3	0.776	234.2	0.272
.300	80.2	0.812	243.5	0.230
.400	81.4	0.860	256.2	0.174
.500	82.6	0.910	270.5	0.112
.600	83.2	0.939	280.0	0.068
.700	84.4	0.975	285.9	0.048
.800	84.7	0.987	289.7	0.031
.900	85.0	0.998	292.1	0.021
1.000	85.0	1.000	293.5	0.014

TABLE 7

EXPERIMENTAL DATA AT $P = 65.0$ MICRONS (COOLED PLATE)

$$x = 0.8 \text{ inches} \quad T_{\infty} = 263 \text{ }^{\circ}\text{K}$$

$$U_{\infty} = 664 \text{ ft/sec} \quad T_w = 82.7^{\circ}\text{K}$$

Distance inches	P_t microns	$\frac{U}{U_{\infty}}$	T_c $^{\circ}\text{K}$	$\frac{T-T_{\infty}}{T_w-T_{\infty}}$
.004	72.8	0.394	102.6	0.919
.005	72.8	0.402	106.5	0.899
.006	72.8	0.410	110.7	0.877
.007	72.8	0.415	113.7	0.861
.008	72.8	0.420	116.6	0.846
.009	72.8	0.424	118.7	0.835
.010	72.8	0.427	120.4	0.826
.020	73.1	0.447	127.1	0.792
.030	73.1	0.451	129.7	0.778
.040	73.1	0.463	136.5	0.742
.050	74.3	0.502	141.9	0.720
.060	74.3	0.509	145.8	0.699
.070	74.3	0.519	151.9	0.667
.100	74.6	0.561	172.5	0.562
.150	75.5	0.599	181.7	0.519
.200	76.7	0.650	194.5	0.460
.250	77.9	0.728	223.9	0.316
.300	79.0	0.778	236.6	0.260
.400	80.8	0.836	246.8	0.220
.500	82.0	0.888	262.6	0.149
.600	82.9	0.926	273.7	0.100
.700	84.4	0.970	281.2	0.074
.800	84.4	0.979	286.1	0.049
.900	84.7	0.990	289.3	0.036
1.000	85.0	1.000	291.5	0.027

TABLE 8

EXPERIMENTAL DATA AT P = 65.0 MICRONS (COOLED PLATE)

$x = 1.0$ inches $T_{\infty} = 263$ °K
 $U_{\infty} = 664$ ft/sec $T_w = 82.7$ °K

Distance inches	P_t microns	$\frac{U}{U_{\infty}}$	T_c °K	$\frac{T - T_{\infty}}{T_w - T_{\infty}}$
.004	71.6	0.374	100.8	0.927
.006	71.6	0.386	107.8	0.890
.008	71.6	0.394	112.0	0.868
.010	71.9	0.409	116.4	0.846
.020	71.9	0.427	126.8	0.791
.030	71.9	0.435	131.5	0.766
.040	72.2	0.451	136.4	0.742
.050	72.2	0.457	140.2	0.722
.060	72.2	0.467	146.6	0.688
.100	73.4	0.529	165.3	0.596
.150	74.3	0.578	180.9	0.520
.200	75.5	0.627	192.7	0.466
.250	76.4	0.689	216.8	0.347
.300	77.6	0.738	229.2	0.292
.400	79.9	0.811	240.3	0.252
.500	81.7	0.877	256.8	0.181
.600	82.3	0.910	268.4	0.127
.700	83.5	0.949	276.9	0.094
.800	83.8	0.965	282.8	0.067
.900	84.4	0.983	286.7	0.052
1.000	85.0	1.000	289.5	0.042

TABLE 9

EXPERIMENTAL DATA AT P = 29.0 MICRONS (UNCOOLED PLATE)

$$x = 0.2 \text{ inches} \quad T_{\infty} = 249 \text{ }^{\circ}\text{K}$$

$$U_{\infty} = 872 \text{ ft/sec} \quad T_w = 301.7^{\circ}\text{K}$$

Distance inches	P_t microns	$\frac{U}{U_{\infty}}$	T_c $^{\circ}\text{K}$	$\frac{T-T_{\infty}}{T_w-T_{\infty}}$
.002	34.4	0.614	301.8	1.000
.003	34.4	0.614	301.8	1.000
.004	34.4	0.614	301.8	1.000
.005	34.4	0.614	301.8	1.000
.006	34.4	0.614	301.8	1.000
.007	34.4	0.614	301.8	1.000
.008	34.8	0.630	301.8	0.963
.009	34.8	0.630	301.8	0.963
.010	35.1	0.645	301.8	0.927
.020	35.7	0.674	301.8	0.857
.030	36.3	0.702	301.9	0.792
.040	37.2	0.740	302.0	0.699
.050	37.9	0.764	302.0	0.635
.060	37.9	0.764	302.1	0.638
.070	38.2	0.775	302.1	0.607
.080	38.5	0.786	302.1	0.577
.090	38.5	0.786	302.2	0.579
.100	38.5	0.786	302.2	0.581
.150	39.1	0.808	302.5	0.530
.200	39.4	0.818	302.7	0.507
.250	40.0	0.838	303.0	0.457
.300	40.6	0.857	303.1	0.405
.400	41.6	0.885	303.5	0.335
.500	42.8	0.919	303.7	0.241
.600	43.7	0.942	303.9	0.172
.700	44.7	0.965	304.1	0.106
.800	45.3	0.979	304.2	0.063
.900	45.6	0.986	304.2	0.043
1.000	46.2	1.000	304.3	0.000

TABLE 10

EXPERIMENTAL DATA AT P = 29.0 MICRONS (UNCOOLED PLATE)

x = 0.4 inches $T_{\infty} = 249^{\circ}\text{K}$

$U_{\infty} = 872 \text{ ft/sec}$ $T_w = 301.7^{\circ}\text{K}$

Distance inches	P_t microns	$\frac{U}{U_{\infty}}$	T_c $^{\circ}\text{K}$	$\frac{T - T_{\infty}}{T_w - T_{\infty}}$
.002	32.3	0.548	301.6	1.000
.003	32.3	0.548	301.6	1.000
.004	32.3	0.548	301.6	1.000
.005	32.3	0.548	301.6	1.000
.006	32.3	0.548	301.6	1.000
.007	32.3	0.548	301.6	1.000
.008	32.3	0.548	301.6	1.000
.009	32.6	0.567	301.6	0.967
.010	32.6	0.567	301.6	0.967
.020	33.2	0.601	301.6	0.903
.030	34.1	0.647	301.6	0.811
.040	34.5	0.661	301.6	0.781
.050	34.8	0.675	301.7	0.753
.060	35.4	0.701	301.7	0.696
.070	35.7	0.713	301.7	0.668
.080	36.0	0.725	301.7	0.641
.090	36.3	0.737	301.7	0.615
.100	36.3	0.737	301.9	0.618
.150	37.5	0.782	302.0	0.518
.200	38.5	0.812	302.2	0.448
.250	39.1	0.831	302.4	0.405
.300	39.7	0.850	302.8	0.369
.400	41.3	0.892	303.0	0.265
.500	42.5	0.924	303.4	0.191
.600	43.4	0.946	303.6	0.135
.700	44.0	0.960	303.9	0.103
.800	44.7	0.974	304.1	0.069
.900	45.6	0.994	304.2	0.016
1.000	45.9	1.000	304.3	0.000

TABLE 11

EXPERIMENTAL DATA AT P = 29.0 MICRONS (UNCOOLED PLATE)

x = 0.8 inches $T_{\infty} = 249^{\circ}\text{K}$ $U_{\infty} = 872 \text{ ft/sec}$ $T_w = 301.7^{\circ}\text{K}$

Distance inches	P_t microns	$\frac{U}{U_{\infty}}$	T_c $^{\circ}\text{K}$	$\frac{T - T_{\infty}}{T_w - T_{\infty}}$
.002	32.6	0.482	301.5	1.000
.003	32.6	0.482	301.5	1.000
.004	32.6	0.482	301.5	1.000
.005	32.6	0.482	301.5	1.000
.006	32.6	0.482	301.5	1.000
.007	32.6	0.482	301.5	1.000
.008	32.6	0.482	301.5	1.000
.009	32.9	0.505	301.5	0.967
.010	32.9	0.505	301.5	0.967
.020	33.5	0.546	301.5	0.903
.030	33.5	0.546	301.5	0.903
.040	33.8	0.565	301.6	0.872
.050	34.1	0.584	301.6	0.841
.060	34.5	0.601	301.6	0.811
.070	34.8	0.618	301.6	0.781
.080	35.1	0.634	301.6	0.752
.090	35.4	0.650	301.6	0.723
.100	35.4	0.650	301.6	0.723
.150	36.3	0.693	301.7	0.643
.200	37.2	0.733	301.7	0.565
.250	37.9	0.757	302.0	0.519
.300	38.8	0.792	302.1	0.449
.400	40.3	0.844	302.5	0.342
.500	41.9	0.890	302.8	0.242
.600	43.1	0.924	303.1	0.168
.700	44.3	0.956	303.5	0.098
.800	45.0	0.971	303.7	0.066
.900	45.6	0.986	303.9	0.033
1.000	46.2	1.000	304.0	0.000

TABLE 12

EXPERIMENTAL DATA AT P = 29.0 MICRONS (UNCOOLED PLATE)

x = 1.0 inche $T_{\infty} = 249 \text{ }^{\circ}\text{K}$ $U_{\infty} = 872 \text{ ft/sec}$ $T_w = 301.7^{\circ}\text{K}$

Distance inches	P_t microns	$\frac{U}{U_{\infty}}$	T_c $^{\circ}\text{K}$	$\frac{T-T_{\infty}}{T_w-T_{\infty}}$
.002	32.6	0.387	301.4	1.000
.003	32.6	0.387	301.4	1.000
.004	32.6	0.387	301.4	1.000
.005	32.6	0.387	301.4	1.000
.006	32.6	0.387	301.4	1.000
.007	32.6	0.387	301.4	1.000
.008	32.6	0.387	301.4	1.000
.009	32.6	0.387	301.4	1.000
.010	33.2	0.446	301.4	0.935
.020	33.2	0.446	301.4	0.935
.030	33.5	0.472	301.4	0.904
.040	33.5	0.472	301.4	0.904
.050	33.8	0.496	301.4	0.873
.060	34.1	0.518	301.4	0.843
.070	34.5	0.540	301.4	0.814
.080	34.8	0.560	301.5	0.785
.090	35.1	0.580	301.5	0.756
.100	35.1	0.580	301.5	0.756
.150	36.0	0.633	301.5	0.673
.200	36.6	0.665	301.6	0.623
.250	37.5	0.709	301.7	0.549
.300	38.2	0.737	301.9	0.503
.400	40.0	0.809	302.2	0.372
.500	41.3	0.852	302.5	0.293
.600	42.5	0.892	302.8	0.219
.700	44.0	0.936	303.2	0.130
.800	45.0	0.961	303.4	0.080
.900	45.6	0.977	303.6	0.048
1.000	46.5	1.000	303.7	0.000

TABLE 13

EXPERIMENTAL DATA AT $P = 64.0$ MICRONS (UNCOOLED PLATE)

$$x = 0.2 \text{ inches} \quad T_{\infty} = 268 \text{ }^{\circ}\text{K}$$

$$U_{\infty} = 688 \text{ ft/sec} \quad T_w = 300.5^{\circ}\text{K}$$

Distance inches	P_t microns	$\frac{U}{U_{\infty}}$	T_c $^{\circ}\text{K}$	$\frac{T - T_{\infty}}{T_w - T_{\infty}}$
.002	70.7	0.608	300.6	1.000
.003	70.4	0.595	300.6	1.000
.004	70.4	0.595	300.6	1.000
.005	70.7	0.608	300.6	1.000
.006	70.7	0.608	300.6	1.000
.007	70.7	0.608	300.6	1.000
.008	70.7	0.608	300.6	1.000
.009	71.0	0.620	300.6	0.970
.010	71.3	0.632	300.6	0.940
.020	72.2	0.667	300.6	0.853
.030	72.8	0.689	300.6	0.797
.040	73.1	0.700	300.8	0.778
.050	73.4	0.710	300.8	0.752
.060	74.0	0.731	300.9	0.699
.070	74.3	0.740	300.9	0.672
.080	74.6	0.750	301.0	0.650
.090	74.6	0.750	301.1	0.655
.100	74.9	0.760	301.2	0.633
.150	76.1	0.796	301.6	0.548
.200	76.7	0.814	301.9	0.510
.250	77.3	0.831	302.2	0.473
.300	77.6	0.840	302.8	0.478
.400	79.3	0.886	303.3	0.353
.500	80.2	0.908	303.5	0.293
.600	81.4	0.936	303.7	0.207
.700	82.0	0.950	303.9	0.171
.800	83.5	0.982	303.9	0.063
.900	83.8	0.990	304.0	0.043
1.000	84.4	1.000	304.0	0.000

TABLE 14

EXPERIMENTAL DATA AT P = 64.0 MICRONS (UNCOOLED PLATE)

x = 0.4 inches $T_{\infty} = 268^{\circ}\text{K}$ $U_{\infty} = 688 \text{ ft/sec}$ $T_w = 300.5^{\circ}\text{K}$

Distance inches	P_t microns	$\frac{U}{U_{\infty}}$	T_c $^{\circ}\text{K}$	$\frac{T-T_{\infty}}{T_w-T_{\infty}}$
.002	69.8	0.559	300.5	1.000
.003	69.5	0.545	300.5	1.028
.004	69.5	0.545	300.5	1.028
.005	69.8	0.559	300.5	1.000
.006	69.8	0.559	300.5	1.000
.007	69.8	0.559	300.5	1.000
.008	69.8	0.559	300.5	1.000
.009	69.8	0.559	300.5	1.000
.010	70.1	0.573	300.5	0.972
.020	70.4	0.586	300.5	0.947
.030	71.0	0.612	300.6	0.893
.040	71.3	0.625	300.6	0.866
.050	71.9	0.648	300.6	0.816
.060	72.5	0.671	300.7	0.766
.070	72.5	0.671	300.7	0.766
.080	73.1	0.693	300.7	0.718
.090	73.1	0.693	300.8	0.722
.100	73.4	0.703	300.8	0.697
.150	74.9	0.753	301.2	0.589
.200	76.1	0.789	301.6	0.510
.250	77.3	0.824	301.9	0.430
.300	78.5	0.856	302.1	0.350
.400	79.6	0.887	303.0	0.300
.500	80.8	0.916	303.5	0.237
.600	82.0	0.943	303.8	0.166
.700	82.9	0.963	303.9	0.113
.800	83.5	0.976	304.0	0.074
.900	84.1	0.988	304.1	0.039
1.000	84.7	1.000	304.1	0.000

TABLE 15

EXPERIMENTAL DATA AT $P = 64.0$ MICRONS (UNCOOLED PLATE)

$x = 0.6$ inches $T_{\infty} = 268$ °K
 $U_{\infty} = 688$ ft/sec $T_w = 300.5$ °K

Distance inches	P_t microns	$\frac{U}{U_{\infty}}$	T_c °K	$\frac{T - T_{\infty}}{T - T_{\infty}}$
.002	68.6	0.495	300.6	1.000
.003	68.6	0.495	300.6	1.000
.004	68.6	0.495	300.6	1.000
.005	68.6	0.495	300.6	1.000
.006	68.6	0.495	300.6	1.000
.007	68.3	0.478	300.6	1.027
.008	68.9	0.512	300.6	0.974
.009	68.9	0.512	300.6	0.974
.010	69.2	0.527	300.6	0.948
.020	69.5	0.542	300.6	0.922
.030	69.8	0.557	300.6	0.896
.040	70.7	0.598	300.6	0.820
.050	71.0	0.611	300.6	0.798
.060	71.3	0.624	300.6	0.774
.070	71.3	0.624	300.7	0.775
.080	71.3	0.624	300.7	0.775
.090	71.6	0.636	300.7	0.754
.100	71.6	0.636	300.8	0.755
.150	74.3	0.735	301.0	0.555
.200	75.2	0.764	301.3	0.501
.250	76.4	0.801	301.7	0.428
.300	77.9	0.843	301.9	0.331
.400	79.3	0.883	302.4	0.250
.500	80.8	0.920	303.2	0.186
.600	82.0	0.948	303.6	0.126
.700	82.6	0.962	303.9	0.099
.800	83.8	0.988	304.1	0.033
.900	84.1	0.994	304.1	0.018
1.000	84.4	1.000	304.1	0.000

TABLE 16

EXPERIMENTAL DATA AT $P = 64.0$ MICRONS (UNCOOLED PLATE) $x = 0.8$ inches $T_{\infty} = 268$ °K $U_{\infty} = 688$ ft/sec $T_w = 300.5$ °K

Distance inches	P_t microns	$\frac{U}{U_{\infty}}$	T_c °K	$\frac{T - T_{\infty}}{T_w - T_{\infty}}$
.002	67.4	0.422	300.6	1.000
.003	67.1	0.401	300.6	1.025
.004	67.1	0.401	300.6	1.025
.005	67.1	0.401	300.6	1.025
.006	67.1	0.401	300.6	1.025
.007	67.1	0.401	300.6	1.025
.008	67.1	0.401	300.6	1.025
.009	67.7	0.442	300.6	0.975
.010	67.4	0.422	300.6	1.000
.020	68.3	0.478	300.6	0.928
.030	68.6	0.495	300.6	0.904
.040	68.9	0.512	300.6	0.880
.050	68.9	0.512	300.6	0.881
.060	69.2	0.527	300.6	0.857
.070	69.5	0.542	300.6	0.834
.080	69.8	0.557	300.7	0.811
.090	70.4	0.585	300.7	0.766
.100	71.3	0.624	300.8	0.702
.150	71.9	0.649	301.0	0.666
.200	73.1	0.694	301.1	0.588
.250	74.3	0.736	301.5	0.518
.300	76.4	0.801	301.8	0.389
.400	77.9	0.844	302.2	0.312
.500	79.6	0.891	302.9	0.228
.600	81.1	0.928	303.4	0.158
.700	82.3	0.955	303.8	0.102
.800	83.5	0.981	304.0	0.042
.900	84.1	0.994	304.1	0.016
1.000	84.4	1.000	304.1	0.000

TABLE 17

EXPERIMENTAL DATA AT P = 64.0 MICRONS (UNCOOLED PLATE)

x = 1.0 inches $T_{\infty} = 268^{\circ}\text{K}$ $U_{\infty} = 688 \text{ ft/sec}$ $T_w = 300.5^{\circ}\text{K}$

Distance inches	P_t microns	$\frac{U}{U_{\infty}}$	T_c $^{\circ}\text{K}$	$\frac{T-T_{\infty}}{T_w-T_{\infty}}$
.002	65.3	0.270	300.6	1.000
.003	65.3	0.270	300.6	1.000
.004	65.3	0.270	300.6	1.000
.005	65.3	0.270	300.6	1.000
.006	65.3	0.270	300.6	1.000
.007	65.3	0.270	300.6	1.000
.008	65.9	0.328	300.6	0.956
.009	65.9	0.328	300.6	0.956
.010	65.3	0.270	300.6	1.000
.020	65.9	0.328	300.6	0.956
.030	66.2	0.353	300.6	0.934
.040	67.4	0.439	300.6	0.849
.050	67.4	0.439	300.6	0.849
.060	67.7	0.458	300.6	0.828
.070	68.0	0.475	300.6	0.808
.080	68.6	0.509	300.6	0.767
.090	68.6	0.509	300.7	0.768
.100	68.6	0.509	300.7	0.768
.150	70.7	0.608	300.9	0.638
.200	71.6	0.645	301.1	0.588
.250	72.5	0.679	301.3	0.542
.300	73.4	0.711	301.5	0.495
.400	75.8	0.788	302.0	0.373
.500	76.7	0.815	302.6	0.343
.600	79.3	0.886	303.1	0.219
.700	81.4	0.936	303.6	0.128
.800	83.8	0.988	303.8	0.021
.900	84.1	0.994	304.0	0.014
1.000	84.4	1.000	304.0	0.000